Polytechnic of Leiria
School of Technology and Management
Department of Mechanical Engineering
Master's Degree in Automotive Engineering

VEHICLE DYNAMICS ANALYSIS IN A FORMULA STUDENT RACING CAR

HENRIQUE NUNO CLÉRIGO DOMINGOS DO AMARAL

Leiria, September 2022

Polytechnic of Leiria
School of Technology and Management
Department of Mechanical Engineering
Master's Degree in Automotive Engineering

VEHICLE DYNAMICS ANALYSIS IN A FORMULA STUDENT RACING CAR

HENRIQUE NUNO CLÉRIGO DOMINGOS DO AMARAL

Project under the supervision of Professor Sérgio Pereira dos Santos and Professor Doutor Carlos Daniel Henriques Ferreira.

Leiria, September 2022

ACKNOWLEDGMENTS

The way we behave as human beings is strongly influenced by our environment, so starting an acknowledgment without first noting my family and friends would be like building a house without its foundations. In particular, special thanks to my grandparents who have always been an example and taught me a lot of things regarding science, engineering and philanthropy when I was a child. I also would like to express my gratitude towards my parents who had a key roll in my education, opening new horizons and always supporting my life decisions financially and mentally. It is impossible to extend enough thanks to my true friends, ain't no words can express on how impact-full was our discussions converted into infinite nights speaking about the meaning of everything, all the trips and projects we did around the world and sometimes beyond, all the parties and good times we have spent together!

My project could not have been accomplished without the support of the FSI-PLeiria team members and team advisors. They helped me bring the old formula student vehicle back to life which was crucial to perform the dynamic analysis of this work. More important they stood by my side, devoting their free time to keep the project going. A special note of thanks to Eng. Pedro Martins who had a huge roll in the team, giving up its academic and social life to help me leading the team in to success.

Last, but not least, I pay my deep sense of gratitude to all the professors I have been working with during my college years. In particular, to professors João Pereira, Luis Serrano, Carlos Ferreira and Olivier Gouveia for the help during the Formula Student project.

Finally, I feel to acknowledge my indebtedness and deep sense of gratitude to my guide professor Sérgio Santos who provided the right guidance and patience not only during this work but also throughout other academic projects, to whom I dedicate the following quote: *"If I have seen further, it is by standing on the shoulders of giants."*

ABSTRACT

One of the most important concepts in motorsport is vehicle dynamics. Being able to predict the manoeuvre behaviour of a racing vehicle, not only reduces test time but also optimizes the development process. Once it is possible to isolate external factors, one can study a particular group of variables and anticipate their consequence on the overall vehicle performance.

This work is focused on two different approaches to the problem of predicting vehicle behaviour. The first procedure consisted in the development of a simulation tool, more precisely, a Lap Time Simulator using Simulink. Given the specific requirements of the team, the simulator was built without the use of any predefined vehicle dynamics block sets, this means, the algorithm is fully customizable. The developed simulator uses a single point mass approach, so the vehicle body was converted to a single point neglecting the effects of body roll and load transfer. Nevertheless, the algorithm can predict the effects of different vehicle systems on lap time. The calculations include, for example, a powertrain model defined by engine torque, gear ratios, rotational inertia and fuel consumption. The aerodynamic module controls the negative lift and drag force present at each step. The tyre behaviour was defined by a basic tyre model, which predicts longitudinal, lateral and rolling resistance forces.

The second method utilizes a commercially available solution using a quasi-steady-state approach with optional transient properties. Instead of a single point mass, the vehicle body model uses a four-track model with the motion of each wheel/suspension to formulate the vehicle manoeuvre. The tyre model was extended to include slip angle, slip ratio and combined slip. For that purpose, the software utilizes the Pacejka magic formula with formula student tyre data.

One of the most important factors of simulation tools is the validation of the results. For that reason, the thesis also includes an experimental procedure regarding the behaviour of a formula student on a controlled environment track. The obtained data were used to compare the simulation results with the real logged data provided by a vehicle instrumentation apparatus.

RESUMO

Um dos conceitos mais importantes no desporto motorizado é a dinâmica de veículos. Ser capaz de prever o comportamento de manobra de um carro de corrida, não só reduz o tempo de teste, mas também otimiza o processo de desenvolvimento. Uma vez que é possível isolar fatores externos, pode-se estudar um determinado grupo de variáveis e antecipar as suas consequências no desempenho dinâmico geral .

O presente trabalho focou-se em duas abordagens diferentes para prever o comportamento de um *formula student*. O primeiro procedimento consistiu no desenvolvimento de uma ferramenta de simulação, mais precisamente, um simulador de tempo de volta utilizando o Simulink. Atendendo aos requisitos específicos da equipa, o simulador foi construído sem a utilização de blocos de dinâmica de veículos predefinidos, ou seja, o algoritmo é totalmente personalizável. O simulador desenvolvido utiliza uma abordagem de massa pontual, isto é, o chassi foi convertido num único ponto, desprezando por exemplo os efeitos de transferência de peso. Apesar dessa limitação, a simulação utiliza um algoritmo dos componentes do motor definido pelo binário, relações de transmissão, inércia rotacional e consumo de combustível. Calcula também as forças aerodinâmicas com um módulo aerodinâmico que controla a força negativa de sustentação e arrasto presente em cada ponto da pista. O comportamento do pneu foi definido por um modelo básico que prevê forças longitudinais, laterais e de resistência de rolamento do pneu.

O segundo método de simulação utiliza uma solução comercial que define o comportamento do veículo através de uma abordagem de estado quase-estático com propriedades transientes opcionais. Em vez de uma massa pontual, o método utilizado calcula o movimento individual de cada roda/suspensão. O modelo de pneu foi estendido para incluir o *slip angle, slip ratio e combined slip* através da aplicação da fórmula mágica de Pacejka utilizando dados de um pneu específico para a competição de *formula student*.

Na parte final do presente trabalho foi proposto um procedimento experimental para estudar o comportamento do *formula student* numa pista pré definida. Os dados foram obtidos através de um sistema de instrumentação eletrónica previamente instalado no veículo e posteriormente usados para validar os resultados das duas abordagens de simulação.

CONTENTS

LIST OF FIGURES

LIST OF TABLES

ACRONYMS

BPS	Brake Pressure Sensor.
BSFC	Brake-specific Fuel Consumption.
CAN	Controller Area Network.
CD	Coefficient of Drag.
CFD	Computational Fluid Dynamics.
CG	Center of Gravity.
CL	Coefficient of Lift.
CP	Center of Pressure.
DLU	Data Logger Unit.
DNS	Direct numerical simulation.
DOF	Degrees of Freedom.
ECU	Engine Control Unit.
IC	Internal Combustion.
IMU	Inertial Measurement Unit.
LAS	Limit Acceleration Surface.
LES	Lotus Engine Simulation.
LTS	Lap Time Simulator.
LUT	Lookup Table.
MM	Milliken Moment Method.

N-S	Navier-Stokes.
QSS	Quasi-Steady State or Quasi-Static State.
QTS	Quasi-Transient State.
RANS	Reynolds-Averaged Navier-Stokes.
Re	Reynolds Number.
SAE	Society of Automotive Engineers.
SAS	Steering Angle Sensor.
SDS	Suspension Displacement Sensor.
SS	Steady State.
SST	Shear Stress Transport.
TPS	Throttle Position Sensor.
TS	Transient State.
WOT	Wide Open Throttle.
WSS	Wheel Speed Sensor.

1

INTRODUCTION

1.1 FORMULA STUDENT COMPETITION

Formula Student is an academic competition in which students from various universities build a single-seat formula type racing car. This competition first started in the United States in 1981. Nowadays, the events are held in countries around the globe merging hundreds of universities (IMechE, 2021).

The project aims to put into practice the skills and theory taught in different areas of study. The team is evaluated in the design, cost, sustainability and business presentation during static events. The prototype is then put to the test at the following dynamic events:

- Acceleration
- Skid Pad
- Sprint
- Endurance

Students from Polytechnic of Leiria have been participating in the competitions since 2006. Despite the popularity of electric vehicles, the FSIPLeiria team started and still competes in the combustion class. One of the cars developed and produced by the team is the T14. This vehicle, showcased in Figure 1, is equipped with a sports motorcycle 600cc engine and was selected to be used in the dynamic analysis of the present thesis.

1.2 OBJECTIVES AND MOTIVATION

One of the key aspects of the competitions is the car behaviour during dynamic events. Due to high competition, every successful team must push their prototype to the limits. Knowing how a vehicle operates, is the baseline to build and tune a winning vehicle. Not only is important to study individual vehicle systems such as

suspension, powertrain, aerodynamics and others but also how systems interact with each other.

The nature of the formula student project makes it difficult to have many hours of real track testing so the use of simulation tools represents an important asset in the research and development phase. The lack of simulators to predict changes in the different systems was noticed making the creation of a computer-based model to predict lap time imperative. Subsequently, the main objective of the present work is the elaboration of a numeric simulator in which team members would be able to study how vehicle parameters change lap times. The model should be capable of computing the performance of vehicle elements such as powertrain, aerodynamic devices and others. Simultaneously, to produce a satisfactory simulation it is important to validate the results using real test data. Thus, vehicle instrumentation and test procedure must be included.

Figure 1: Formula T14.

1.3 THESIS OUTLINE

An overview of the research standards, including vehicle dynamics nomenclature and an overall description of the single-seated vehicle, was conducted in Chapter 2 .

The current solutions regarding lap time simulators and the most common approaches to define the dynamic behaviour of the vehicle are described in Chapter 3.

The Chapter 4, provides a literature overview focused on key vehicle modelling theories and complementary details used in the development of the lap time simulator.

A lap time simulator created in Simulink is proposed in Chapter 5. The auxiliary CFD and Thermodynamic simulations required to obtain some inputs respecting

aerodynamics and engine performance are also evidenced in this section. Furthermore, the modelling strategy used in a commercially available vehicle dynamic software is also described.

The validation of the theoretical approaches (Simulink and Carmaker) is present in Chapter 6. The chapter provides the reader with a description of the required vehicle instrumentation and test settings.

A result analysis including real logged data, Simulink and Carmaker outputs of the most commonly analysed results is delineated in Chapter 7.

Finally, the conclusions of the thesis are summarized in Chapter 8. In addition, the recommendations for future work are also included.

2

VEHICLE DYNAMICS FUNDAMENTALS

2.1 INTRODUCTION

The definition of a vehicle's movement and the relative motions of certain vehicle systems can often be misleading, so this chapter features an overview of concepts used when studying vehicle dynamics. It also provides an overlook of the open-wheel type vehicle used in the present work, with clarification of the overall dimensions, suspension and steering system. Lastly, the problem of optimum trajectory applied to lap time simulations is evidenced.

2.2 COORDINATE SYSTEM

The dynamic behaviour is determined by applied forces throughout the various systems that compose a vehicle. Usually, papers and books define the same degrees of freedom but nomenclature disparities are common. In the present work, all equations are under the SAE axis convention (SAE, 1976). This ground vehicle axis system uses the same principle as air vehicles. It defines motion using an orthogonal coordinate system (x, y, z) that moves with the vehicle and has its origin coincident with the centre of gravity (see Figure 2).

An earth-fixed complementary axis system (X, Y, Z), illustrated in figure 3, is also needed to describe the relative motion of the vehicle to the ground, expressing for example its relative velocity. The rates of change in velocity (accelerations), can be defined according to the direction of the vehicle's path:

- Longitudinal Acceleration - The component of the vector acceleration of a point in the vehicle in the x-direction;
- Normal Acceleration - The component of the vector acceleration of a point in the vehicle in the z-direction;

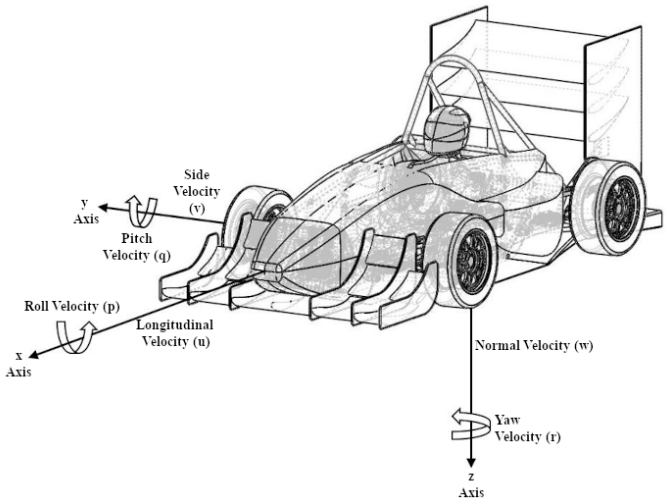

Figure 2: Vehicle axis system (SAEJ670).

- Lateral Acceleration - The component of the vector acceleration of a point in the vehicle perpendicular to the vehicle x-axis and parallel to the road plane (for small sideslip angles it can be considered equal to centripetal acceleration);

The three Euler angles (yaw, pitch and roll), describe the orientation of a rigid body concerning a fixed system and thus are defined by the relationship of the two-axis systems described above.

The tyre of a given vehicle is subjected to internal and external forces that produce moments and deformations. In order to clarify the concepts used to define the tyre's behaviour, the SAEJ670 orthogonal tyre axis system was adopted. As shown in Figure 4, it sets its origin at the centre of the contact patch and uses the road plane as a reference for inclination angle, normal force and other notions.

2.3 VEHICLE ARCHITECTURE OVERVIEW

2.3.1 *General Dimensions*

Formula student vehicles must fulfil very specific rules regarding their dimensions. The rules define the boundaries of the aerodynamic devices constraining not only the maximum length, width and height but also the wheelbase and wheel track relationship. The wheelbase and wheel track have a relevant impact on longitudinal, lateral and diagonal load transfer thus affecting the vehicle's performance. A relatively long wheelbase increases straight-line stability and reduces longitudinal load transfer

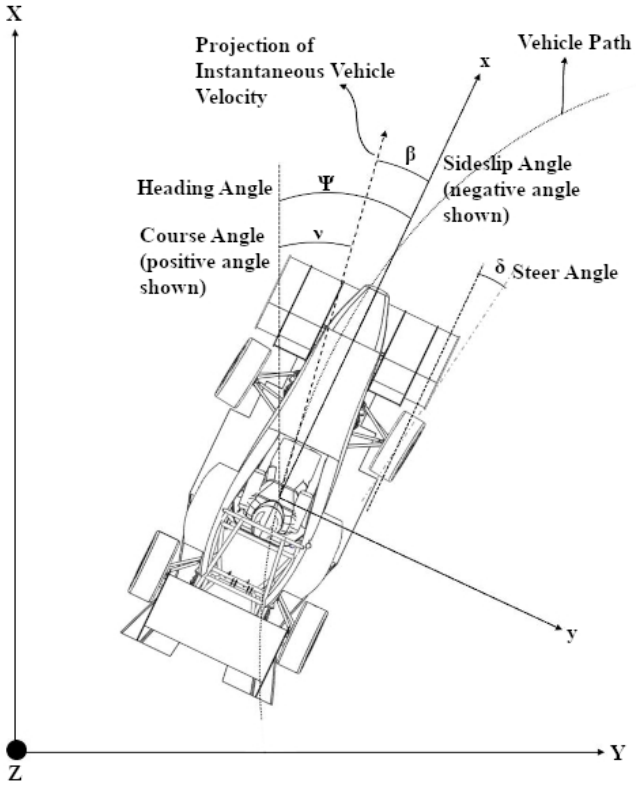

Figure 3: Ground axis system (SAEJ670).

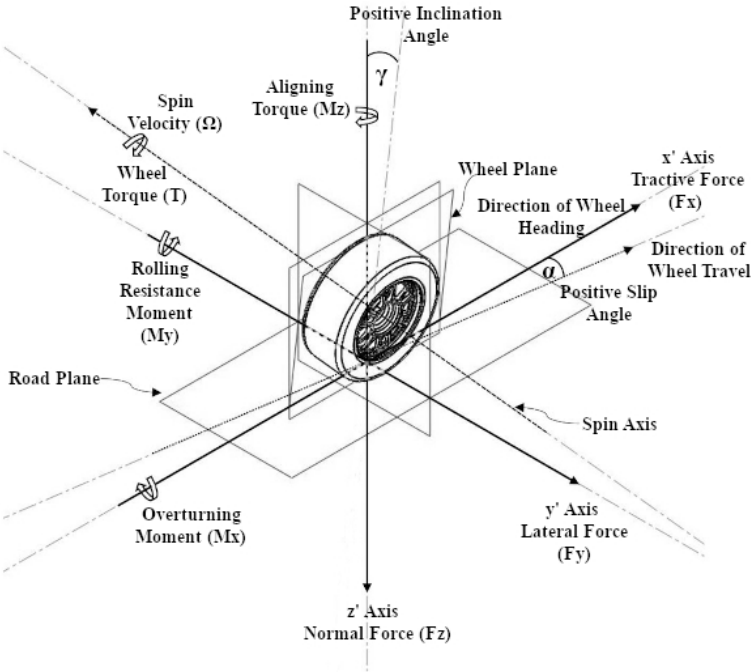

Figure 4: Tyre axis system (SAEJ670).

(Smith, 2004), while long track widths reduce the lateral load transfer. As shown in Figure 5 and Figure 6 formula student vehicles usually have considerable small wheelbases/ track widths and centre of gravity (CG) as low as possible. A low CG location will result in lower load transfer and body roll, both favourable aspects for the dynamic behaviour of a given vehicle.

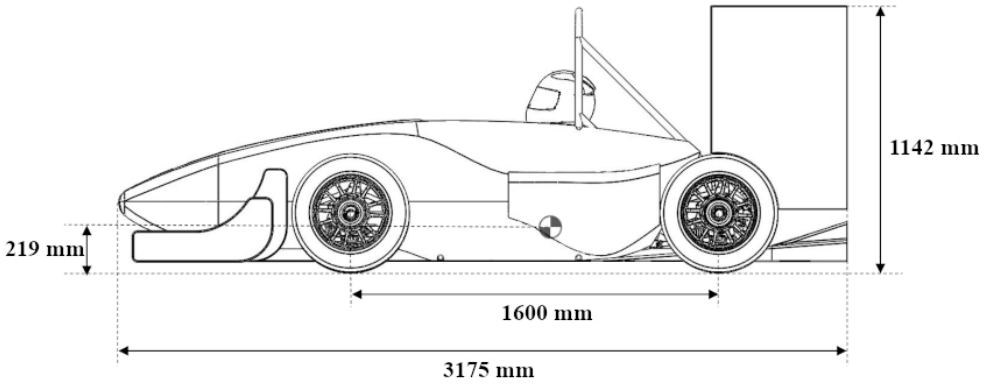

Figure 5: Formula T14 overall dimensions.

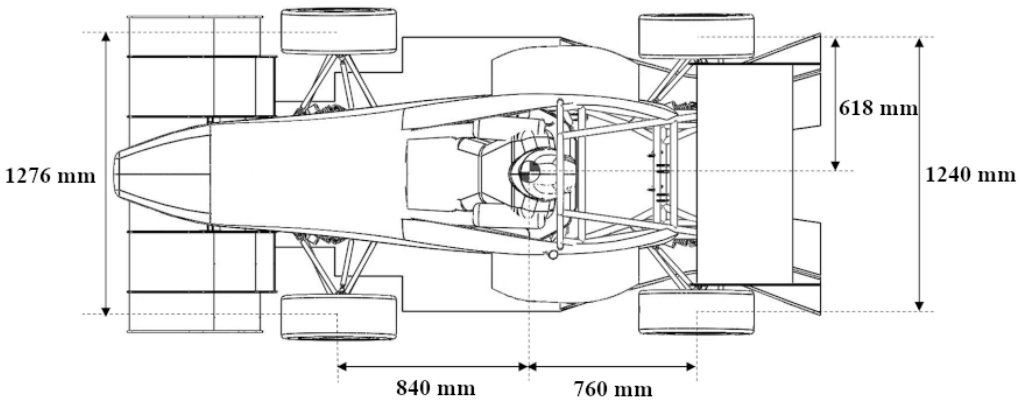

Figure 6: Formula T14 front and rear track dimensions.

2.3.2 *Suspension and Steering*

Modern race cars use double wishbone suspension systems. This type of geometry (see figure 7) allows better motion control of the wheels and has more degrees of freedom to adjust parameters like camber, toe and caster. The length and position of the suspension arms have a major impact on the dynamic behaviour of the wheels for a given amount of vertical travel. Unequal length arms (short upper link) result in fewer camber angle changes (tending to negative camber) as the car rolls and the suspension compresses. A non-parallel link geometry can also be used to further control camber curves and roll centre position.

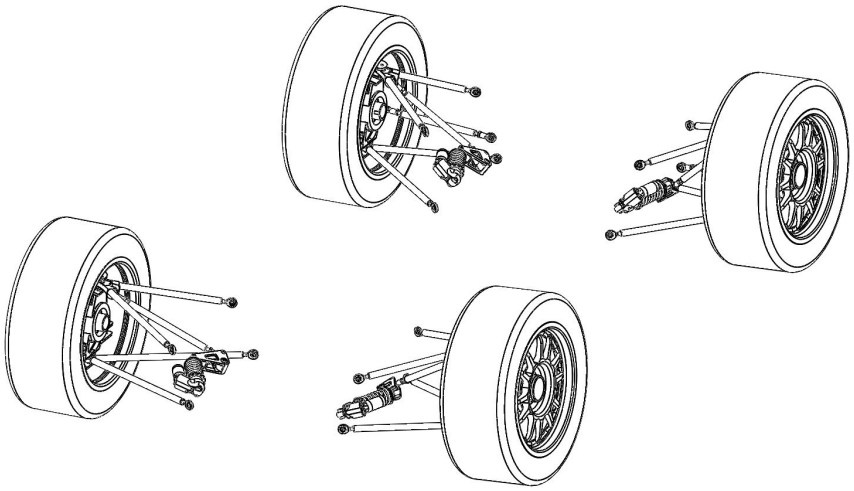

Figure 7: Formula T14 suspension geometry.

The Ackermann steering geometry is an important concept to keep in mind when designing or tuning the steering system. As the vehicle corners, the four tyres follow unique trajectories around the cornering centre. It means that to avoid sliding in a low-speed corner, the inside front tyre steering angle must be higher than the outside front tyre as illustrated in Figure 8. One can use pro-Ackermann to influence the slip angle on the inside tyre. This might be useful to maintain tyre temperature at the expense of increasing drag in cars with a lot of negative camber. In high-speed corners, bigger outside front tyre steering angles, in other words, anti-Ackermann steering, is sometimes used to reduce drag and rise the laden wheel slip angle.

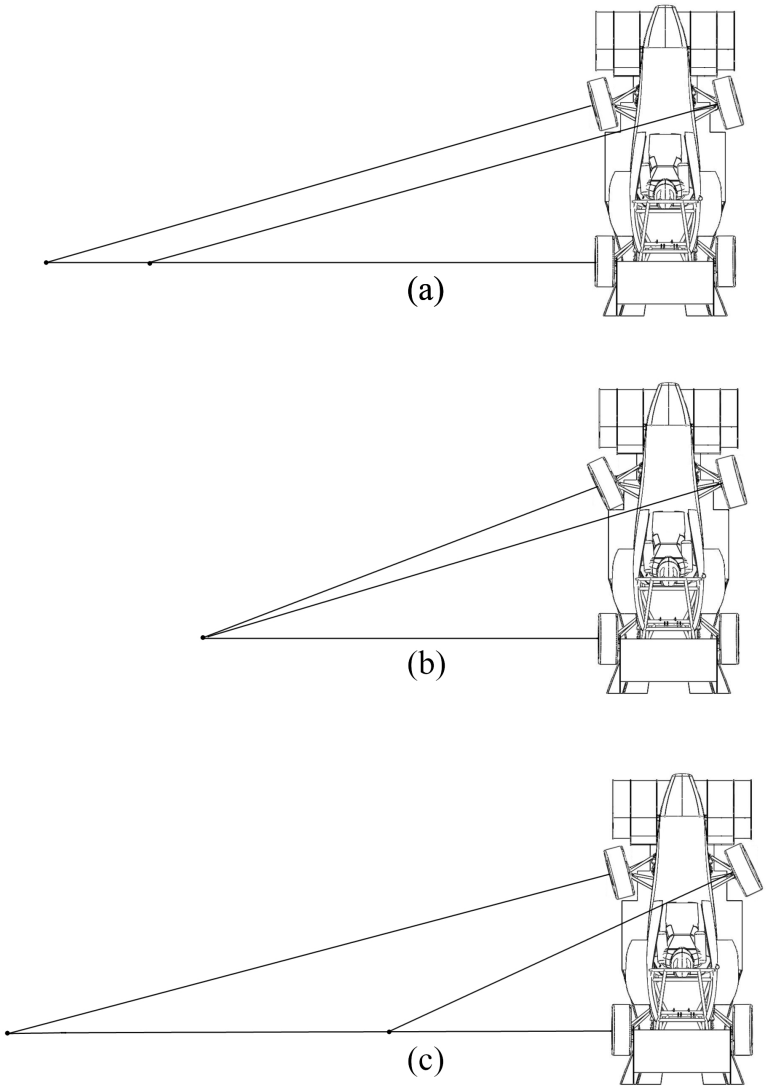

Figure 8: Different steering geometries ((a)- Parallel; (b)- Ackermann; (c)- Anti-Ackermann).

2.4 OPTIMUM TRAJECTORY

The main goal of a racing driver is to reduce lap times. The best way to do that is to take advantage of every piece of the racing track, in other words, driving in the ideal racing line. Likewise, minimum lap time simulations should also include the ideal trajectory. Regarding optimum paths, there is not much to say about straights, once it is all about keeping the vehicle at maximum acceleration and in a good position for cornering entry. Notwithstanding, during corners, the path becomes a critical factor that can be divided into four points (Figure 9):

- (A) Braking: Minimum distance to slowdown until corner entry speed is reached;
- (B) Turn-in: Moment when the vehicle turns to the corner;
- (C) Apex: Inside (minimum radius) stage of the corner;
- (D) Exit: Outside point of the corner where the vehicle starts to go straight again.

The geometrically calculated optimum trajectory is not always the best practice to solve minimum lap time problems. For example, high-powered vehicles may benefit from earlier corner exits at the expense of lower cornering speeds, changing the entire racing line as represented in Figure 9.

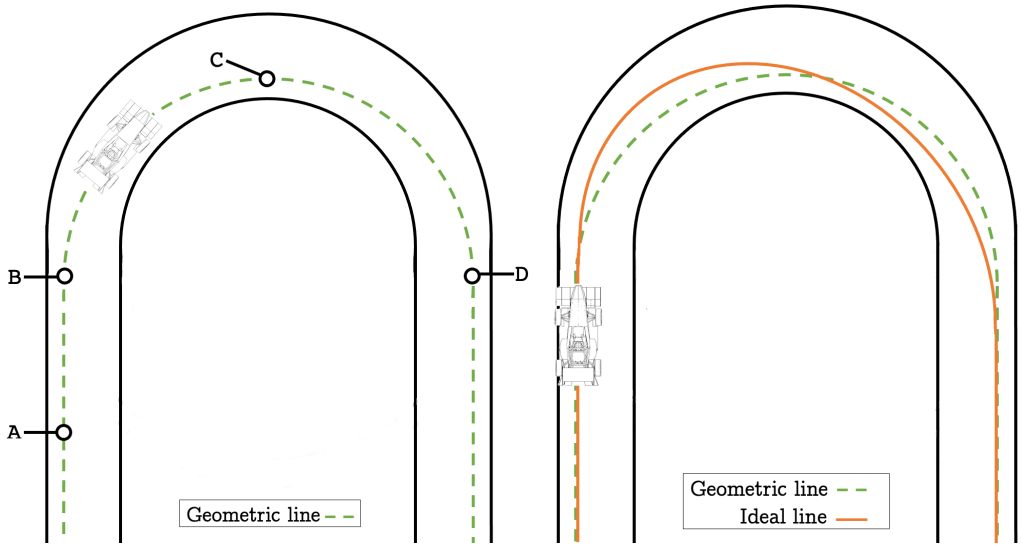

Figure 9: Steps of cornering maneuver and race lines.

2.5 SUMMARY

The formula student vehicle used in this work follows the tendency of this type of racing formulas with narrow track widths/ wheelbase and a fully independent multi-link suspension system. Regarding optimum trajectory, the best pathway to achieve minimum time is always at constant change during a race. When considering the variables involved, one must choose between finding the optimum path for a certain vehicle or the optimum vehicle for a previously defined path.

3

STATE OF THE ART IN LAP TIME SIMULATIONS

3.1 INTRODUCTION

Lap time simulators (LTS) are widely used in motorsports. They provide fundamental information to design and optimize vehicles complementing other simulation tools such as structural and fluid dynamics analysis. Not only it allows engineers to predict the behaviour of a concept vehicle reducing design flaws and build costs but it also offers a solution to reduce real testing when setting up a car. This maximizes efficiency by decreasing the costs and increasing the consistency of the results once human errors and other external variables are mitigated. LTS fall into three main categories to predict the performance of a vehicle:

- Steady-State (SS);
- Quasi-Steady State or Quasi-Static State (QSS);
- Transient State (TS).

3.2 STEADY-STATE

The SS approach is the easiest and common way of predicting lap times. It implies the division of the racing track straights in small lengths where the longitudinal acceleration is set to be constant and the speed is:

$$v = \sqrt{v_0^2 + 2 \cdot ax \cdot d} \tag{1}$$

where:

- vo = Initial speed;
- ax = Longitudinal acceleration;
- d = Displacement.

During corner stage the speed is constant. This speed is known as critical speed:

$$vc = \sqrt{\frac{Fty \cdot Rc}{m}} \tag{2}$$

where:

- Fty = Maximum lateral tyre force ;
- Rc = Corner radius;
- m = Total mass.

The braking points are calculated by running the simulation in reverse (Brayshaw and Harrison, 2005). In this phase, the longitudinal acceleration is the sum of braking force with the other forces such as drag, rolling resistance and road inclination, which was negative when the vehicle was set to accelerate with the engine (under normal straight-line acceleration).

A point mass procedure is the simplest way of defining the vehicle model. It only requires the longitudinal and lateral coefficients of friction, once the maximum longitudinal and lateral force is only a function of the coefficients of friction and normal force (mass of the vehicle). The Figure 10 illustrates the output of a point mass car manoeuvre on a track compose of two different radius corners.

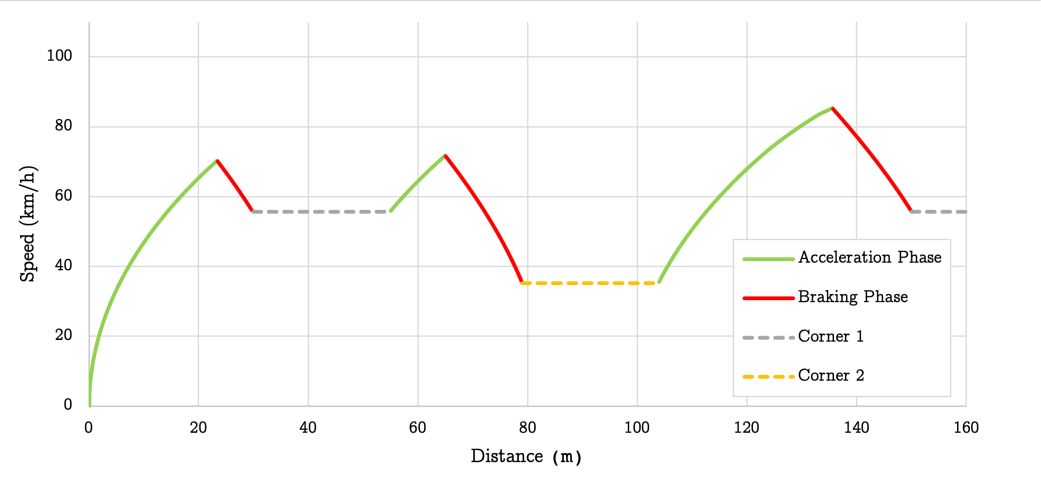

Figure 10: Vehicle speed results of a steady-state cornering approach.

3.3 QUASI-STEADY-STATE

The SS approaches usually result in bad convergence when compared to real measured data (Siegler et al., 2000). The main reason for this is the unrealistic definition of the cornering phase (Novotny, 2016), i.e., implying a constant radius trajectory around

the corner. QSS methods solve this problem with the division of the corner in small different radius lengths and in some cases with steering angle inputs. The tyre steady-state force is replaced by force using the friction circle (or more precisely ellipse) combined with Pacejka Magic Formula Tyre model (Pacejka, 2005) (see Figure 11). This combines the longitudinal and lateral forces establishing a relationship that resembles real tyre behaviour. This methodology have been study for some years and is formalized and expanded in (Siegler et al., 2000) ,(Candelpergher et al., 2000) and (Brayshaw and Harrison, 2005).

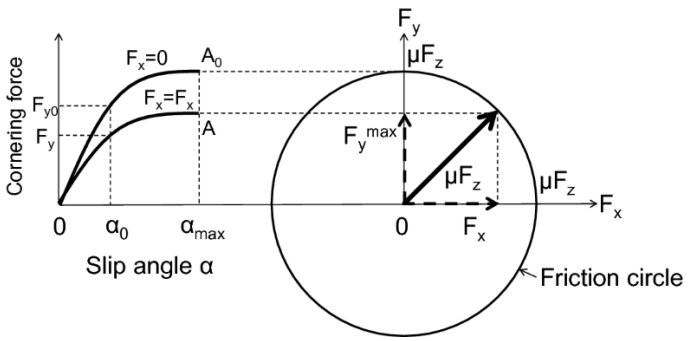

Figure 11: Combined tyre force (Nakajima, 2019).

Regarding vehicle models, the single point mass definition is usually replaced by detailed models. The simplest way is by defining the vehicle as a 2 DOF two-track model representing the lateral and yaw motions (see Page 39). Furthermore, advanced configurations use four-track models with 3 DOF (longitudinal and lateral and yaw motions) that can be extended to higher DOF models with the implementation of vertical motion, in particular wheel motion, roll, pitch and yaw. In (SangDo et al., 2015) the previous approach combined with an higher level tyre model (4 DOF) resulted in a 14 DOF representation.

3.4 TRANSIENT-STATE

In reality, the vehicle is undergoing a non-steady behaviour because as it corners, it is always suffering accelerations in the 3 axes of motion. Typically, the dynamic response of yaw is included in the QSS simulation to characterize this TS behaviour, producing a quasi-transient-state (QTS) simulation. The Milliken Moment Method (MM) (W. Milliken and D. Milliken, 1995) can be used to describe this phenomenon since it correlates the yaw moments versus lateral accelerations as a function of vehicle slip and steer angle. (Kang et al., 2005) provides a straightforward implementation of this method in commercially available dynamic simulation and control software programs.

Further research was extended in (Patton, 2013), where Limit Acceleration Surface (LAS) profiles were used to combine lateral, longitudinal and yaw acceleration. The use of LAS method resulted in a QTS lap time simulator with transient inputs. Regardless of the extended simulation environment, the use of 3D diagrams produces lap times identical to that in QTS algorithms.

How much tyre force is available at a given time is not only a function of the approaches mentioned on the SS and QSS sections. In fact, there are physical delays in force generation so the response time of a system is taken into account during transient analysis. This time delay promotes lateral acceleration lag, as depicted in Figure 12. Again the tyre magic formula still applies, but it needs to be complemented with the transient properties that can be found in (Pacejka and Besselink, 1997).

Even though transient models are very complex, previous work concluded that the results are very similar to QSS models. Research in this area (Kelly, 2008) found some steering discrepancies in QSS simulations when the yaw accelerations are relevant. Nevertheless, QSS solution gained time during braking and corner exit and the overall time manoeuvre was only 0.77% faster when compared to the TS solution. Another study (Siegler et al., 2000) had similar results with QSS elapsed time higher 0.73%. A more sophisticated work (Casanova, 2000), with 7 DOF formula 1 vehicle model and transient algorithms, concluded that the yaw rate variations are quite large (the more yaw inertia there is, the higher are the peaks). Regardless, the length of each transient phase was short to such a degree, that the minimum time manoeuvre remain almost the same.

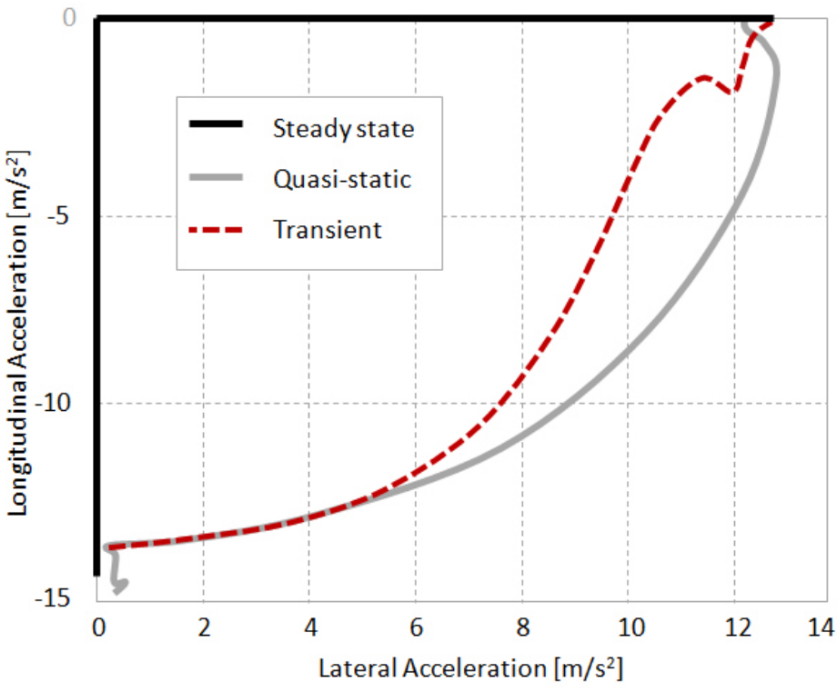

Figure 12: Acceleration results for different states algorithms during a corner maneuver (Novotny, 2016).

3.5 SUMMARY

The state of the art research has shown that the three main approaches for LTS have different levels of accuracy. Starting with SS, it represents the vehicle behaviour with the lowest number of inputs thus being the less computational demanding of the three. The QSS procedure is usually the most cost-benefit solution with high levels of precision and a wide range of applications. When the problem of minimum lap time is focused on tuning certain subsystems, oftentimes the best solution is to perform transient analysis but it might not be the most suitable way for generic vehicle behaviour, because of higher simulation times.

4

VEHICLE DYNAMICS MODELLING THEORY

4.1 INTRODUCTION

Usually, the modelling of a given system has two approaches: a straightforward mathematical formulation that one can call law, or theories, which by definition, do not fully define the behaviour of a system but instead tries to characterize it. This chapter summarizes the most common methods used to formulate vehicle dynamics and complements the modelling strategy presented in Chapter 5.

4.2 TYRE BEHAVIOUR

The tyre is one of the most important, if not, the most important component in vehicle dynamics. It not only provides the forces needed to accelerate, brake and steer the vehicle but also the stabilizing and resisting forces at the expense of inducing rolling resistance. It develops friction by the contact interaction between the rubber and the road surface, which in this case 'bends and twists' the elastic tread compound affecting its coefficient of friction.

4.2.1 *Rolling Resistance*

The rolling resistance can be defined as the resistance of a free-rolling tyre to forward motion. This resistance is primarily generated by the deformation of the rubber in the contact patch and is dependent on different factors such as speed, tyre pressure, road surface, wheel alignment, and others. The analytic method for predicting the rolling resistance is very difficult to obtain with such a number of variables. The determination of the rolling resistance, therefore, relies almost entirely on experiments (Wong, 2001).

The rolling coefficients for air filled tires on dry roads can be estimated using the following formula (*Eng. ToolBox* 2008):

$$c = 0.005 + \frac{1}{p} \cdot (0.01 + 0.0095 \cdot (\frac{v}{100})^2) \tag{3}$$

where:

- c = Rolling coefficient;
- p = Tyre pressure (bar);
- v = Velocity (km/h).

4.2.2 *Slip Angle*

The slip angle is the angular displacement between the plane of rotation of the wheel (direction of wheel travel) and the path that the tyre will follow (Smith, 2004). The maximum lateral force capacity of the tyre contact increases as the patch acquires more slip angle. As illustrated in Figure 13, when the maximum slip angle is reached, the tyre will lose its potential to withstand higher lateral forces, thus losing traction. At low slip angles, the relationship between lateral force and slip angle is linear, the slope defines the cornering stiffness of the tyre which is influenced by rubber compound, number and orientation of the plies, tyre dimensions, tyre pressure and others.

4.2.3 *Slip Ratio*

The slip ratio of a tyre is the difference between the angular velocity of a free-rolling tyre ($\Omega 0$) and the effective angular velocity of the tyre when braking or driving torque (Ω) is applied. The definition is the following, for tires pointing straight ahead:

$$SR = \frac{\Omega}{\Omega 0} - 1 \tag{4}$$

As the slip ratio increases, the maximum longitudinal force also increases up to a maximum value which usually occurs in the range of 0.10-0.15 slip ratio, after which the forces fall off (W. Milliken and D. Milliken, 1995). The tyre will either lock or spin once the peak force is exceeded.

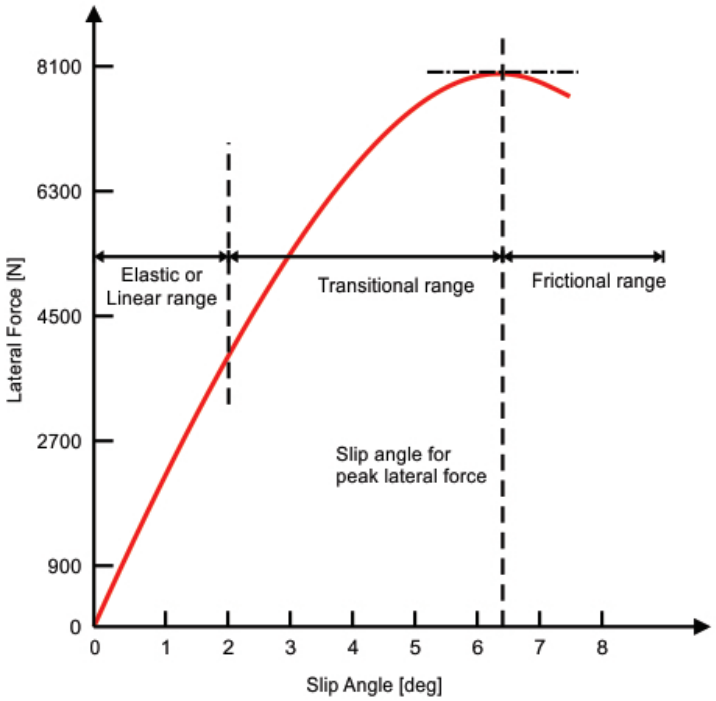

Figure 13: Tyre Lateral Force vs Slip Angle (Santos, 2014).

4.2.4 *Combined Slip*

Tyres are frequently subjected to longitudinal and lateral forces simultaneously. The interaction is not favourable since the peak longitudinal force is achieved when the lateral force is zero, and vice versa. The effects of combined slip, in other words, the presence of slip angle and slip ratio at the same time, in a right-hand turn are portrayed in Figure 14.

Despite the data regarding combined slip is not many times available, this type of information can be useful to define the tyre model and acquire information about utilizing most of the tyres, hence reducing real lap time.

4.2.5 *Load Sensitivity*

The coefficient of friction decreases with the increase of the normal load (Fz). This phenomenon is called load sensitivity and it has a negative impact on tyre´s performance. Despite reductions in the coefficient of friction, the overall lateral load

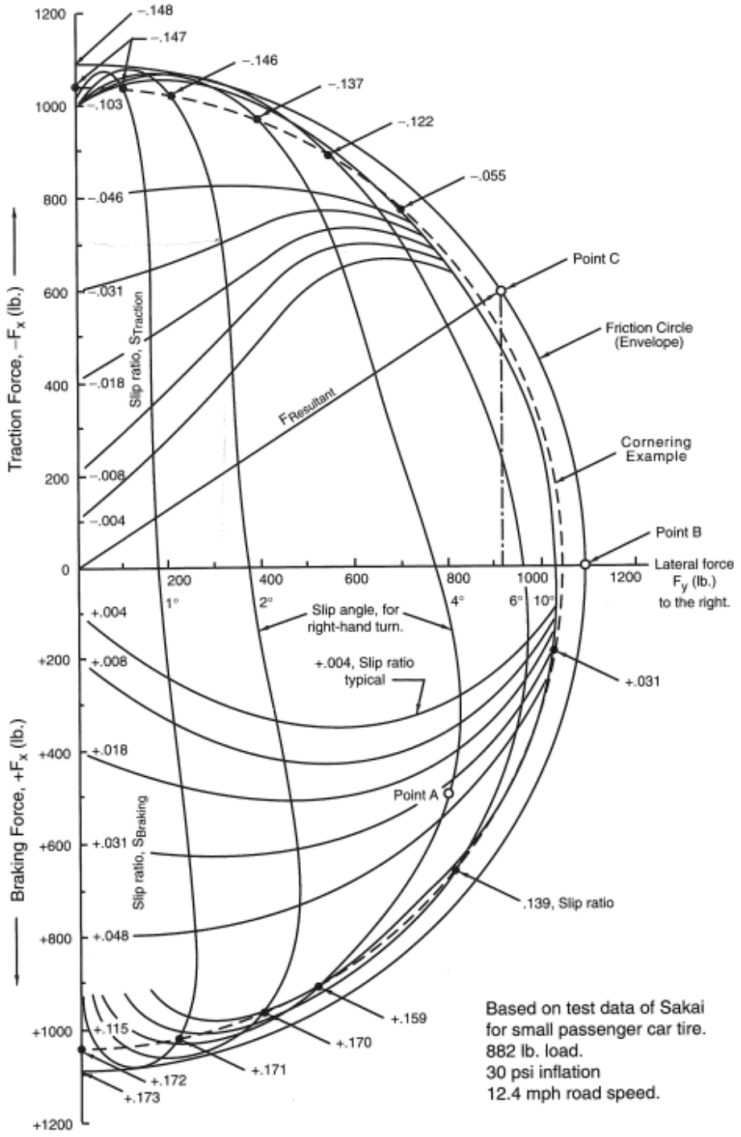

Figure 14: Tyre Friction Circle Diagram (W. Milliken and D. Milliken, 1995).

capacity of the tyre has a positive gain with higher normal loads according to Figure 15 and Figure 16.

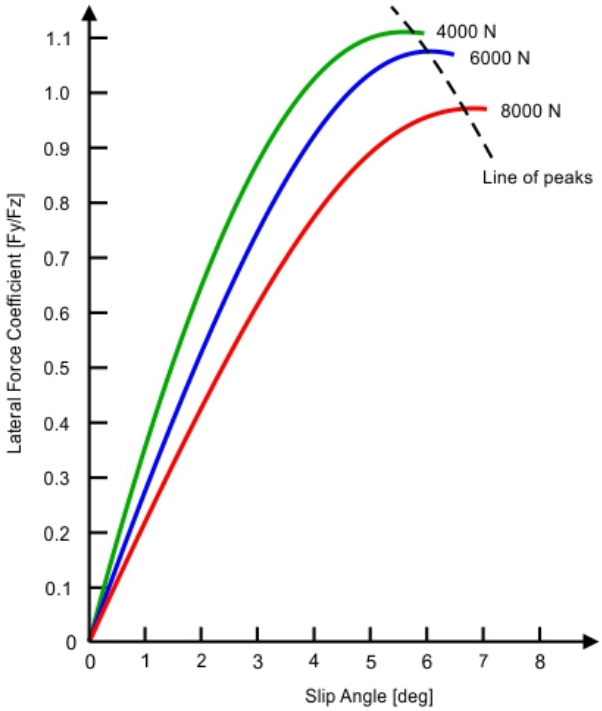

Figure 15: Variation of coefficient of friction with normal load (Santos, 2014).

4.2.6 *Camber Thrust*

When a wheel leans inwards towards the vehicle body it develops an inclination angle that is positive on the left side of the car and negative on the right side (see Figure 4). This inclination angle can also be referenced as the camber angle, which is negative on both sides when the wheel leans as described above. As illustrated in Figure 17, negative camber angles will give rise to a horizontal force (camber thrust) in the same direction in which the tyre leans, rising the lateral load capacity of the tyre (Figure 18). The camber thrust also increases with a vertical load within tyre limits. It is important to note that low profile tyres have different behaviour when subjected to lean angles. When this kind of tyre cambers, the lateral distribution of the tyre load in the contact plane, could shift the load to the inner side, unloading the outer side. This unequal distribution causes a decrease in the lateral force (Abe, 2015).

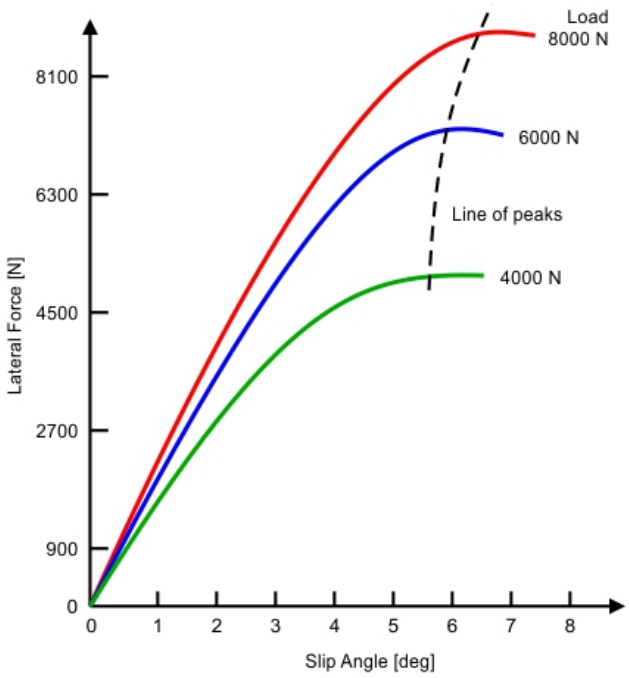

Figure 16: Variations of lateral force with normal load (Santos, 2014).

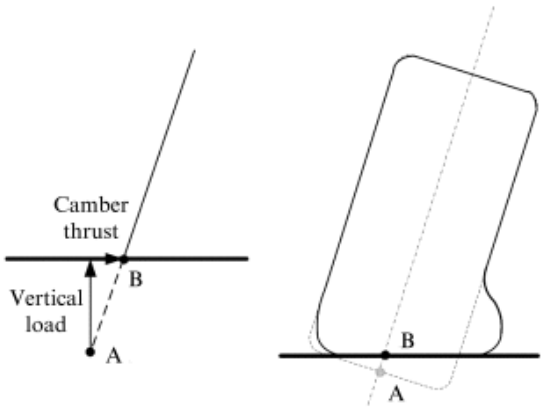

Figure 17: Principle of camber thrust (Balkwill, 2018).

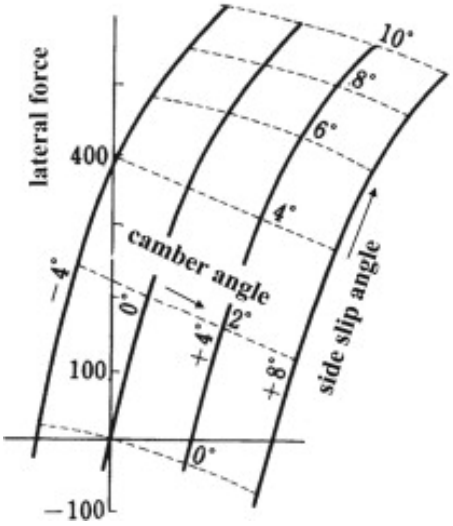

Figure 18: Effects of camber angle in lateral force (Abe, 2015).

4.2.7 *Magic Formula Model*

One of the most widely used semi-empirical models is the Tyre Magic Formula (Pacejka, 2005), which uses a curve fitting approach to output lateral and longitudinal tyre force and aligning moment with the following inputs:

- load;
- slip angle;
- slip ratio;
- camber;

Since its start in the mid-eighties, the formula has been through some improvements. New formulations cope with higher camber angles and inflation pressure changes (I.J.M. Besselink and Pacejka, 2010).

For given values of vertical load and camber angles formula reads:

$$y(x) = D \cdot \sin[C \cdot \arctan(Bx - E(Bx - \arctan(Bx)))] \tag{5}$$

with:

$$Y(X) = y(x) + Sv \tag{6}$$

$$x = X + Sh \tag{7}$$

where:

- Y = Output variable (Fx, Fy or Mz);
- X = Input variable ($\tan\alpha$ (slip angle) or κ (slip ratio).

and:

- B = Stiffness factor;
- C = Shape factor;
- E = Curvature factor;
- Sh = Horizontal shift;
- Sv = Vertical shift.

4.3 LONGITUDINAL DYNAMICS

4.3.1 *Forces Acting on the Vehicle*

The interaction between the vehicle-road-environment set generates a considerable amount of force. These forces can be condensed into equivalent forces that represent the behaviour of the distributed loads on a single point. Figure 19 illustrates the simplification mentioned above, where, for example, the aerodynamic forces are represented only with two components (drag and lift force) reacting on an instantaneous centre of pressure. As depicted, during a longitudinal movement of the vehicle, the point of action of most forces is not located in the vehicle's centre of gravity causing moments. The determination of these moments can be performed using simple physics, applying Newton's second law. With this type of method, one can predict for example the effects of load transfer during straight-line acceleration. Assuming equilibrium around the contact patch of the rear tyre, the total weight on the front axle (Wf) reads:

$$Wf = \frac{P\cos(\theta)\cdot lr + Fl.lp + (m\cdot ax + P\cdot\sin(\theta))\cdot -hcg - Fd\cdot hcp}{lr + lf} \tag{8}$$

where:

- P = Vehicle weight (N);
- θ = Road inclination (deg);
- Fl = Lift force (N);
- lp = Distance from the rear contact patch to CP (m);

- m = Vehicle mass (Kg);
- ax = Longitudinal acceleration(m/s^2);
- hcg = CG height (m);
- Fd = Drag force (N);
- hcp = CP height (m);
- lr = Distance from CG to rear contact patch (m);
- lf = Distance from CG to front contact patch (m).

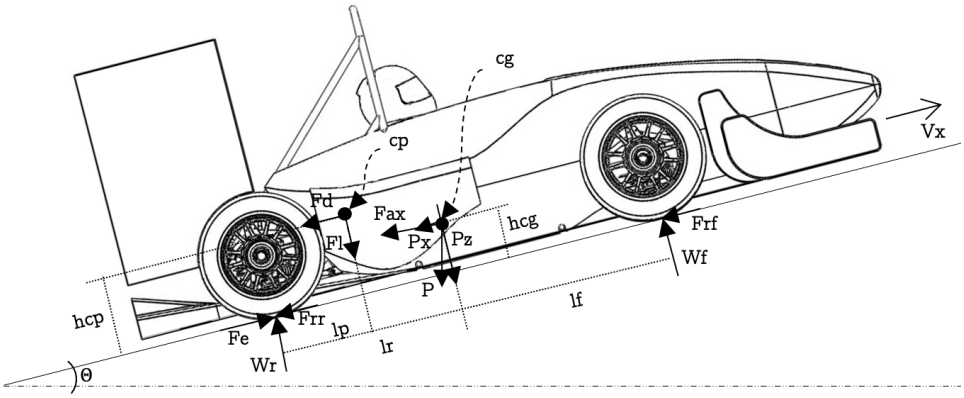

Figure 19: Longitudinal free body diagram with road inclination.

4.3.2 *Powertrain*

Formula Student vehicles are usually equipped with either internal combustion engines or electric motors. The vehicle under analysis has a Suzuki GSXR 600 cc, 4 cylinders internal combustion engine so the following subtopic will focus on reciprocating IC engines.

4.3.2.1 *General Characteristics of IC engines*

The majority of engines used in commercial and competition vehicles have four separate stages during a cycle. These stages are called strokes and they have a big role in how an engine would behave under certain conditions and how efficient it would be.

The performance of an IC engine is usually represented in a plot comparing its angular speed ne (rpm) with torque output Te (N.m) or power output Pe (kW).

This type of generic analysis is typically performed under wide-open throttle (WOT) condition, so due to many factors such as gas inertia, the torque output may not be the best result for every angular speed measured. Despite that, this type of data is a quite common approach to model the powertrain unit on lap time simulators.

$$we = \frac{2\pi \cdot ne}{60} \tag{9}$$

$$Pe = Te \cdot we \tag{10}$$

Due to low torque outputs, IC engines have a gearbox complemented by a final drive located at the differential, thus wheel torque can be calculated using the following formula:

$$Tw = Te \cdot i \cdot \eta \tag{11}$$

where:

- Te= Engine torque $(N.m)$;
- i = Gear box and final drive ratio;
- η = Drive-train efficiency.

4.3.2.2 *Fuel Consumption*

Nowadays, one of the most important parameters defining engine performance is efficiency. As a matter of fact, road vehicle engines are in constant development to increase efficiency and decrease emissions of pollutants. In the branch of competition, emissions are often neglected but the efficiency is very important because most races set a maximum amount of fuel usage. The fuel consumption is often plotted (see Figure 20) with relation to a certain power output and angular velocity also know as brake-specific fuel consumption (BSFC). Using this type of information one can understand the efficiency of an IC engine under a particular load condition and predict its fuel consumption during a particular condition of operation.

$$BSFC = \frac{r}{P} \tag{12}$$

where:

- r= Fuel consumption rate (g/h);

- P= Engine Power (kW).

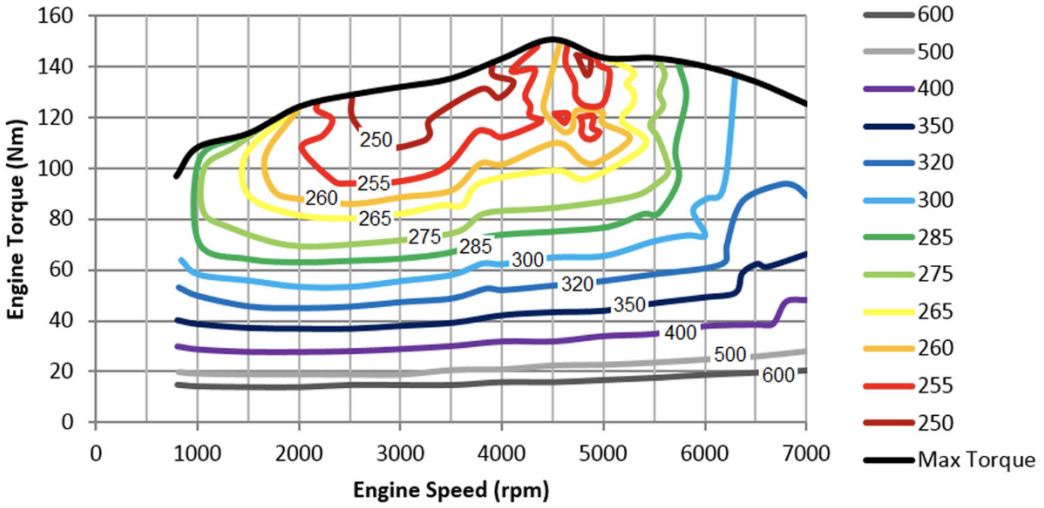

Figure 20: Break-specific fuel consumption results of a road vehicle (Oglieve et al., 2017).

4.3.3 *Brake System*

The brake system of a Formula Student vehicle has many similarities to other systems used in modern competition vehicles. As depicted in figure 21, it is composed of a pedal (mechanical leverage) that applies force to the master cylinder, which then generates pressure that is transmitted to the slave cylinder (brake calipers). Increasing the system pressure means more force generated at the calipers and consequently more force applied to the brake pads thus more braking force. The difference in pressure of the front and rear brakes (brake bias) can be regulated using a pressure regulator valve or with a mechanical system that applies different forces to the front and rear master cylinders, as commonly used in race cars.

The brake torque (Tb), applied to each wheel, can be calculated using the force transmitted by the brake calipers to the disc. The following simplified formulation (13) assumes that the pad contact area is equal to the piston area, and the coefficient of friction remains constant during braking. For wheel speeds different from zero, the coefficient of friction used should be kinetic.

$$Tb = Fb \cdot Rm \tag{13}$$

with:

$$Fb = Ap \cdot ph \cdot \mu p \cdot np \tag{14}$$

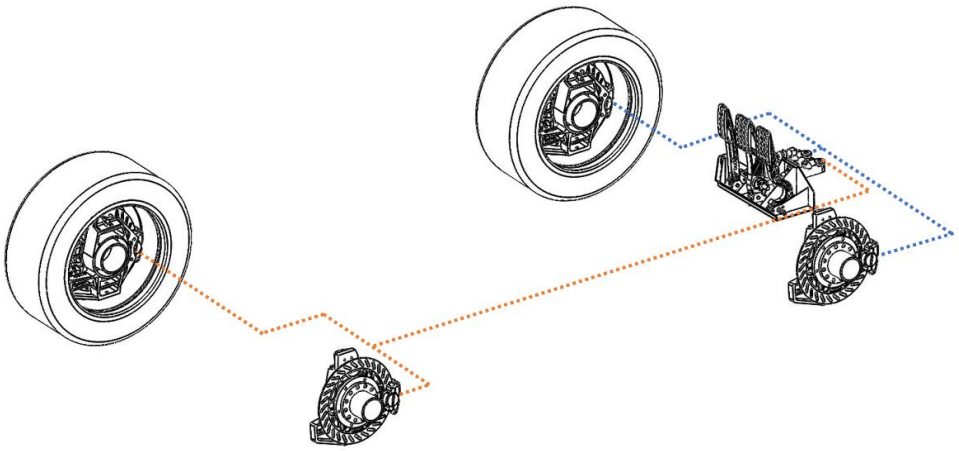

Figure 21: Formula T14 brake system.

where:

- F_b = Braking Force (N);
- R_m = Mean pad radius (m);
- A_p = Brake piston area (m^2);
- p_h = Hydraulic pressure (Pa);
- μ_p = Brake pad coeff. of friction;
- n_p = Number of friction pads.

4.3.4 *Aerodynamic Devices*

A moving vehicle is always in interaction with the surrounding environment. In this case, it results in air being displaced around the body of the car imposing aerodynamic forces illustrated in Figure 22. These forces fall into two basic sources:

- Pressure distribution: This is a force that acts perpendicular to the body surface because of the pressure created by the flow.
- Friction shear stress distribution: Occurs due to friction between the flow and the surface causing a force tangent to the surface.

The integrated distribution of pressure (ρ) and shear effects (τ) over the surface results in the total aerodynamic force which also creates a moment on the body. The resultant force can be simplified in two components: lift (force component perpendicular to the flow stream) and drag (force component parallel to stream velocity).

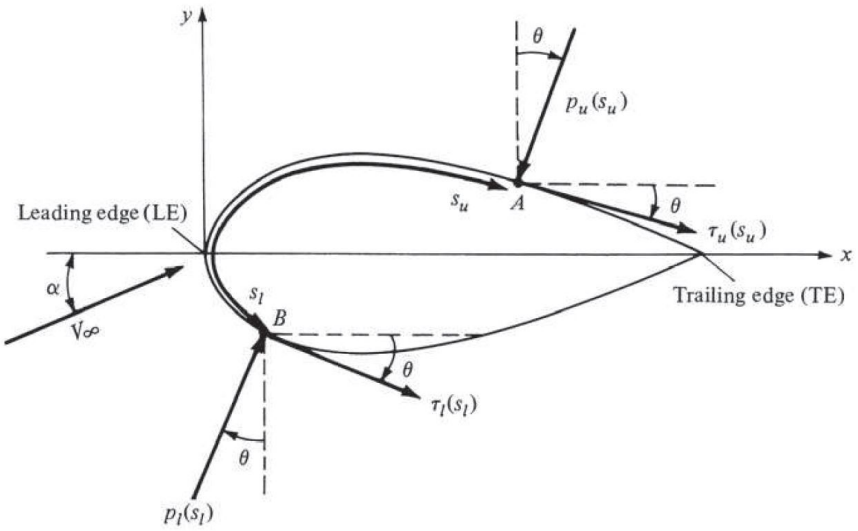

Figure 22: Integration of pressure and shear stress distributions over a 2D body surface (Anderson, 2017).

4.3.5 *Flow Types*

The viscous fluid flow is frequently classified into two main categories:

- Laminar flow: This type of flow occurs when the fluid moves smoothly and regularly along the streamlines. During this regime, it is possible to calculate the velocity and pressure fields by solving the Navier-Stokes equations.
- Turbulent flow: Occurs when a fluid flows in a chaotic path. The smooth streamlines are replaced by eddies and swirls produced by random fluid movement. In this case, numerical solutions can be introduced in an effort to define the disordered flow.

The following example of a fluid flow over a flat plane present in Figure 23, illustrates the flow behaviours listed above. The three regions (laminar, transition and turbulent), are usually defined in terms of Reynolds number (Re), expanded in subsection 4.3.5.2. The drawn flow velocity profiles define the boundary layer, on which the fluid velocity changes from zero at the surface of the plate to the free stream value at a given distance from the surface. This region is extremely important to aerodynamic problems such as wing stall, friction drag, high speed heat transfer and others (*NASA* 2021).

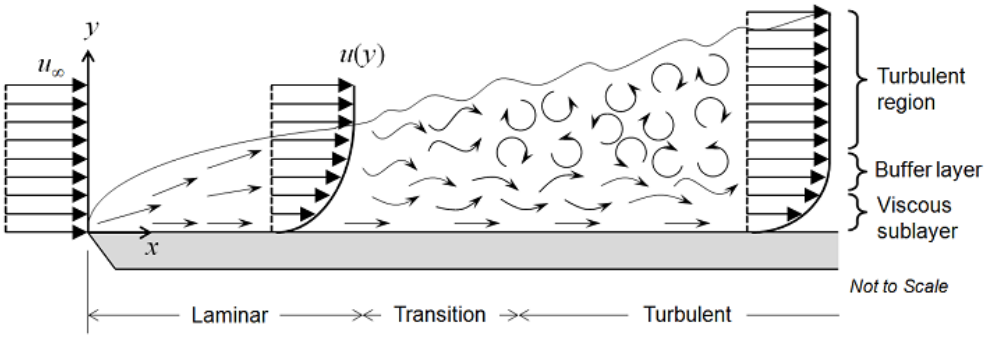

Figure 23: Fluid flow profile over a flat plate (*COMSOL* 2017).

4.3.5.1 *Generation of Drag and Lift*

The drag force as the name states is a force opposite to the movement of an object with respect to the fluid. Occurs in the presence of the high-pressure zone formation at the front and low-pressure zone at the rear of a given part of the vehicle, varying with geometry shape, area and inclination. It is also induced by viscous friction until the flow reaches a turbulent state. At this point, the flow separates from the surface leading to much higher values of pressure drag. The resultant of these forces oppose to forward (upstream) movement of the vehicle and it has a major impact on the acceleration of a vehicle, once the power needed to maintain speed, varies with the 3rd power of the speed. When the vehicle is braking, the drag force adds to the braking force promoting higher negative accelerations. The formula to calculate drag force reads:

$$Fd = \frac{1}{2} \cdot v^2 \cdot \rho \cdot Ap \cdot Cd \tag{15}$$

where:

- v = Speed of the flow (m/s);
- ρ = Air density (kg/m^3);
- Ap = Projected area (m^2);
- Cd = Drag coefficient.

The lift force is generated by the same principle of pressure difference. In this particular case, the formation of low pressure under zone and a high-pressure upper zone creates a negative lift force also called downforce. This force can be useful to apply load to the tyres, maximizing the overall force capacity of the tyre. Similar to the force imposed by drag the lift force reads:

$$Fl = \frac{1}{2} \cdot v^2 \cdot \rho \cdot Ap \cdot Cl \tag{16}$$

where:

- Cl = Lift coefficient.

Note: There are many incorrect theories about how an object generates lift. One can find many arguments with miss applications of Newton's and Bernoulli's equations. In fact, the lift is a very complex phenomenon because when working with a gas, one has to conserve the mass, momentum and energy in the flow. A more detailed explanation can be found using the Euler equations and Navier-Stokes (N-S) equations which incorporate the effects of flow viscosity.

4.3.5.2 *Reynolds Number*

The Reynolds number (Re) is the dimensionless quotient between the inertial forces and viscous forces of a given flow:

$$Re = \frac{V \cdot \rho \cdot L}{\mu} \tag{17}$$

where:

- V = Flow speed (m/s);
- ρ = Fluid density (kg/m^3);
- L = Characteristic length of the object (m);
- μ = Dynamic viscosity of the fluid ($Pa.s$).

This number is very important in fluid dynamics once it can be used to predict the flow transition from laminar to turbulent. Even more, the Re is used to predict the behaviour of a full-size model using measured data from wind-tunnel scaled analysis.

4.3.5.3 *Center of Pressure and Instability*

The centre of pressure (CP) is the location where the average pressure variation reacts. The location of the CP can be manipulated to reduce over-steer or under-steer increasing the rear or front downforce, respectively. This practice, also known as aerodynamic balance, is a quite common adjustable parameter in competition cars. Typically, the CP is located near the CG. When the track has low/mid-speed corners

the tendency is to shift the CP towards the rear to avoid over-steer, hence reducing lap time. At high-speed corners, the pressure bias is usually set to neutral or slightly forward to decrease under-steer.

4.3.5.4 *Formulations in Computational Fluid Dynamics*

The high complexity associated with flow behaviour during turbulent stages, implies the use of computational fluid dynamics (CFD) or experimental approaches. Nowadays, the use of software to study flow is quite common and models with higher complexity are being used more, because of the increase in computational power. Despite, CFD simulations are still very time consuming and for complex geometries such as formula student vehicles, some approaches are not feasible, even with high-end computers.

For the majority of problems regarding flow dynamics, there are three main numerical formulations used:

- Reynolds-Averaged Navier-Stokes models (RANS): The RANS model is currently the most common approach. It is based on the assumption that the problem can be solved using average quantities (time, space or ensemble averaging). This statistical application neglects small scale phenomena which represent lower demands on the numerical calculation and mesh requirements;
- Direct numerical simulation (DNS): This method requires a lot of computational power once the N-S equations are solved without any turbulence model and with very small time steps. According to (Molland and Turnock, 2007), DNS computations are limited to simple problems at low Re numbers;
- Large-eddy simulation (LES): The formulation is based on filtered N-S equations and is used to calculate large-scale eddies. It is seen as an intermediate approach between RANS and DNS, requiring less model effort because small-scales are more universal in nature (Franck, 2007). Nevertheless, it is still very demanding on computer resources when compared to RANS.

4.3.5.5 *Turbulence Models*

There are a substantial amount of employed models in engineering solutions. In summary, in the present work, the three models considered for CFD analysis were the following:

- $\kappa - \epsilon$: It is based on a two-equation model with two additional partial differential equations to define the properties of the flow. The first transport equation is the turbulent kinetic energy (κ), which determines the energy in the turbulence. The second called the turbulent dissipation (ϵ) predicts the scale of the turbulence. This model is quite popular due to its high convergence rate and low computational requirements. It performs well for external flow problems for example to solve the airflow around a bluff body (*COMSOL* 2017) such as an Ahmed body.
- $\kappa - \omega$: It works on the same principle of the model described above but instead of using turbulent dissipation, it uses the specific rate of dissipation (ω). It is used to study the flow inside a pipe with strong curvatures and separated flows.
- Shear stress transport (SST): This model combines the $\kappa - \epsilon$ and $\kappa - \omega$ turbulence model, taking advantage of turbulent dissipation for free stream flow and specific rate of dissipation for the inner region of the boundary layer. For this reason, this approach represents a large increase in computational effort but creates at the same time an opportunity for higher levels of accuracy.

4.3.5.6 *Numerical Wall Treatment*

One of the biggest challenges in CFD is how to treat the near-wall sublayer. In detail, the walls are the main source of turbulence so the overall results of a simulation are very dependent on near-wall defining parameters. The two most common approaches to solve this problem are low-Reynolds-number and wall function. The low-Re-number formulation integrates the near-wall region all the way down the wall, so there is no need to choose a wall distance. Nevertheless, the fully integrated solution comes with the price of requiring very fine meshes thus increasing substantially the computational resources (Frazza et al., n.d.). In alternative, the semi-empirical method of wall function applies the boundary conditions to merge the viscosity-affected region between the wall and the turbulent region. Besides, it requires defining the distance to the wall as an input which directly influences the final results. However, the demands of processing power are considerably low when compared to the low-Re-number technique.

4.3.6 *Inertia*

The resistance of a change in the velocity of rotating components has considerable relevance in the dynamic behaviour of vehicles. For example, the rotational inertia of the drive-train resists changes in the vehicle's speed (v), which is not good for the net acceleration of the powertrain parts and consequently negative to the overall acceleration of the vehicle. Despite the resistance, this phenomenon may be positive during gear shifts, once it maintains engine speed, avoiding significant speed drops and engine stall at low engine speeds/torque.

The effects of rotational inertia can be expressed using an equivalent non-rotating mass approach (Mason, 2020). Assuming there is no clutch and tyre slip, the motion ratio of a given rotation component (n) is directly proportional to the speed of the vehicle:

$$n = \frac{w}{v} = \frac{w_{tyre} \cdot i}{r_{tyre} \cdot w_{tyre}} = \frac{i}{r_{tyre}} \tag{18}$$

where:

- w = Angular velocity of a vehicle part (rad/s);
- i = Gear ratio;
- w_{tyre} = Angular velocity of the tyre (rad/s);
- r_{tyre} = Tyre radius (m).

The total kinetic energy stored in the object (E) is the sum of translational with rotational kinetic energy:

$$E = \frac{1}{2}(m \cdot v^2 + I \cdot w^2) \tag{19}$$

From (18) and (19) the formula for equivalent mass reads:

$$me = m + I \cdot n^2 \tag{20}$$

where:

- m = Vehicle mass (kg);
- I = Moment of inertia ($kg.m^2$);
- n = Motion ratio.

4.4 LATERAL DYNAMICS

4.4.1 *Forces Acting on the Vehicle*

Changes in a vehicle trajectory produce centripetal accelerations that point to the corner centre. The development of the cornering forces induces a moment around the roll centre causing the vehicle to roll and a moment around the centre of gravity lading the outside tyres. The use of inwards banked corners reduces substantially these problems once the generation of centripetal forces can be provided by tyre lateral and normal forces instead of just tyre lateral forces when the vehicle is driven on flat ground. This interaction is illustrated in the Figure 24.

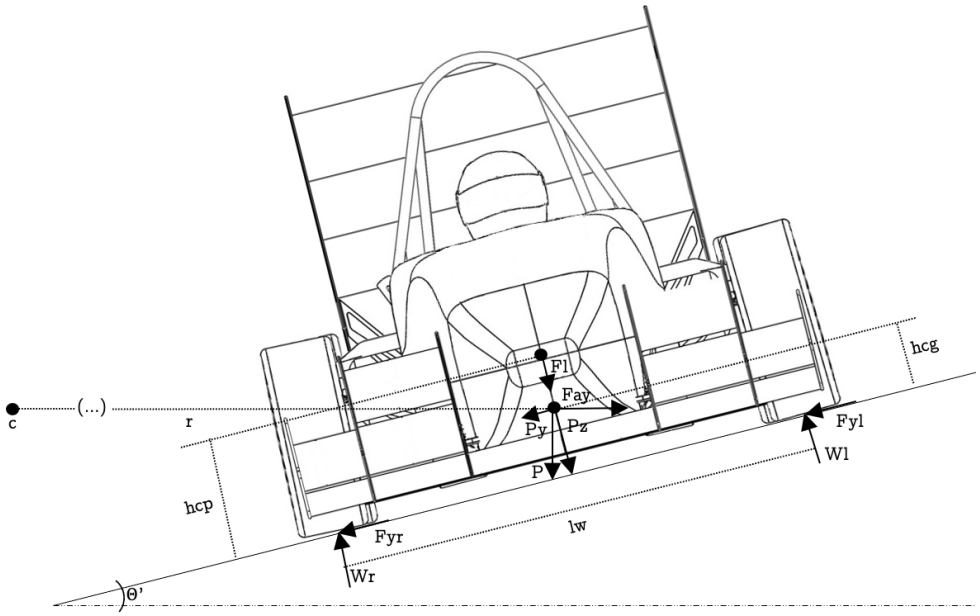

Figure 24: Lateral free body diagram with banked corner.

Following the section 4.3, one can predict quite easily the load transfer behaviour during a given manoeuvre. Considering equilibrium, the total force of the outside wheels (Wl) reads:

$$Wl = \frac{(Fl + P \cdot \cos(\theta') + Fa \cdot \sin(\theta')) \cdot \frac{lw}{2} + (Fa \cdot \cos(\theta') - P \cdot \sin(\theta')) \cdot hcg}{lw} \quad (21)$$

where:

- Fl = Lift Force (N);

- P = Vehicle weight (N);
- θ' = Corner inclination (deg);
- Fa = Cornering force (N);
- lw = Wheel track length (m);
- hcg = CG height (m).

4.4.2 *Low-speed cornering*

At low speeds longitudinal and lateral accelerations are negligible, so the tyres do not need to develop lateral forces, therefore slip angles are not present. Since the rear wheels don't acquire slip angles, the projection of the rear axle must pass through the turn centre. Under these conditions, the vehicle behaviour is predictable therefore a simple model for basic analysis may be used. The most common approach is the linear two-wheel vehicle model also called the single-track model or bicycle model where there is no body roll, lateral load transfer and other lateral effects as shown in Figure 25.

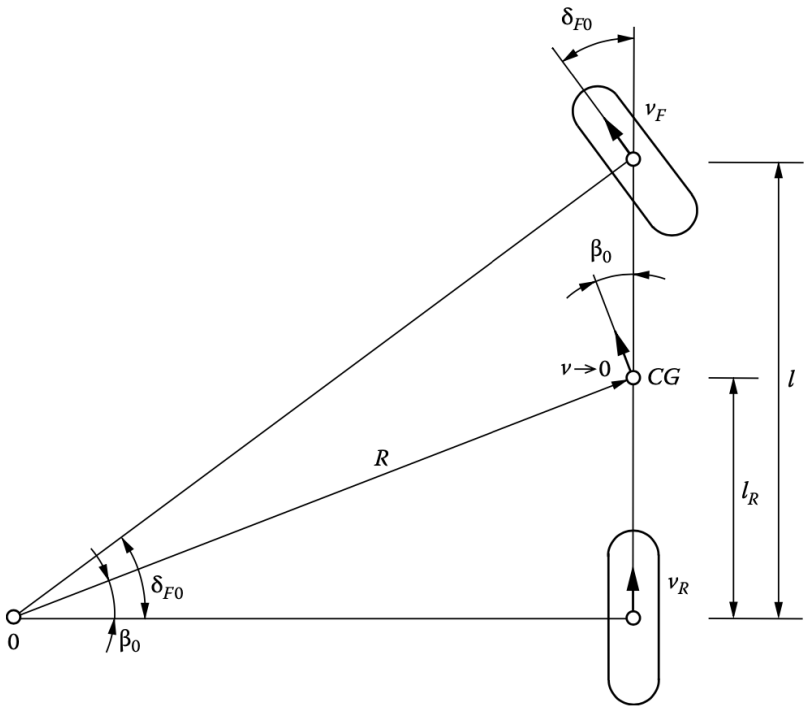

Figure 25: Bicycle model of a vehicle without lateral forces (Gianpiero Mastinu, 2014).

For this particular scenario, in the absence of tyre forces the steer angle can be calculated directly from the geometric approach yielding Ackerman steering angle δ_{ack}:

$$\delta_{ack} = \frac{l}{R} = \frac{l}{v_x^2} \cdot a_y \tag{22}$$

where:

- l = Wheel base lenght (m);
- R = Corner radius (m);
- v_x^2 = Longitudinal velocity (m/s);
- a_y = Lateral aceleration (m/s^2);

4.4.3 *High-speed Cornering*

At high speeds, the radius of turn is much larger than the wheelbase of the vehicle, as a result, small angles can be assumed and the difference between the steering angle on the inner and outward front wheels is negligible (Gillespie, 1992). In other words, the representation of the vehicle can still be defined using a single track bicycle model but the limitations regarding lateral dynamics would be more impactful in the results.

For smalls values of front and rear slip angles (α_f and α_r), the total steering angle (δ) for a right-hand turn is given by the following relationship:

$$\delta = \delta_{ack} + (\alpha_f - \alpha_r) \tag{23}$$

In steady-state cornering, the maneuver of the vehicle can be described using Newton´s second law applied to circular motion. The sum of front and rear tyre forces must equal the mass times the centripetal acceleration:

$$\sum f_y = f_{yf} + f_{yr} = m \cdot \frac{v^2}{R} = \frac{m \cdot l_r}{l} \cdot \frac{v^2}{R} + \frac{m \cdot l_f}{l} \cdot \frac{v^2}{R} \tag{24}$$

In the linear range cornering force is simply the relation between slip angle and cornering stiffness:

$$F_y = C_\alpha \cdot \alpha \tag{25}$$

From 24 and 25 the front steering angle is:

$$\alpha_f = \frac{\frac{m \cdot l_r}{l} \cdot \frac{v^2}{R}}{C_{\alpha f}} = \frac{W_f \cdot v^2}{C_{\alpha f} \cdot g \cdot R} \tag{26}$$

and

$$\alpha_r = \frac{W_r \cdot v^2}{C_{\alpha r} \cdot g \cdot R} \tag{27}$$

Now substituting the α_f and α_r from equations 26 and 27 back into equation 23 the total amount of steering angle yields:

$$\delta = \frac{l}{R} + (\frac{W_f}{C_{\alpha f}} - \frac{W_r}{C_{\alpha r}}) \cdot \frac{v^2}{g \cdot R} \tag{28}$$

4.4.4 *Stability Behaviour*

The equation (28) introduces one very important term in vehicle dynamics. The K gradient also known as understeer gradient $(\frac{W_f}{C_{\alpha f}} - \frac{W_r}{C_{\alpha r}})$ dictates the additional angle required per increase of lateral force, that is, to manoeuvre the vehicle on a constant radius high-speed corner. This vehicle handling response is often classified into three possible outcomes:

- neutral steer $((\frac{W_f}{C_{\alpha f}} = \frac{W_r}{C_{\alpha r}}))$: This scenario occurs when the lateral force at the CG increases proportionally the front and rear slip angles. Thus on a constant radius turn the steering angle remains the same as the speed increases $(K = 0)$ and is equivalent to the Ackerman angle $(\frac{l}{r})$.
- understeer $((\frac{W_f}{C_{\alpha f}} > \frac{W_r}{C_{\alpha r}}))$: In this situation the front tyres do not develop enough lateral force to maintain the constant radius corner at a given speed. Therefore, the only way of keeping the required trajectory is by rising the steering angle $(K > 0)$.
- oversteer$((\frac{W_f}{C_{\alpha f}} < \frac{W_r}{C_{\alpha r}}))$: Conversely, when the vehicle oversteers the lateral force leads to an increase slip angle at the rear tyres resulting in an outwards movement of the rear pushing the front inwards thus decreasing the corner radius. Consequently, to maintain the constant radius the steering angle must be decreased $(K < 0)$.

It is important to reference that when a vehicle is understeering at its limits it cannot develop more cornering force but is dynamically stable. When the steering angle required doubles the amount of the Ackerman angle, the characteristic speed is reached. Inversely, when the manoeuvre leads to the limit of oversteer the vehicle is no longer stable once it is very likely to spin out if there is no applied counter steer. The point where this occurs is pointed in Figure 26 as critical speed.

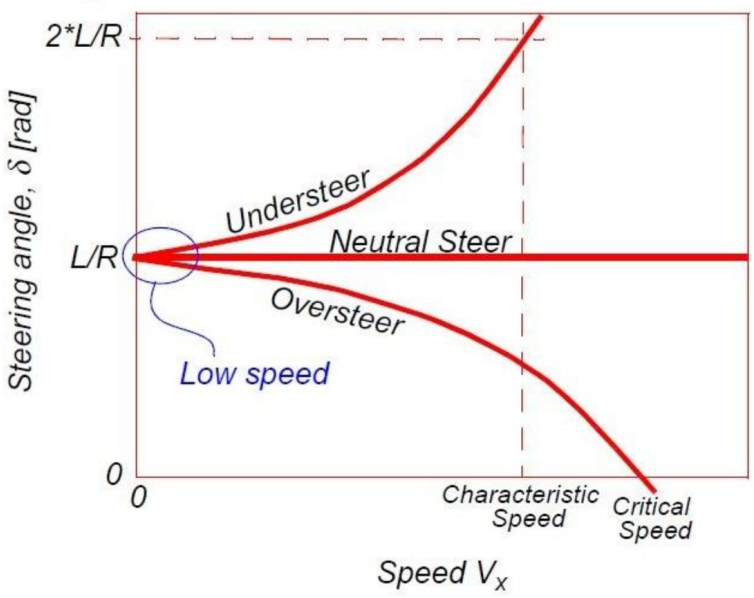

Figure 26: Change of steer angle with the speed (*Cornering of Vehicle* 2015).

4.5 SUMMARY

The tyre modelling represents a huge stepping stone in lap time simulators but comes with the cost of very complex mathematical formulations. Nevertheless, semi-empirical models such as 'Tyre Magic Formula' with slip angle and slip ratio inputs, provide great information about the behaviour of the tyres.

In general, the longitudinal performance of the vehicle can be developed using straightforward calculations and the transient properties of the engine can be simplified using WOT operation conditions. Despite this, the aerodynamic behaviour of the vehicle using N-S equation is up to this date mathematically unsolvable so a numerical method must be used to obtain CL and CD. In that matter, the CFD formulation of RANS with SST turbulence model provide a good relation between computational cost/results.

The lateral behaviour of the vehicle can be simplified using a single-track bicycle model where body roll, lateral load transfer and suspension effects are not taken into account. Concerning lateral load application, the vehicle often exhibits understeer or oversteer. The first is a stable condition where steer angles must increase to withstand the increasing lateral force. The second is defined by excessive slip angles at the rear so the front steer angle must be lowered to maintain trajectory and lead the car out of an unstable manoeuvre.

5

MODELLING AND SIMULATION

5.1 INTRODUCTION

The following chapter provides an overview of the two vehicle dynamics models used. All systems of the single point mass lap time simulation were modelled using a MATLAB based graphic programming environment, Simulink. The program offers a repertoire of vehicle dynamics with some predefined documented block sets. Despite that, all block sets used to perform the simulations were built from scratch to avoid possible black boxes and to make the blocks totally customizable. The simulator is composed of two Simulink environments that share the same MATLAB script where input variables are defined. The first program file (processor) creates two-speed profiles, one with the vehicle moving in a normal track direction and the other with the vehicle taking a reverse path. The two profiles are then merged in the second program (post-processor) to create a global speed profile with the effects of cornering and longitudinal accelerations.

The commercial software (IPG Automotive Carmaker), uses a graphical user interface were the vehicle and track parameters are defined. This QSS with some transient features offers a wide range of options to model the different vehicle systems. It also has post-processing capabilities with data plotting and 3d simulation.

5.2 SIMULINK MODEL

This approach to compute elapsed lap time assumes the vehicle as a point of moving mass through each point of a previously defined track. Each track point (step) has the same length and it is defined with three variables: elapsed distance from starting line, corner radius and track inclination.

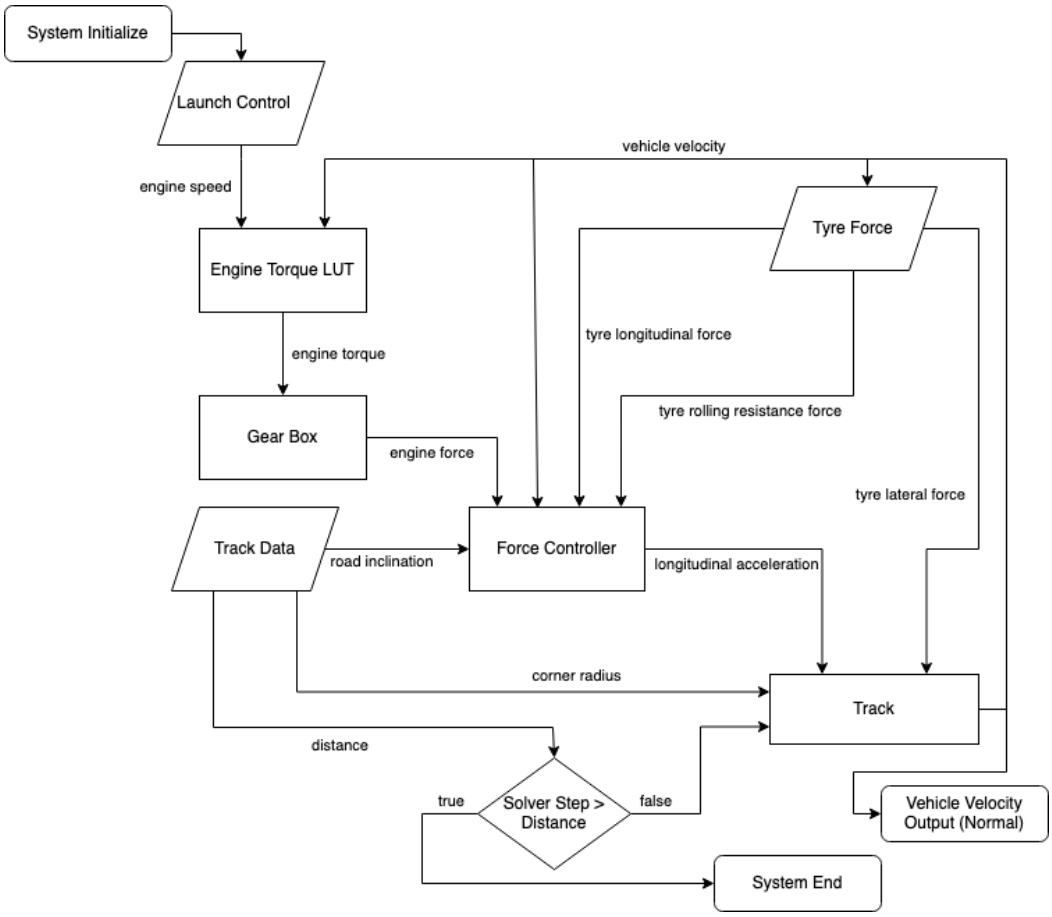

Figure 27: Flowchart of the processor model (normal path).

5.2.1 *Base Algorithm Description*

The algorithm used in this particular approach is as purported in Chapter 3 thus utilizes normal track direction to output the positive acceleration speed profile and reverse direction to calculate negative accelerations.

Initially, it starts with a preset launch control engine speed that is used to calculate the longitudinal force produced by the drive-train as illustrated in Figure 27. After that, the engine force enters the 'force controller' where it is compared to the longitudinal tyre force potential and the lowest value is chosen. Furthermore, the negative forces such as aerodynamic drag and rolling resistance add to road inclination which is then subtracted resulting in the available net force, needed to output longitudinal acceleration of that particular step. At the 'track' block-set the longitudinal acceleration is converted to velocity during zero corner radius input. When the corner radius is different from zero, the output velocity is overwritten by a function of lateral tyre force and corner radius.

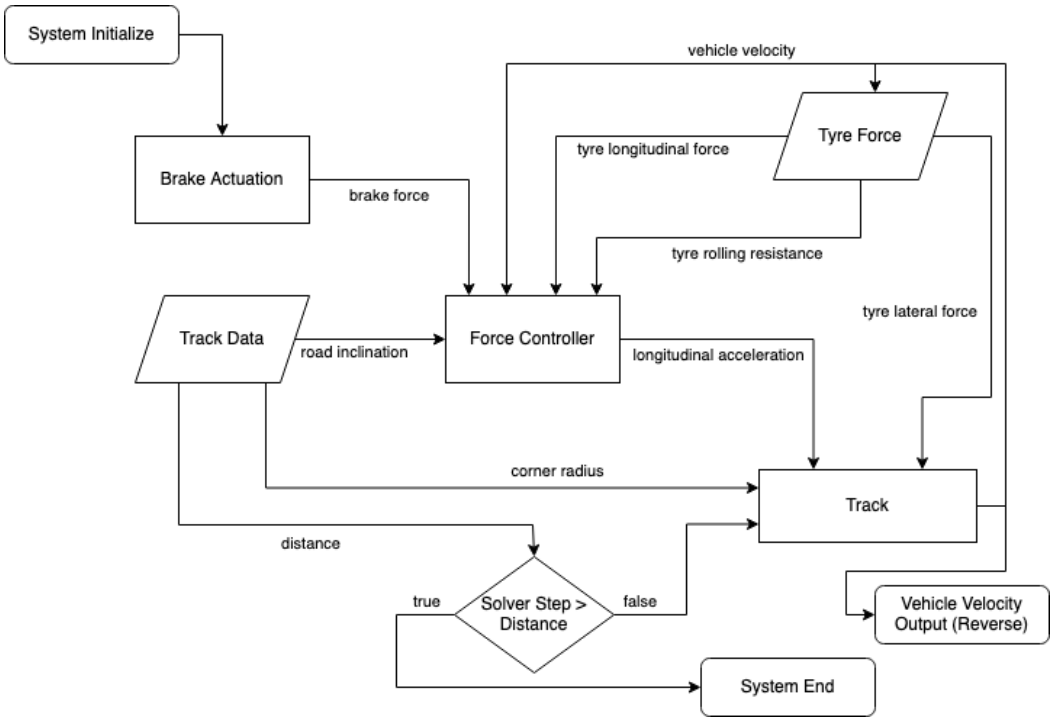

Figure 28: Flowchart of the processor model (reverse path).

The same logic applies to calculate the speed in the reverse direction as shown in Figure 28. The main difference is that the engine force is replaced by a braking force, to calculate the braking points. It also compares it with the total longitudinal tyre force, but instead of creating a traction control, the block-set creates an anti-lock brake system. The speed output, in this case, represents the braking phase, so the contribution of the aerodynamic drag and rolling resistance is always positive (generates more negative acceleration).

Subsequently, the forward and the flipped rearward velocity profiles are merged in the post-processor (Figure 29) with 'select minimum value' criteria. This creates a fully defined speed profile with optimum acceleration/ braking points and constant corner velocity. As a result of the velocity profile, the post-processor calculates step time and elapsed time. Furthermore, it outputs longitudinal accelerations based on step time and steep speed, and lateral accelerations with corner radius and corner velocity. In this stage, the powertrain data system is used to output a complete profile of engine performance information such as fuel consumption, available torque output, engine speed and gear position. It also utilizes the aerodynamic data to output the drag and lift profiles. Finally, based on the speed profile and tyre data it generates the total tyre forces in each step.

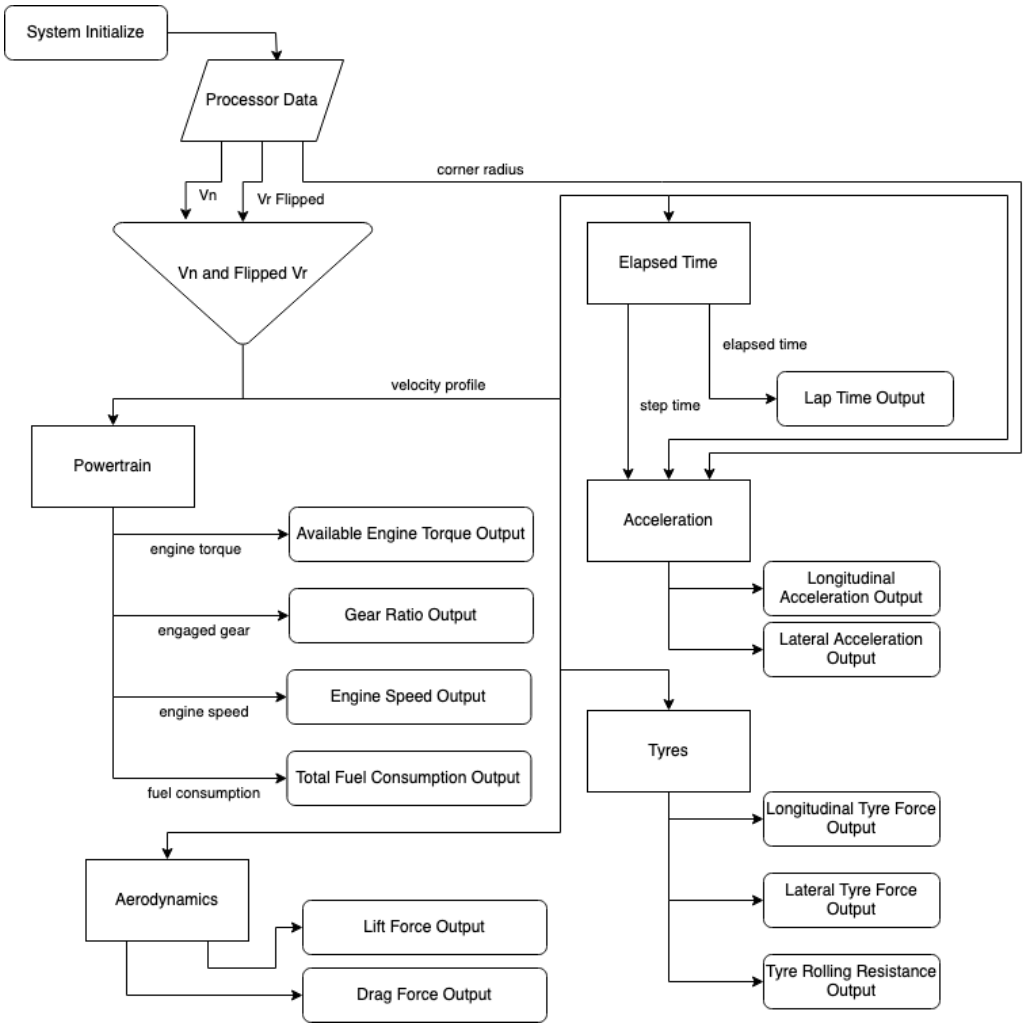

Figure 29: Flowchart of the post-processor model.

5.2.2 *Processor Block-set Overview*

5.2.2.1 *Powertrain System*

The propulsion of the vehicle was modelled accordingly to measured data from a car dynamometer and thermodynamic engine simulations. Specifically, the main powertrain system (see Figure 30), works by reading a lookup table (LUT) to compute the engine torque available at a specific engine speed. This engine speed is calculated using a vehicle speed to engine speed converter that assumes no clutch slip. The torque curve present in the LUT was defined using the data from a dyno run, depicted in Figure 31. This approach focused only on wide-open throttle conditions, so partial engine loads were neglected.

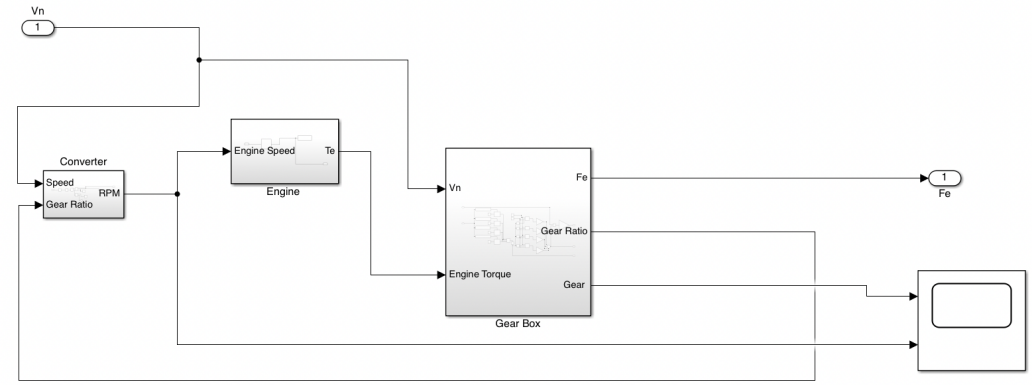

Figure 30: Powertrain system.

The gearbox algorithm works simply by comparing the speed with the previously defined threshold of shift engine speeds (up and downshifting rpm targets). After calculating the gear position, the engine torque is converted into wheel torque and subsequently into an equivalent propelling force (Fe) as shown in Figure 32 .

The main powertrain system does not include fuel usage, nevertheless, a subsystem to predict fuel mass consumption was modelled in the post-processor file, according to sub-section 5.2.3.

5.2.2.2 *Braking System*

The system where brakes were modelled is very straightforward. It is based on the principle evidenced in sub-section 4.3.3 with only six variables needed to output braking force (Fb), as described in Figure 33.

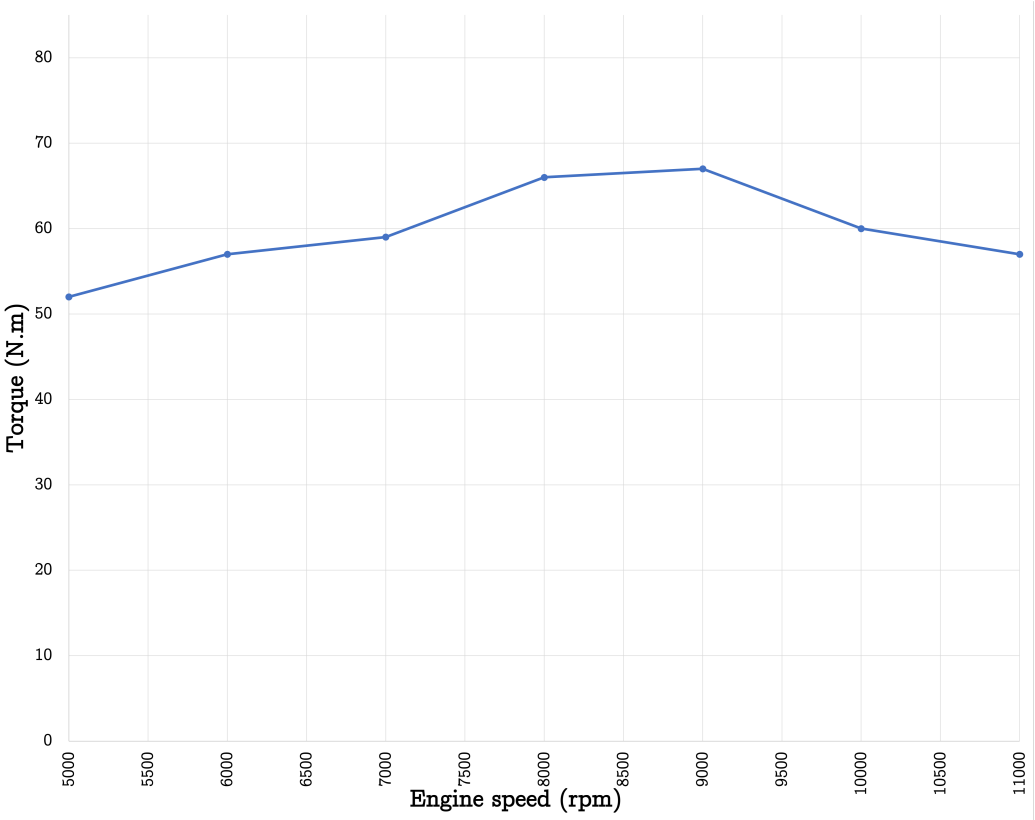

Figure 31: Engine torque results at WOT condition.

5.2.2.3 *External Force System*

The external force system, represented in Figure 34 combines the tyre rolling resistance force with track inclination force and aerodynamic drag force to predict the net force that opposes the movement of the vehicle. The block-set calculates weight force influence using the inclination angle of each step and the vehicle's mass input. It also calculates lift resultant force, which in this case always points to the ground. This force is combined with the weight of the vehicle to calculate tyre longitudinal and lateral capacity (see sub-section 5.2.2.4).

It is noteworthy to mention that when the vehicle is accelerating with the engine the net force can be positive, null or negative. The drag and rolling resistance are always negative but track inclination can be either, thus the sum may be positive. However, the output is called Fn (negative force), because the simulator uses another external force system to calculate the reverse speed, which sets drag and rolling resistance as always positive because the vehicle is accelerating with the brakes. Because of that, the output of the other system is called Fp (positive force) according to Figure 35.

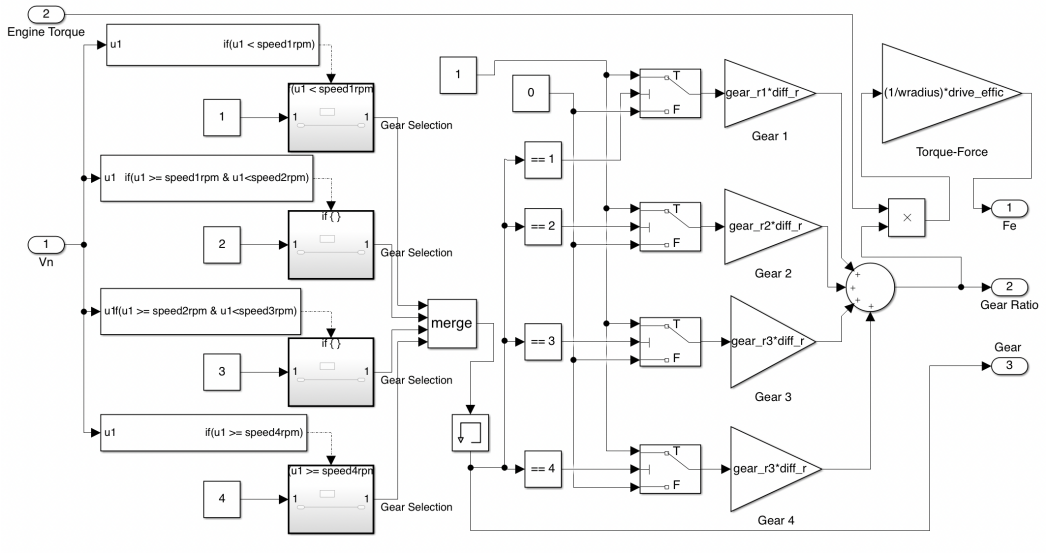

Figure 32: Gearbox subsystem.

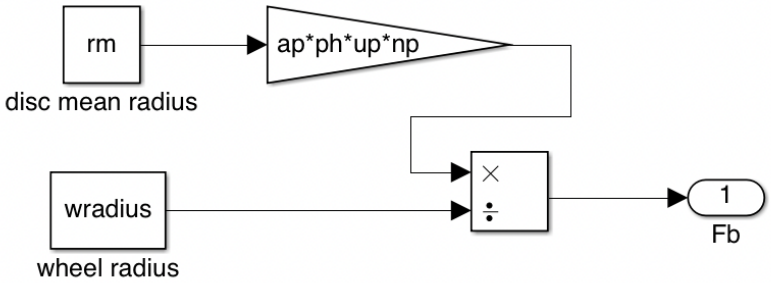

Figure 33: Braking system.

The aerodynamic sub-system works by resolving drag and lift force as a function of the formulation present in sub-section 4.3.4. The forces change with air velocity, in this case, represented only by the motion of the vehicle, so to compute the lift and drag it utilizes a look-up table that outputs CD and CL according to the step speed.

Once the information regarding the aerodynamic properties of the vehicle in study was not detailed and fully available, an CFD analysis of the formula t14 at different speeds was conducted to obtain the required aerodynamic properties of the vehicle in the lap time simulator. The study was performed using a commercially available solution, in particular, ANSYS ICEM to generate the mesh and ANSYS CFX for processing and running the simulations. The general properties of the study represented in Table 1 were defined based on the information provided in Chapter 4 and similar work regarding the development of the new formula student

vehicle (Miguel Ribeiro, 2021), where a detailed study about mesh dependency of a formula vehicle CFD analysis was conducted. In particular, the definition of element size for different aerodynamic devices (wings, fairings, side pods and others) and the characterization of the control volume, i.e., the dimensions and settings of the simulation volume were based on the work mentioned above.

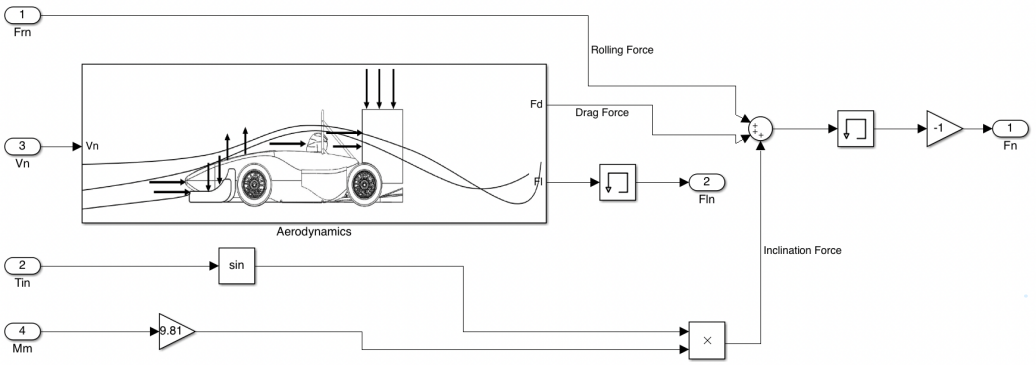

Figure 34: External force subsystem for normal path.

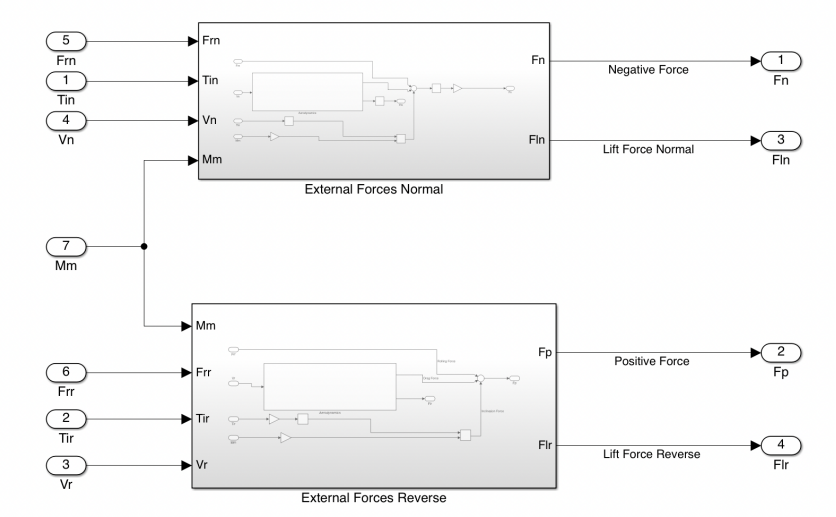

Figure 35: External force system for normal and reverse path.

As expected, the flow inside the control volume of the simulation follows the tendency of turbulent behaviour before the rear of the vehicle generating additional pressure drag as illustrated in Figure 36. Despite the increasing drag forces, the outputs of the aerodynamic analysis present in Table 2 indicate that the aerodynamic devices generate a considerable amount of negative lift at relatively low speeds. This normal force of lift will load the tyres promoting the generation of higher tyre lateral and longitudinal forces, pointing to the need to consider the effects of lift in the lap time simulator.

Parameter	Value
Fluid Temperature	Air @ 25^{o}C
Fluid Density	1.162 kg/m^3
Molar Mass	28.96 g/mol
Dynamic Viscosity	1.86E-05 Pa.s
Numeric Approach	RANS
Turbulence Model	SST
Maximum Iterations	100
Residual Target	5E-05

Table 1: General properties of the CFD analysis.

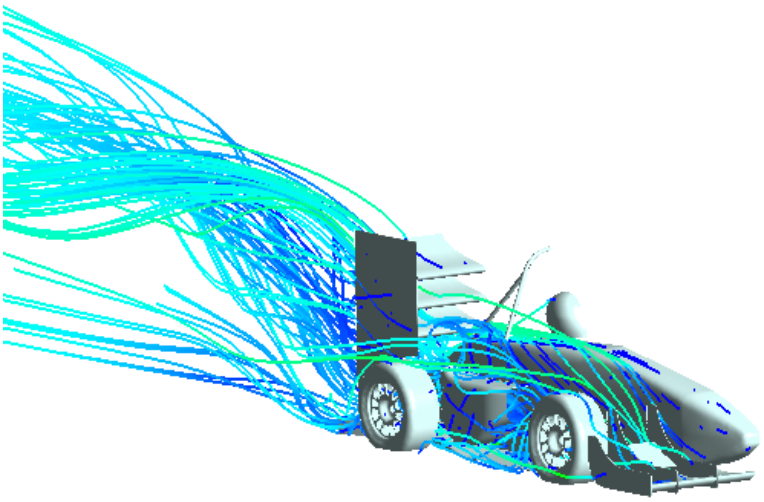

Figure 36: Results of flow stream line at 120km/h.

5.2.2.4 *Tyre System*

The single mass point simulator uses a straightforward steady state tyre model where tyre force is estimated by means of vehicle weight and tyre lateral/longitudinal coefficient of friction. The rolling resistance of the tyre used in the block-set was formulated using the equation defined in sub-section 4.2.1. It also receives inputs from a very simplified pilot system where users can characterize the efficiency of the pilot while braking, cornering or accelerating forward. The pilot efficiency enters as a reducing factor, altering lateral and longitudinal tyre coefficients, as depicted in Figure 37. The simulator utilizes another similar tyre system for reverse path calculations. This allows to have different longitudinal coefficients of friction and pilot behaviours when the vehicle is accelerating with the engine or brakes.

Speed (Km/h)	Cd	Cl	Fd (N)	Fl (N)
20	0.74437794	1.1370514	16.098	24.59
40	0.7580651	1.5701621	65.576	135.826
60	0.75893853	1.51535952	147.716	294.942
80	0.76107072	1.51776595	263.344	525.174
100	0.75984073	1.53799265	410.81	831.52
120	0.75926478	1.55720965	591.118	1212.35

Table 2: Results of drag and lift obtained via CFD simulations.

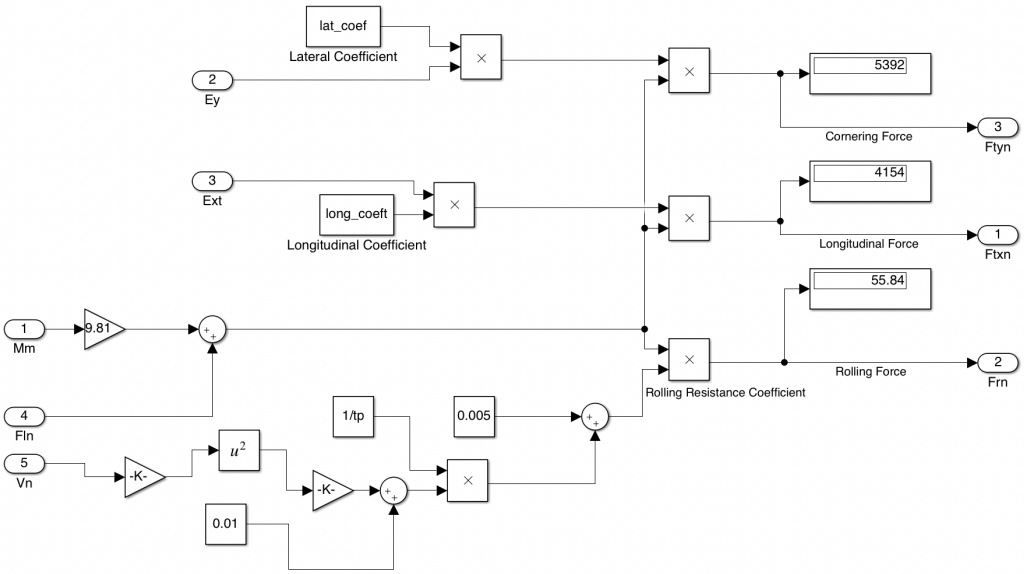

Figure 37: Tyre force system.

5.2.2.5 *Inertia System*

The last vehicle system of the simulator is the block-set where the effects of rotational inertia are linked to acceleration. This is done by converting the rotational inertia of certain components in mass according to the method described in subsection 4.3.6. The output mass is then added to the vehicle mass to compute throttle and brake accelerations. Since the rotational inertia is related to angular velocity and some vehicle components are moving at different speeds, the block-set accounts for that phenomenon with the input of different motion ratios relative to wheel movement, as illustrated in Figure 38.

Note: Once the powertrain system is equipped with a gearbox, the engine flywheel has variable motion ratios but to reduce complexity the motion ratio was set to be constant, using the second gear ratio. Engine internals such as camshafts, crankshaft and others were not taken into account.

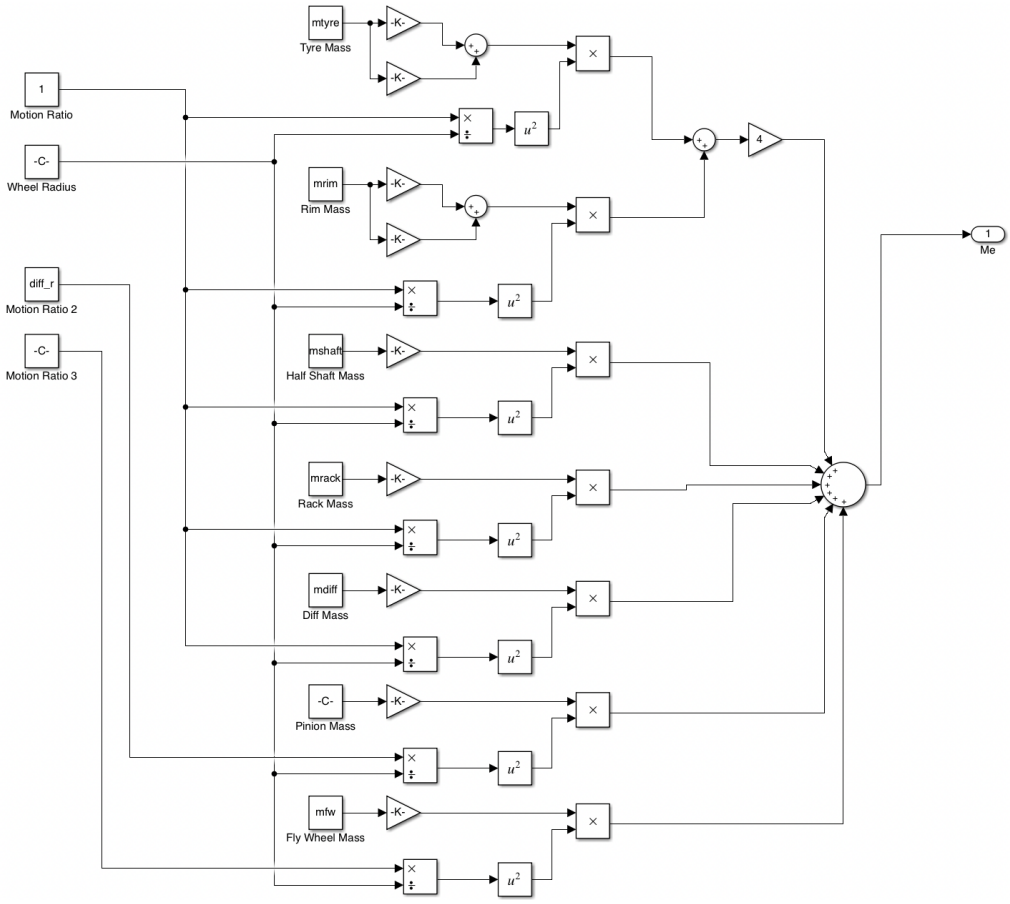

Figure 38: Inertia system.

5.2.2.6 *Force controller System*

The force control system, as the name suggests, was modelled to manage the two acceleration forces available, Fe and Fn for a normal path or Fb and Fp for a reverse trajectory. It compares the step engine force with tyre longitudinal capability when a normal path is implied. This enables the system to have traction control, once the engine force is limited to wheel force, in particular, engine force is only used to accelerate the vehicle when it is lower than tyre force. The propellant force is then added to the external force output and divided by total mass (vehicle mass + inertia equivalent mass) which results in the step acceleration output portrayed in Figure 39 .

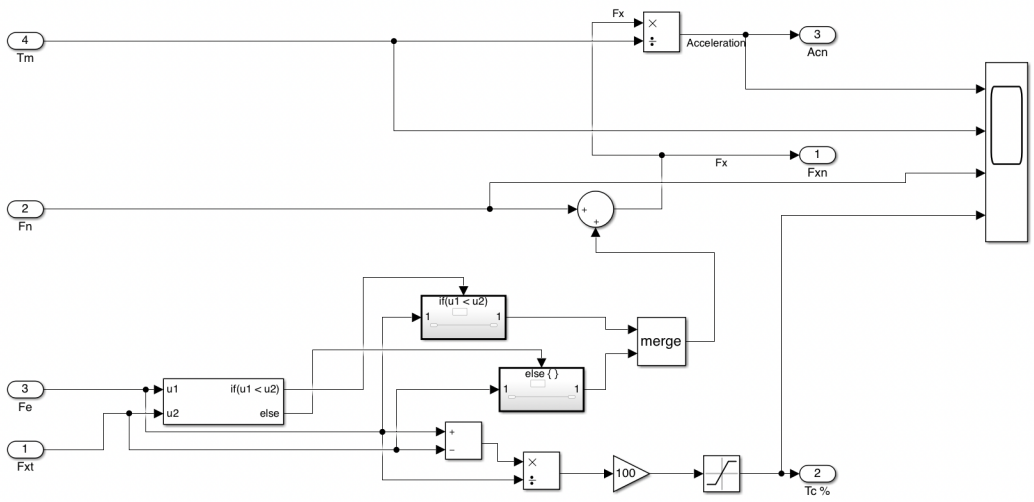

Figure 39: Force controller system for normal trajectory.

5.2.2.7 *Track System*

The last block of the lap time processor is the track system visible in Figure 40. It reads user input arrays for distance, corner radius and track inclination. The system works by merging the two possible motion scenarios, i.e., straight and cornering phases. It computes straight velocity using the previously calculated acceleration in the force controller system and cornering critical speed from moving mass and tyre lateral force. After merging the two-speed conditions it outputs vehicle velocity which is used as a next step input in the powertrain and external force systems. The processor saves the normal and reverse velocity profiles, that will be used afterwards in the post-processor for computing elapsed time, fuel consumption and other performance outputs.

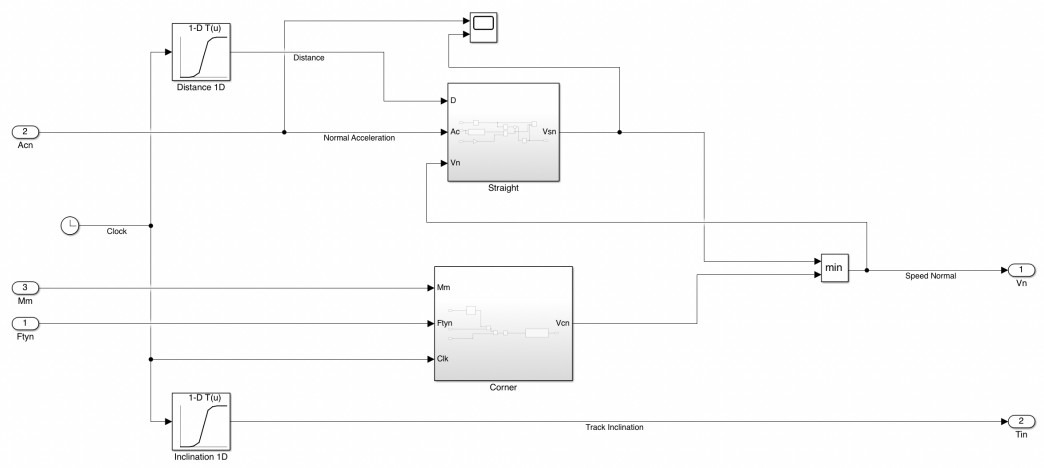

Figure 40: Track system for normal trajectory.

5.2.3 *Post-Processor Block-set Overview*

5.2.3.1 *Powertrain System*

Besides common information about engine performance such as engine torque output, operation speed and others, the post-processor also predicts the total fuel consumption. For that purpose, the model contains a subsystem with engine BSFC data, which is linked to engine power to output the elapsed fuel usage in mass, according to Figure 41. In addition, the program only adds fuel consumption when the car is accelerating or maintaining the speed with the engine and to minimize the previous WOT simplification it uses traction control as an input. This allows to reduce fuel consumption, once, in real life, the pilot modulates the throttle to avoid traction losses. It is important to note that BSFC does not decrease with lower engine loads. In fact, it usually increases with the reduction of engine load, but since the engine power output is smaller the overall fuel consumption decreases.

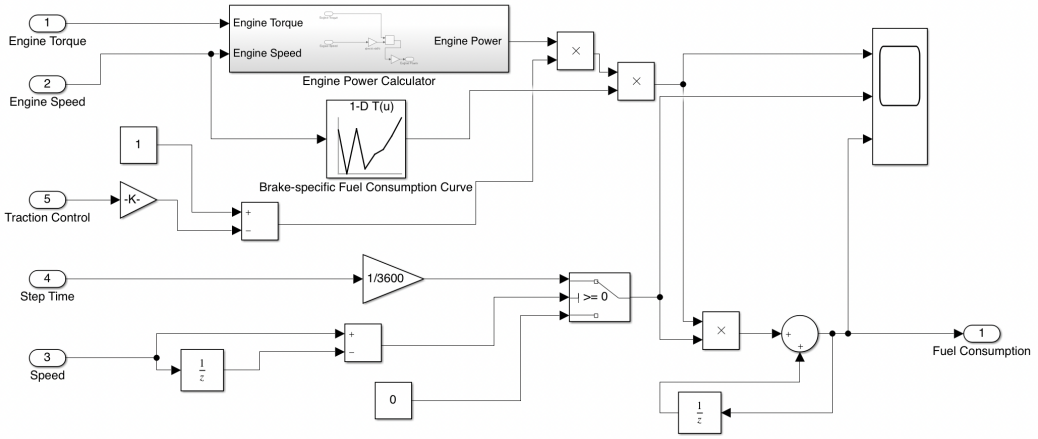

Figure 41: Fuel consumption subsystem.

The difficulty to obtain real data about the fuel consumption of the engine in study during various conditions of operation, imposed a different approach to define BSFC. For that matter, a commercial software of thermodynamics simulation called Lotus Engine Simulation (LES) was used to predict the required inputs. It works by defining the geometric parameters of the engine like intake runner lengths, exhaust geometry, valve timing diagram and displacement, along with others variables. After specifying the thermodynamic parameters such as gas properties, combustion model and other engine control variables (see Table 3), one can obtain an abroad range of engine performance outputs. The model represented in Figure 42 used in this work was developed and validated in a previous undergraduate project regarding the development of a variable-length intake system (Henrique Amaral, 2018).

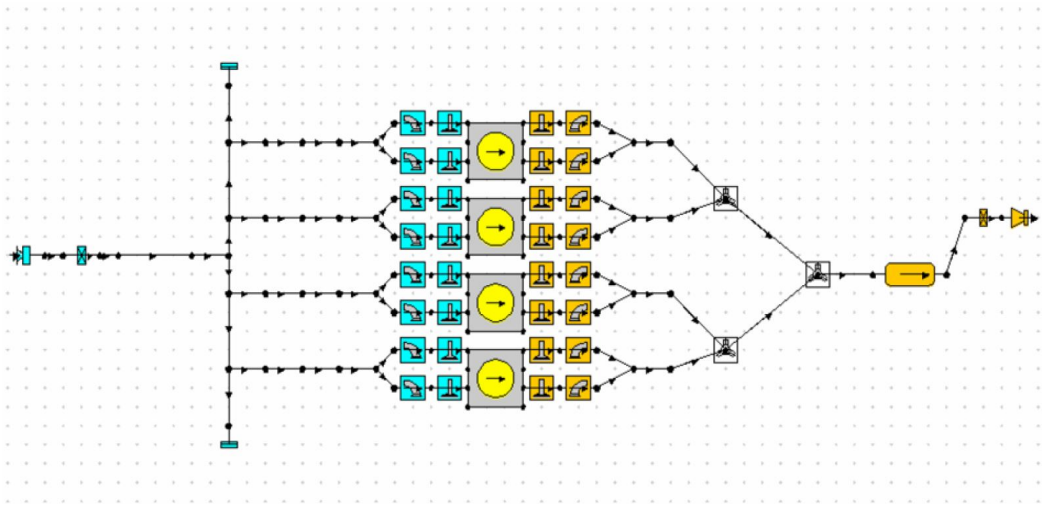

Figure 42: LES model of the engine used in the t14 formula (Henrique Amaral, 2018).

Parameter	Value
Air Temperature	20^{o}C
Absolute Air Pressure	1 Bar
Combustion Efficiency	0.97
Air/Fuel Ratio	14.6
Combustion Model	Single Wiebe
Heat Transfer Model	Annand
Friction Model	Honda

Table 3: General properties of the thermodynamic analysis.

Engine Velocity (rpm)	BSFC (g/kW. h)
4000	305.4
5000	287.8
6000	306.1
7000	289.9
8000	295.6
9000	297.7
10000	303.2
11000	310.5

Table 4: Brake-specific fuel consumption simulation results.

5.2.3.2 *Elapsed Time System*

The lap time calculator system, present in Figure 43, receives the velocity of each step and mesh size, in other words, user-defined track distance between points. It can compute step time with a simple division of distance per velocity and predict total lap time by the sum of the time needed to go through each step.

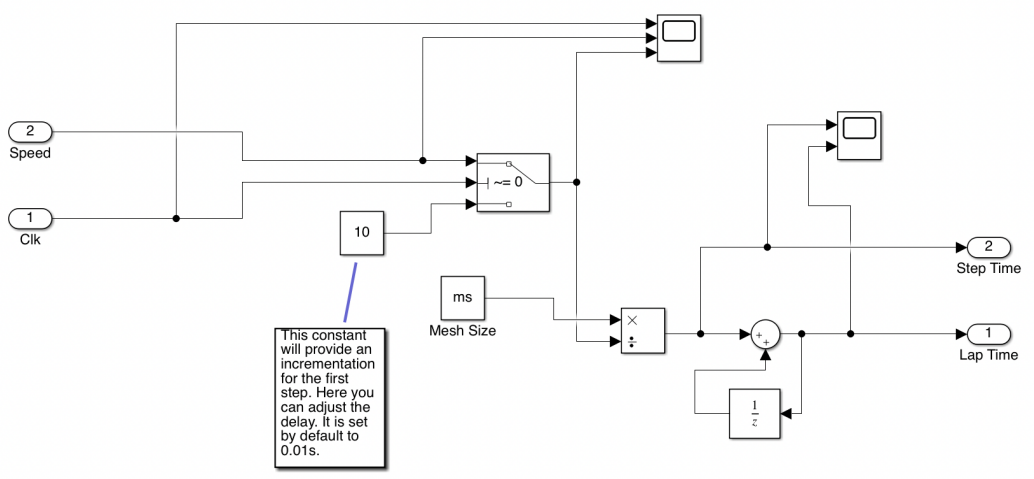

Figure 43: Elapsed time subsystem.

5.3 CARMAKER MODEL

Carmaker offers a vast range of models to define the vehicle systems. This commercial approach is used beyond motorsports with proven industry solutions in autonomous driving and advanced driver assistance systems (Automotive, 2021a). Due to the nature of the software, the algorithm is not fully available so this section was based on the generic information provided by the software documentation (Automotive, 2021b).

5.3.1 *Vehicle Body*

The vehicle body is a multibody system that uses the D'Alembert's principle of motion with the forces and induced moments applied to the main body and to each of the four wheels. The vehicle model algorithm starts by calculating the steering rack position, which is needed to calculate the tyre slip ratio/ slip angle. Before computing the forces and torques, such as, aerodynamic, suspension and tyre forces,

the simulation predicts the kinematic and elastokinematic behaviour of the system. After that, comes the kinetic part where the general forces and respective inertias and loads are evaluated. One interesting feature of the software is the characterization of a flexible vehicle model. With this option, one can define the vehicle using two body parts, i.e., the rear and the front of the vehicle are connected by a rotational joint with spring-damper mechanism. This allows to predict for example the effects of chassis's torsional rigidity.

5.3.2 *Suspension and Steering*

According to the software information, the suspension element is composed of five types of interactions:

- suspension spring;
- parasitic effects (bushing preloads and internal friction);
- suspension damper;
- suspension buffer (bump stops);
- anti roll bar;

It offers the possibility of selecting a fourlink suspension kinematic model up to 38 DOF with optional compliance effects.

5.3.3 *Powertrain*

Despite the software allowing complex models, the powertrain system was kept simple with a model very similar to the Simulink algorithm. It utilizes a engine model with a torque look-up table to predict the engine performance under a certain engine speed/load. The approach to calculate the fuel consumption is also similar, once it calculates the volume of fuel based on a user defined brake-specific fuel map. Because the algorithm utilizes the engine load, the WOT operation condition is replaced by a partial load condition therefore one can define multiple fuel consumption maps to produce more reliable outputs.

The gearbox model works similar to the simulink model. The program simply controls the engaged gear ratio according to a preset maximum and minimum range of engine speed. At the same time it calculates the drivetrain losses based on user defined torque loss gear maps and other parameters. This does not happen in the

Simulink model, once it only has one variable for torque loss to define the entire drivetrain.

5.3.4 *Brakes*

The brake definition is also comparable to the Simulink simulator. The major difference is the introduction of build-up time. Instead of having a on/off brake force it defines a target time (time delay) for the braking force to reach 75% of the desired brake force.

5.3.5 *Tyres*

The tyre model is one of the most important thing regarding the simulation. The built lap time simulator had the most simple tyre model possible so the other systems were always affected by that. In contrast, the Carmaker algorithm uses a well defined model based on the popular tyre magic formula (see section 4.2.7). This allows to consider the effects of slip angle, slip ratio and combined slip on the tyre force generation. It is also possible to extend others parameters such as rolling resistance and tyre inflation pressure. Furthermore, the software has some tyre transient properties because it incorporates first-order lags for longitudinal and lateral deformations. To create the simulation environment the tyre properties of a formula student vehicle were previously defined.

5.3.6 *Aerodynamics*

Likewise the calculation method previously describe in section 4.3.5.1, the Carmaker simulator works by applying drag and lift force to the vehicle body but at the same time introduces a side force based on the angle of attack of wind. Despite, due to the lack of data regarding side force, the coefficient of lift and drag was set to be constant for different attack angles.

5.3.7 *Main Vehicle Parameters*

The model characterisation was influenced by two main factors: data consistency concerning the Simulink approach and new data inputs resulting from the advanced methods mentioned above. More precisely, whenever the two approaches were similar the input variables were kept the same in comparison with the two software, for example, the engine performance and gearbox characterization. At the same time, the complex models required the definition of more data, based on known parameters and formula student resources provided by the software company. Table 5 summarizes the models and approaches used to define the vehicle data-set in Carmaker.

Parameter	**Model Type**	**Approach**
Vehicle Body	Flexible	Defined Body Split
Suspension (Spring)	Hookean	Linear Stiffness
Suspension (Damper)	Newtonian	1D LUT
Suspension (Kinematics)	Kinematics & Compliance	FS Resource Database
Steering	Static Steer Ratio	Defined Value
Powertrain (Engine)	Conventional	1D LUT
Powertrain (Fuel Consumption)	Specific	2D LUT
Powertrain (Gearbox)	Characteristic Value	Defined Gear Ratio
Brakes	Hydraulic	FS Resource Database
Tyre	Magic Formula	FS Resource Database
Aerodynamics	Conventional	1D LUT

Table 5: CarMaker modelling approaches.

5.3.8 *Summary*

The Simulink algorithm provides a simple approach to lap time simulation, i.e., the vehicle body was condensed into a single point of mass. This steady-state approach neglects the effects of load transfer, suspension and individual tyre behaviour. The inputs used were obtained by experimental and numerical procedures. For example, the engine torque was acquired via power dyno run, while the brake specific fuel consumption was calculated from a thermodynamic simulation. The aerodynamic forces were also the result of a numerical CFD simulation.

The commercially available solution requires not only the same inputs but also more advanced specifications and geometrical inputs regarding the vehicle body (four-track model). Additionally, It needs comprehensive tyre data to calculate the tyre forces based on slip angle and slip ratio (magic formula).

6

SIMULATION VALIDATION

6.1 INTRODUCTION

This chapter describes the approach taken to validate the results obtained via computational simulation. It provides a brief description of the sensors and control modules used to obtain dynamic data of the vehicle. The overall track where the dynamics tests occur is also detailed in this section.

6.2 VEHICLE INSTRUMENTATION

The formula vehicle (t14) used in the tests was previously equipped with sensors and control modules by team members. Not only this can be used to measure certain individual parameters to validate different components and control systems, but also to record the behaviour of the vehicle, if the data is stored on a time or vehicle position data set. In other to achieve that, the signals from the sensors mentioned in Figure 44 are first processed in individual control units or shared control units and then sent to a data logger unit (DLU) via controller area network (CAN).

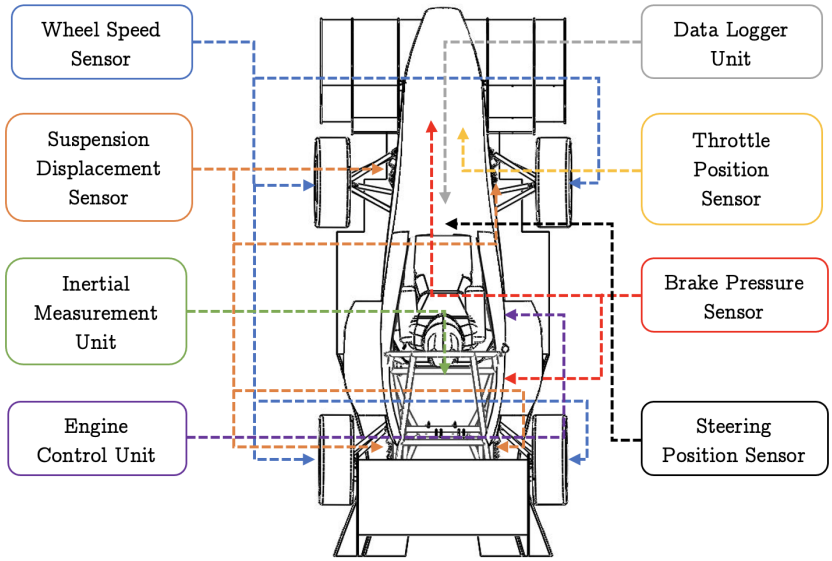

Figure 44: Test vehicle measurement apparatus - sensors and electronic units diagram.

The sensors used during the dynamic study are the following:

- Wheel Speed Sensor (WSS):

Four Hall effect sensors (see Figure 45), located at each wheel hub were responsible for measuring the angular speed of the wheel.

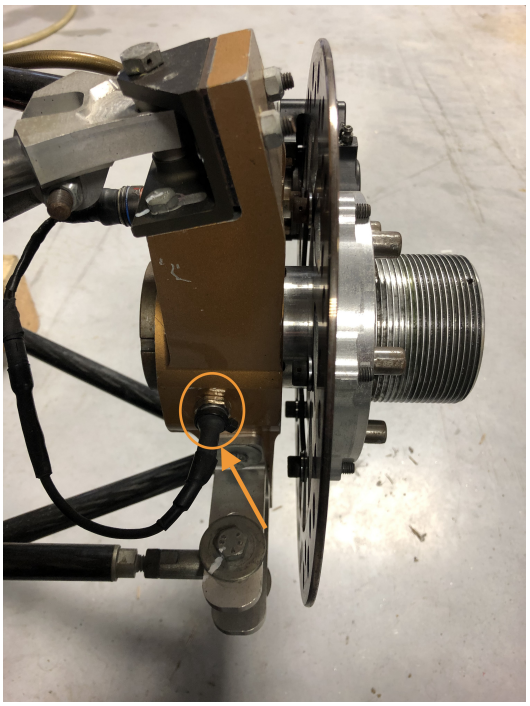

Figure 45: Wheel upright and hub assembly with integrated angular velocity sensor.

- Suspension Displacement Sensor (SDS):

One linear potentiometer at each shock absorber was used to capture the suspension movement as depicted in Figure 46.

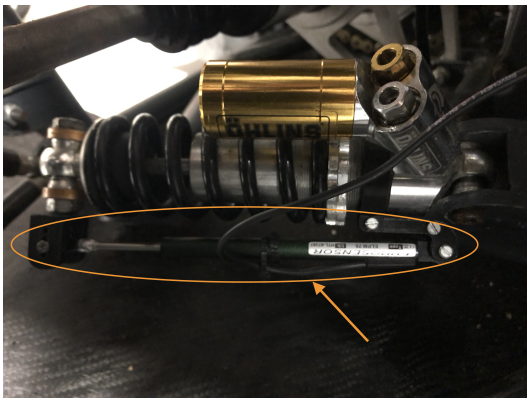

Figure 46: Suspension displacement measurement approach.

- Steering Angle Sensor (SAS):

A multi turn potentiometer connected to the steering column was used to measure the angle of the steering wheel, according to Figure 47 .

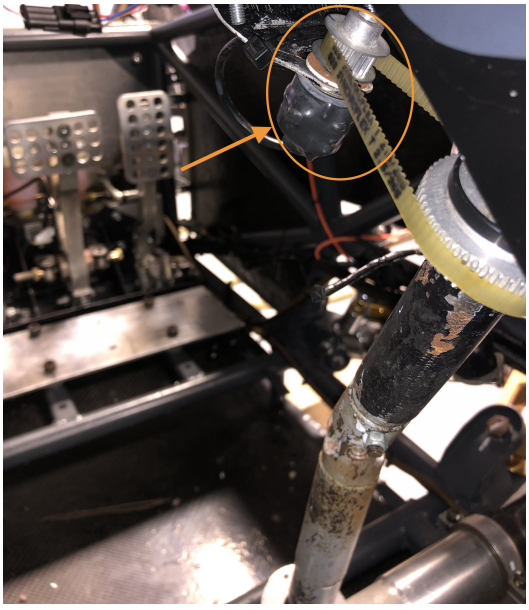

Figure 47: Steering angle measurement system.

- Inertial Measurement Unit (IMU):

The IMU (Figure 48) measures the three angular motions of the vehicle (yaw, pitch and roll) and the acceleration on the three axis of motion.

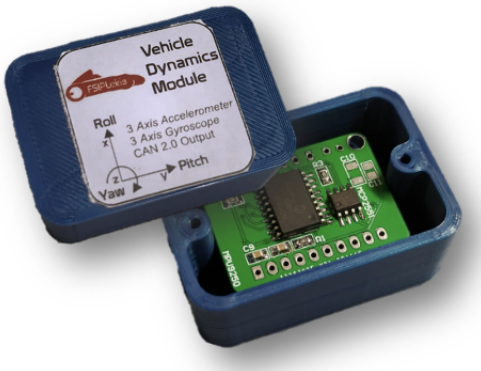

Figure 48: FSIPleiria IMU

- Brake Pressure Sensor (BPS):

The pressure of the brake system is measured using the piezoresistive effect. There were two sensors installed in the vehicle. One at the front (depicted in Figure 49) and the other at the rear, used to measure the effective pressure and difference pressure between front and rear, in other words, brake bias.

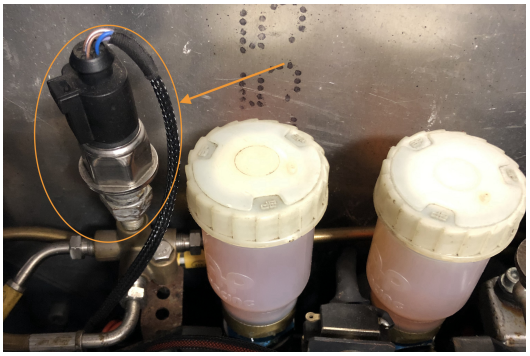

Figure 49: Brake pressure sensor - front brake hydraulic line.

- Throttle Position Sensor (TPS):

The TPS used is found in many vehicle commercial applications. It is an angular Hall effect sensor directly connected to the throttle pedal as shown in Figure 50:

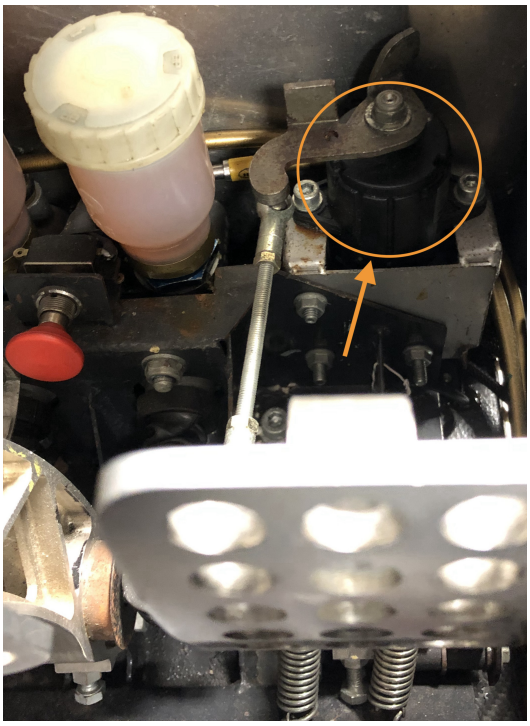

Figure 50: Throttle position sensor implemented.

- Engine control unit (ECU):

The ECU used was a Motec-M400 (see Figure 51). It controls the entire engine with inputs from TPS, WSS, BPS and other installed sensors not mentioned. In this particular application, it was also used to receive the signals from sensors without individual processor units (TPS and BPS) and send the information to the CAN bus.

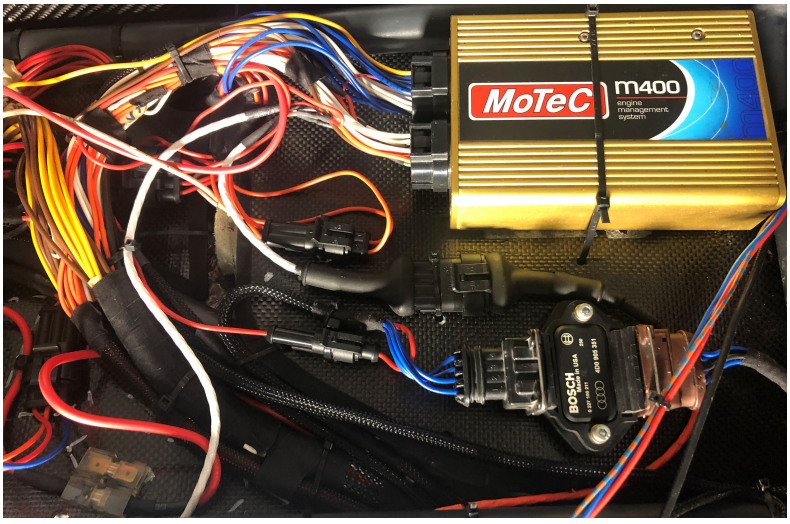

Figure 51: Motec-M400 engine control unit applied.

- Data logger unit (DLU):

The DLU, illustrated in Figure 52, receives all information via CAN bus and stores it on a data set where each array is registered with a time index created at the beginning of the record. The frequency of the recording process during the test was set to 200HZ but the individual modules send the variables at different rates as shown in the Table 6. It is noted that this speed of acquisition is enough for most applications but may induce substantial errors when the main focus of the analysis is the suspension behaviour due to high-frequency suspension movements.

Figure 52: FSIPleiria Data Logger.

Logged Variable	Acquisition Speed (Hz)	Unit type
Wheel Speed	100	km/h
Suspension Displacement	200	mm
Steering Angle	100	deg
Acceleration (XYZ)	50	m/s^2
Brake Pressure	100	bar
Throttle Position	100	%
Engine Speed	100	rpm
Gear Position	100	1

Table 6: Specifications of the acquired variables.

Despite the instrumentation apparatus disregard some data such as GPS and tyre temperature, the information provided by the available sensors was enough to have solid data on the dynamic behaviour of the formula vehicle, during the test run.

6.3 EXPERIMENTAL PROCEDURE

6.3.1 *Circuit Representation*

Two main factors were taken into account when the test track was created. The first one was the available area of the school parking lot. There were a lot of debris areas with sand and dust so the track was constructed to avoid those areas. The other factor was the rule book of the competitions where the minimum corner radius and track are defined. Due to the first design constraint, the minimum corner radius was lower than what is expected in the competitions.

The anti-clockwise circuit starts with a straight, followed by the first corner which is a hairpin type corner with a variable radius. After, comes another straight that ends on a large radius corner combined with a small straight that is used to brake into the last hairpin turn (constant radius). The track ends with a small corner exit straight as delineated in Figure 53. It is important to note that, although the track was swept, the racing line was affected by pavement debris. The trajectory drawn in orange was the approach of the pilots. This trajectory was then used in the simulation tool to define the vehicle path.

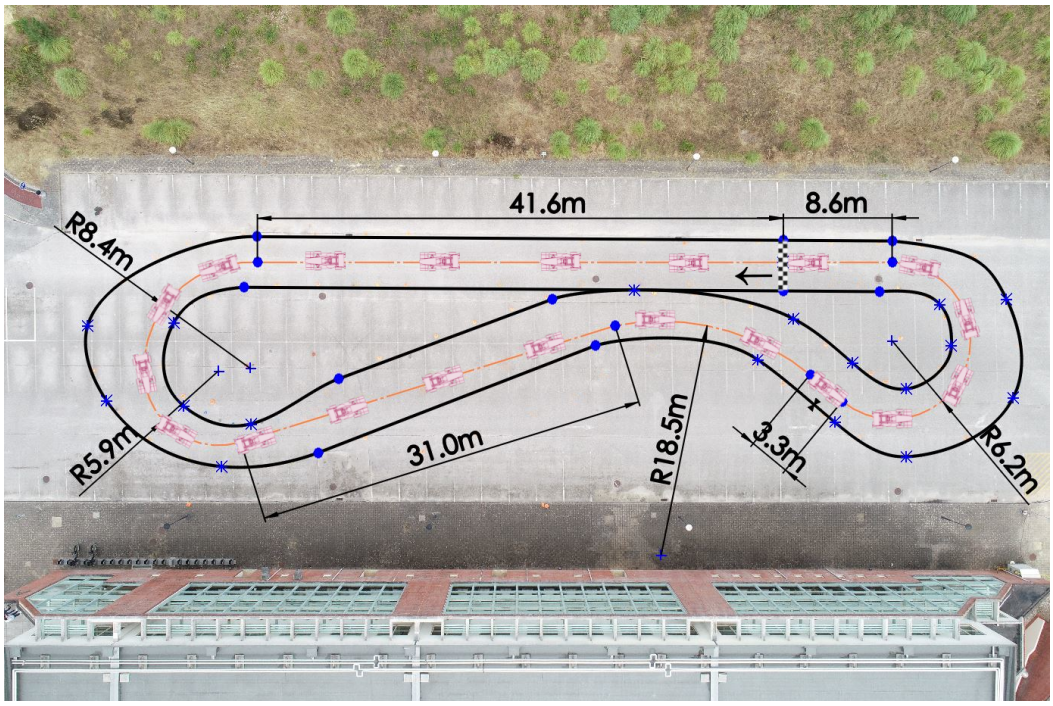

Figure 53: Aerial view of the circuit.

6.4 TESTING STRATEGY

The test runs (see Figure 54), were performed by two amateur pilots with backgrounds in drift and kart racing. After some warm-up laps, the pilots were instructed to start a recording run of two laps. A standing start condition, in other words, a stationary car start at the beginning of the first lap was used. Subsequently, the best results of each pilot were used to validate the lap time simulator in chapter 7.

Figure 54: Vehicle during the test run (pilot 1).

6.4.1 *Summary*

The formula student vehicle was tested in a controlled environment circuit to validate the outputs generated by the two simulations. To obtain the data from the various sensors, a student made data logger capable of recording at 200Hz was used. This device worked by receiving the data from analog inputs and CAN bus. The data was then converted and saved on an SD card generating a txt file with an array of data as a function of recorded time.

7

RESULT ANALYSIS

7.1 INTRODUCTION

This chapter provides a critical analysis of the theoretical data obtained via lap time simulation tools and experimental data acquired by real testing. It is divided into two main sections: Simulink Model and Commercial Software (IPG Carmaker) where a full track described in the section 6.4 was modelled to predict the manoeuvre behaviour of the formula student vehicle. It provides comparison of isolated parameters such as speed, profile, lap time, longitudinal/ lateral accelerations, powertrain and aerodynamic performance.

7.2 SIMULINK MODEL

The model was validated according to the experimental data, so the two pilot profiles were simulated in an effort to evaluate the performance of the LTS during the two different test runs. It is important to note that only the speed and lap times were the object of comparison, i.e., due to similarities between theoretical and experimental data provided by the two runs, the other outputs (accelerations, powertrain performance and aerodynamics) were only analysed and compared to data provided by the first pilot run.

7.2.1 *Speed and Lap Time*

The speed results of the simulation and the actual logged data from pilot 1 (blue line) and pilot 2 (orange line) are plotted in Figure 55. At the beginning (distance fewer than 10 meters), the transient conditions, imposed by all powertrain systems and driven tyres, are very difficult to predict. To avoid that, the simulation forces the initial speed to be constant at the first step and after that, the vehicle accelerates according to the available tyre and engine forces. This allows to have quite accurate results during the first stages of acceleration as illustrated in Figure 55. After

that, some discrepancies in speed are noted, with the sim data reaching higher values when compared to logged data. This occurs mainly because the simulator continues to ideally accelerate the vehicle, neglecting for example the torque cut-offs during shift changes, uneven wheel torque distributions due to the limited-slip differential, tyre slip after gear exchange among others. Nevertheless, during braking, the tendency is very similar with negative acceleration slopes of the same magnitude. The behaviour of the vehicle during the corner stage is by far more complex to calculate then straight line acceleration. The mathematical simplification of the simulator induced considerable errors regarding the transition between longitudinal and lateral accelerations, once in real life, the forces acting on the vehicle are not exclusively in the X-X or Y-Y direction. Even though the corner entry and exit stages were not fully equated, the apex speeds, in other words, the minimum speed point at the corner, is similar with percentage differences between 3% and 6% for corner 1 and 3, respectively.

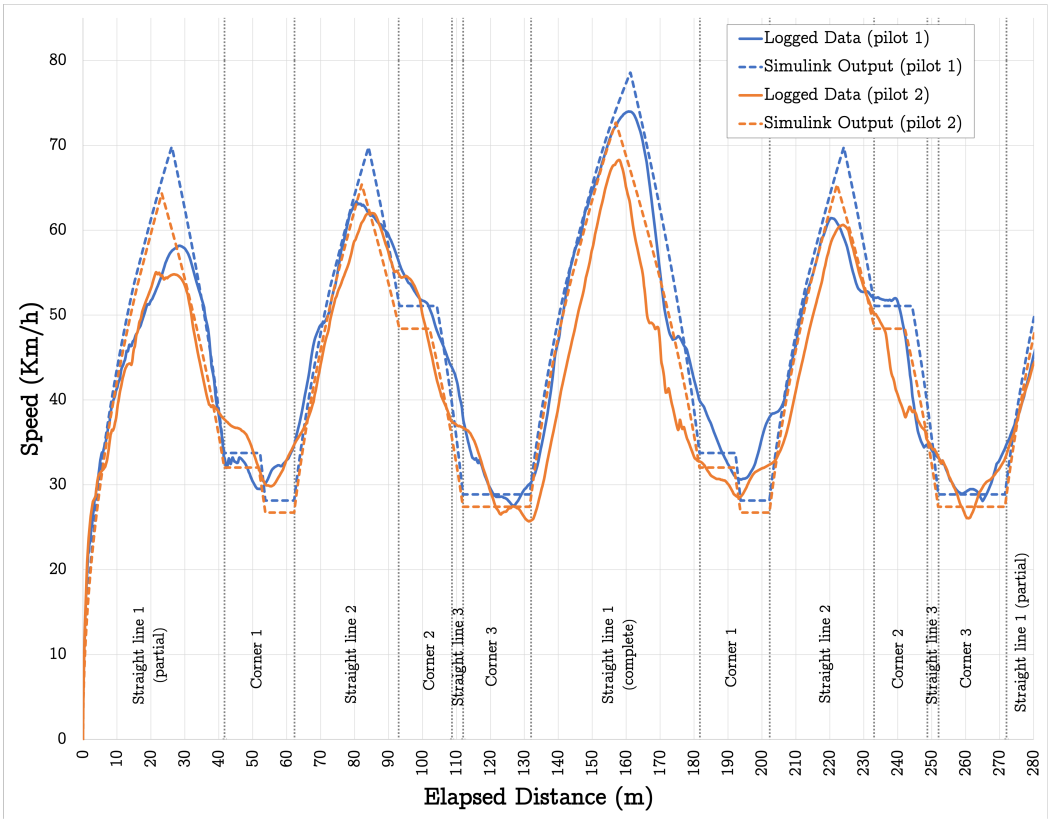

Figure 55: Simulink simulation and real speed results for pilot 1 and pilot 2.

The disparities concerning the simulated and logged speed profiles had quite an impact on the elapsed time. The high values of maximum straight-line speed adding to constant velocity corner manoeuvres induce substantial lap time errors, with a

percentage difference rounding 16% when compared to the actual time, as indicated in Table 7. Regardless, in this particular case, the overall difference is not very important because it can be reduced quite easily by changing for example the tyre's longitudinal and lateral force. The most important factor is the simulator's potential to predict changes following a certain data tendency. For example, the time between the two pilots represented a percentage difference of 5% and the simulator predicted a difference of about 6% between the two runs.

	Real Time (s)	**Simulation Time (s)**	**Difference %**
Pilot 1	29.81	24.66	-17.28
Pilot 2	31.37	26.19	-16.51
Difference	-5.23	-6.20	

Table 7: Simulink model elapsed time results.

7.2.2 *Longitudinal and Lateral Accelerations*

In a real scenario, the vehicle is always subjected to forces in both directions of movement so purely cornering or straight-line acceleration is not possible. Once the simulator works by forcing the vehicle to accelerate strictly in the X or Y direction, the output results will display zero value longitudinal acceleration when cornering and likewise show no lateral acceleration when throttle or braking forces are present. Nonetheless, the acceleration results displayed similar profiles, with both X and Y acceleration peaks reaching the maximum values of the logged data (filtered).

7.2.2.1 *Acceleration X-X*

The results of longitudinal accelerations are quite important because they allow one to understand key points on the vehicle brake and throttle performance:

- Engine Acceleration: During the first stages (elapsed distance«1m) the simulator imposed a user-defined launching engine speed creating the acceleration peak seen in Figure 56. After that, represented by the positive values of acceleration, the engine acceleration appeared where expected with the simulated acceleration peaks staying for longer distances but falling sharply to zero which does not appear in the real data profile. The most interesting phenomenon regarding positive acceleration is that the acceleration has a positive slope despite the drag forces increase with the square of velocity at the beginning of the straight line. This can be justified by the tyre grip because at that

particular moment the vehicle's longitudinal acceleration is limited by tyre grip and not by engine power. In addition, the aerodynamic devices generate more negative lift than drag, increasing the tyre longitudinal force which reduces the traction control rising the overall longitudinal acceleration. On the contrary, when the vehicle acceleration starts to be engine limited the longitudinal acceleration decreases with the increase in velocity. Due to the dimensions of the test track, this shift only takes place at the end of the complete straight line 1 (elapsed distance = [145;161]).

- Brake Acceleration: When the vehicle is accelerating with the brakes the overall acceleration is grip limited (assuming that the pilot can reach maximum brake capacity). Once the simulation algorithm works at the maximum, the overall longitudinal negative acceleration always increases with the speed. This is because the drag, lift and rolling resistance work together during the brake stage. On other words, at higher velocities, the drag forces and rolling resistance combine with tyre longitudinal forces (induced by high values of negative lift) enabling the vehicle to reduce the speed faster. In addition, it is notable that the braking peaks are superior than the positive acceleration ones, due to the fact that the vehicle brakes with the four wheels while, in this particular application, it only accelerates positively with the two rear wheels. At corner 2 the results show something curious because the simulator is applying some sort of longitudinal acceleration during the cornering stage. This happened as an outcome of corner 3 speed and vehicle brake capability, i.e., if the vehicle continued at constant speed during corner 2 the straight line 3 would not be large enough for the vehicle to brake and reach corner 3 at a given speed, therefore, the simulator must implement an exit corner braking.

7.2.2.2 *Acceleration Y-Y*

Given the defined constant radius path and corner critical speed algorithm, the lateral acceleration outputs resulted in a constant acceleration during the cornering manoeuvre. As illustrated in Figure 57, the simulated Y-Y acceleration reached similar values when compared to the logged data filtered. Once the simulator is always working at maximum cornering force without predicting body roll and other factors, the acceleration is almost the same at the different corners with a percentage difference of approximately 5% between the slowest corner and fasted corner, the second part of the corner 1 and corner 2, respectively. As expected, the lateral

acceleration was not constant during corner 2 because the vehicle started to reduce speed as mentioned in the sub-section 7.2.2.1.

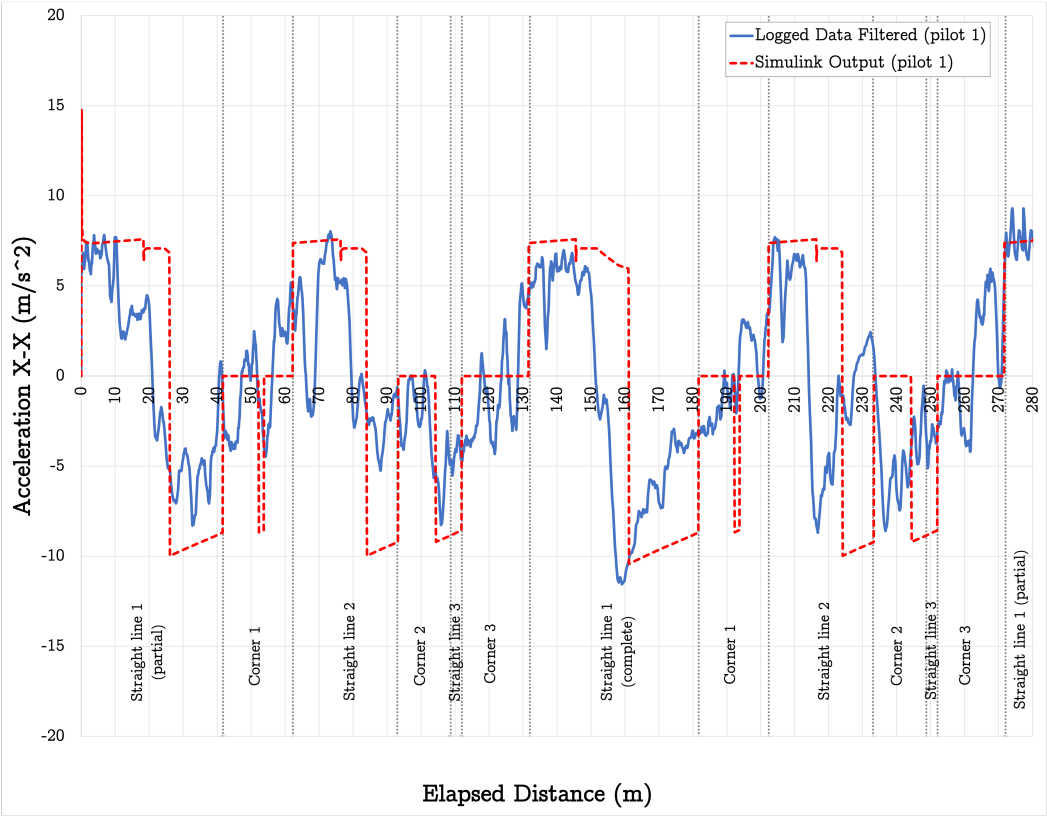

Figure 56: Simulink simulation and real longitudinal acceleration results for pilot 1.

7.2.3 *Powertrain*

The powertrain block set outputted relevant information about engine performance that one can utilize to develop certain components and also to validate the pilot behaviour and correct eventual mistakes.

7.2.3.1 *Gear position*

The gear position calculations were in fact more optimistic than what happened in real life. The ideal working conditions of the simulator allowed the vehicle to accelerate faster therefore the gear change occurred sooner than the real gear change. For example, during the first straight line, the simulator predicted the use of the third gear at the end of that segment, which was not the case in the real data profile as depicted in Figure 58. The other dissimilarity was the engaged gear at corners,

once the pilot use always second gear instead of first gear. Both discrepancies can be justified by the lack of tyre grip, for example, the first instance might be justified by an excessive amount of wheel spin at launch and the second circumstance probably in an effort to reduce the wheel torque available at the corner exit.

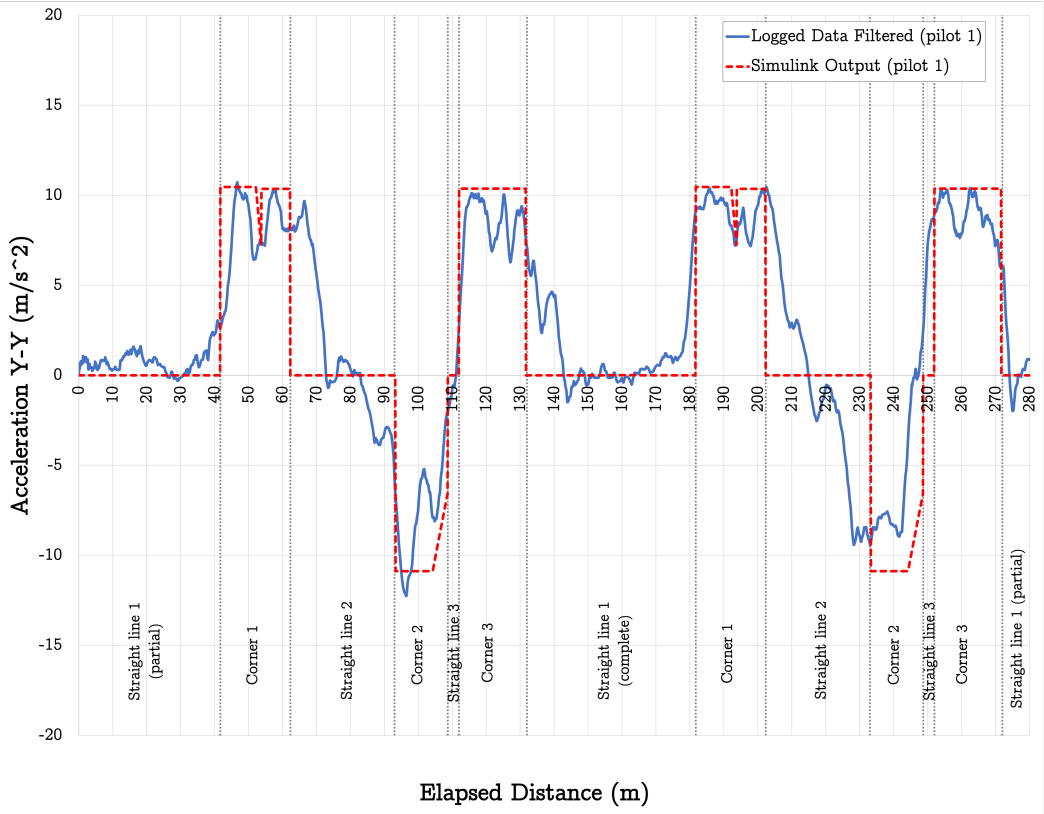

Figure 57: Simulink simulation and real lateral acceleration results for pilot 1.

7.2.3.2 *Engine speed*

The engine speed data represented one of the most, if not the most error when compared with the simulated outputs. There was one main operation condition that dictated the errors obtained, the available tyre grip. The first major inconsistency appears at the beginning of the run (elapsed distance $<$ 10m) because the launching speed induced a quite amount of wheel spin reducing the overall tyre grip and allowing the engine to reach the maximum range of operation, while the simulator worked at full tyre potential. The other primary divergence was at corner manoeuvre once the pilot stayed in second gear instead of first gear which represents lower engine speeds for the same vehicle speed according to Figure 59.

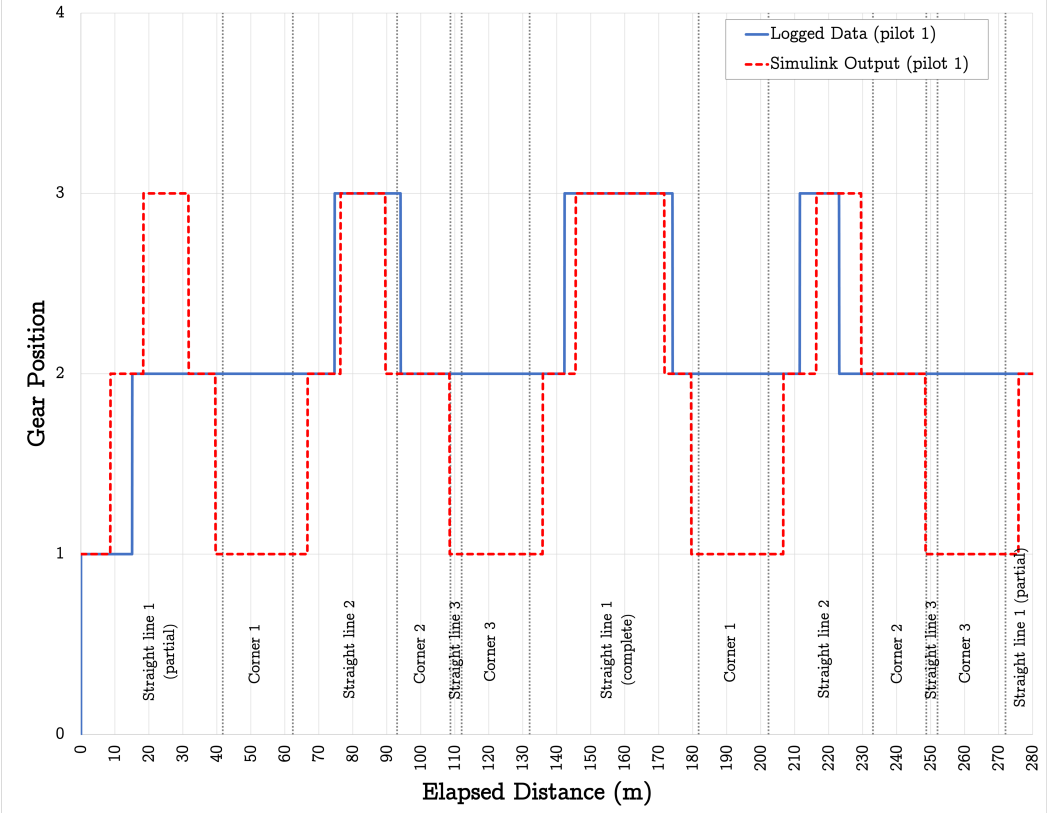

Figure 58: Simulink simulation and real gear position results for pilot 1.

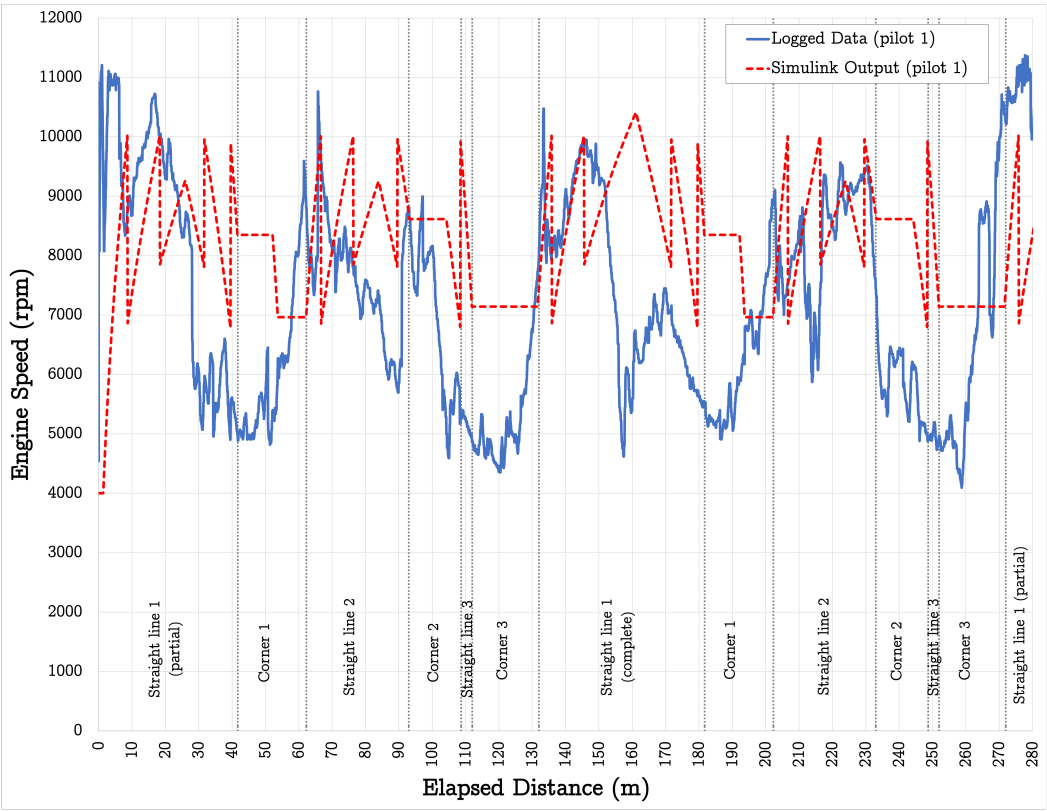

Figure 59: Simulink simulation and real engine speed results for pilot 1.

7.2.3.3 *Available wheel force*

When the vehicle is exclusively accelerating with the throttle, the simulator utilizes engine torque, gearbox ratio and efficiency as an input to calculate the available force at the wheels. As outlined in Figure 60, the engine force equivalent at the rear wheels was higher than the longitudinal force generated by the tyres roughly throughout the entire run. In fact, that was only one exception where the vehicle longitudinal acceleration was engine limited, at the end of the complete straight line 1 (elapsed time = [153;161]). Despite the engine performance, the program selects the minimum available force value for each step (tyre or engine).

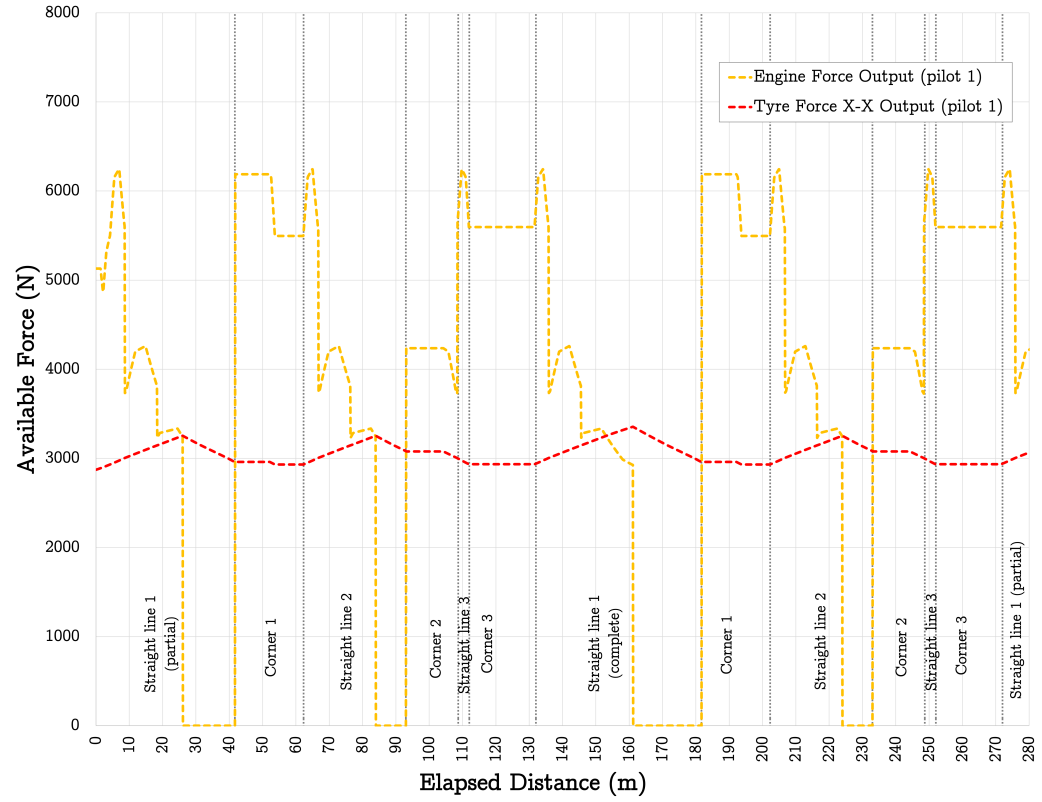

Figure 60: Simulink simulation engine and wheel force results for pilot 1.

7.2.3.4 *Fuel consumption*

As referred in Section 5.2.3, the fuel consumption estimation might induce substantial errors regarding the WOT condition of operation. Nevertheless, the fuel usage output seems to be in the higher range of the sport motorcycle's average fuel consumption. The total value obtain in the pilot 1 simulation was 55.48g of fuel which represents an average of approximately 24.7L/100km. It is important to note that during braking the fuel usage was programmed to be zero once the engine is rotating with

the inertia of the vehicle transmitted through the drive-train and not with the fuel itself. This behaviour is shown in Figure 61.

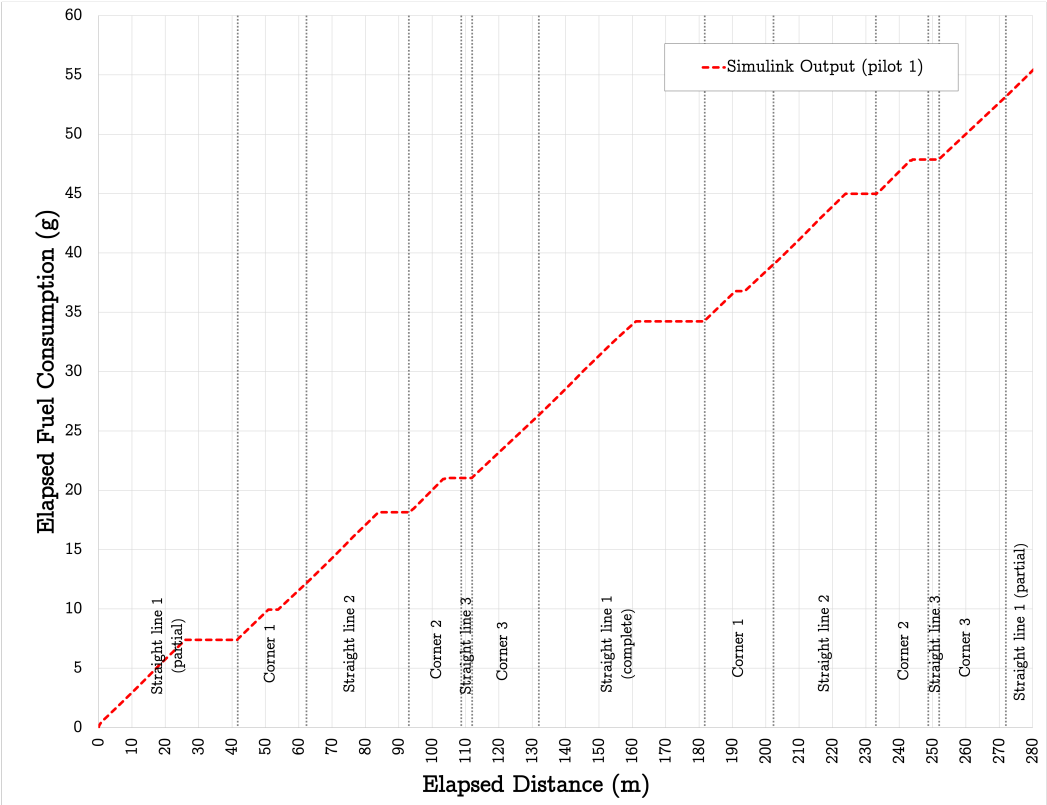

Figure 61: Simulink simulation fuel consumption results for pilot 1.

7.2.4 *Aerodynamics*

The aerodynamic applications are oftentimes neglected in this type of vehicle due to high production costs and low speeds. Notwithstanding, the simulation results regarding the generation of negative lift and drag shows that aerodynamic devices create an opportunity to reduce lap times. In conformity with the CFD analysis, the simulation predicts that the downforce was higher than the drag force (see Figure 62), which had an overall positive roll in longitudinal and lateral accelerations. In Table 8, the results of pilot 1 simulated run with and without aerodynamic devices showed significant lap times reductions with 1.80% percentage difference in elapsed times. Once the vehicle grip was affected by the lack of down-force, the fuel consumption was also affected with less fuel usage in the simulation without aerodynamic devices.

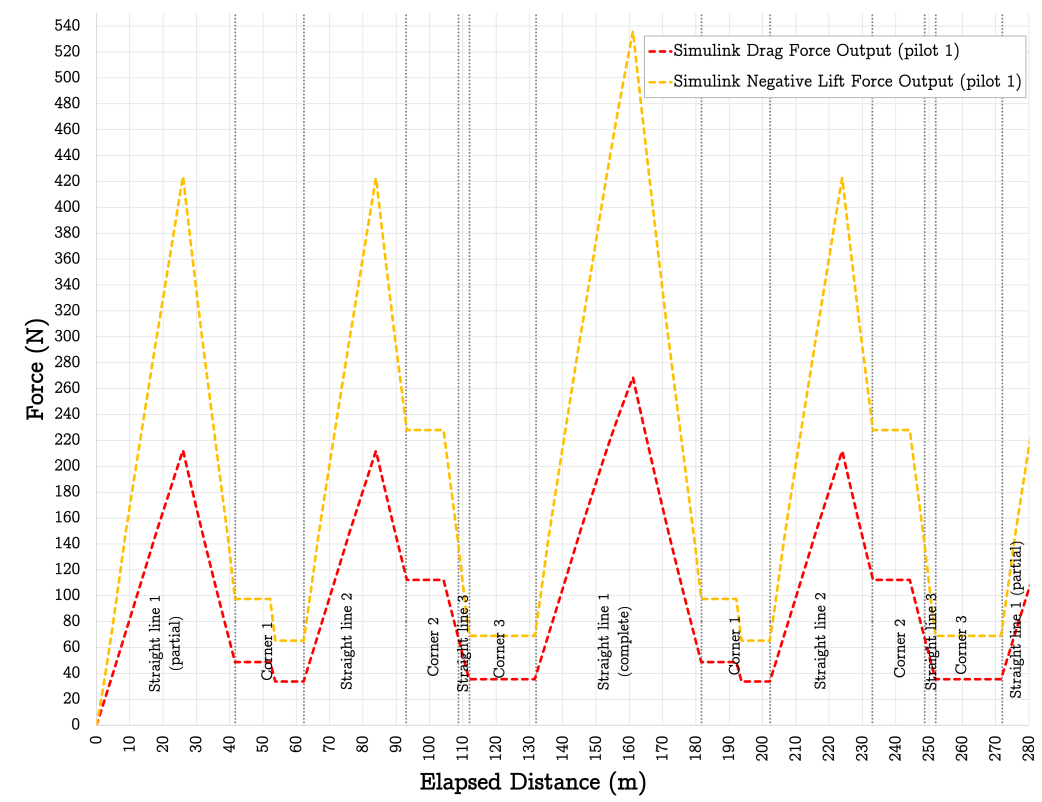

Figure 62: Simulink simulation aerodynamic results for pilot 1.

	Simulation Time (s)	Fuel Consumption (g)
Aero	24.66	55.49
No Aero	25.08	52.04
Difference %	1.70	-6.22

Table 8: Simulink simulation aerodynamic vs no aerodynamic devices results for pilot 1.

7.3 IPG CARMAKER MODEL

This section provides a critical breakdown of some simulation outputs and compares them to the previously analysed model. To simplify the data analysis and comparison to the Simulink model the commercial software results only account the pilot 1 run.

7.3.1 *Speed and Lap Time*

Regarding speed profile, the model created in Carmaker proved its value generating quite good results without much effort. The model used was able to achieve 6% of lap time difference when compared to the real data (see Table 9). The nature of the algorithm makes it difficult to justify the speed behaviour based on isolated events (variables). Nevertheless, some characteristics of the profile might be justified according to certain approaches used by the software. For example, the shape of the transition between throttle and braking is very similar to logged data. Instead of quickly imposed change from full throttle to full braking as the Simulink model, the software accounts not only for driver reaction delays but also physical delays such as generation of hydraulic pressure, change of tyre slip ratio, load transfer and other factors that smooth the positive to negative longitudinal acceleration transition. The same happened during corner because the force generation occurs smoothly, once the model utilizes the tyre magic formula where the generation of the cornering force is not only a function of the coefficient of friction but also a merge of slip angle, slip ratio and others. The corner speed output of the Carmaker simulation tends towards being higher than the logged data. This phenomenon may be justified by the lack of grip on some stages of the track, which was not taken into account during the definition of the simulation model. Another interesting factor about the commercial solution is its particularity to have different corner speed profiles for the same corner but for different corner entry speeds, as evidenced in Figure 63 (corner 1 after partial and complete straight).

	Real Time (s)	**Simulation Time (s)**	**Difference %**
Pilot 1	29.81	27.93	6.31

Table 9: Carmaker model elapsed time results.

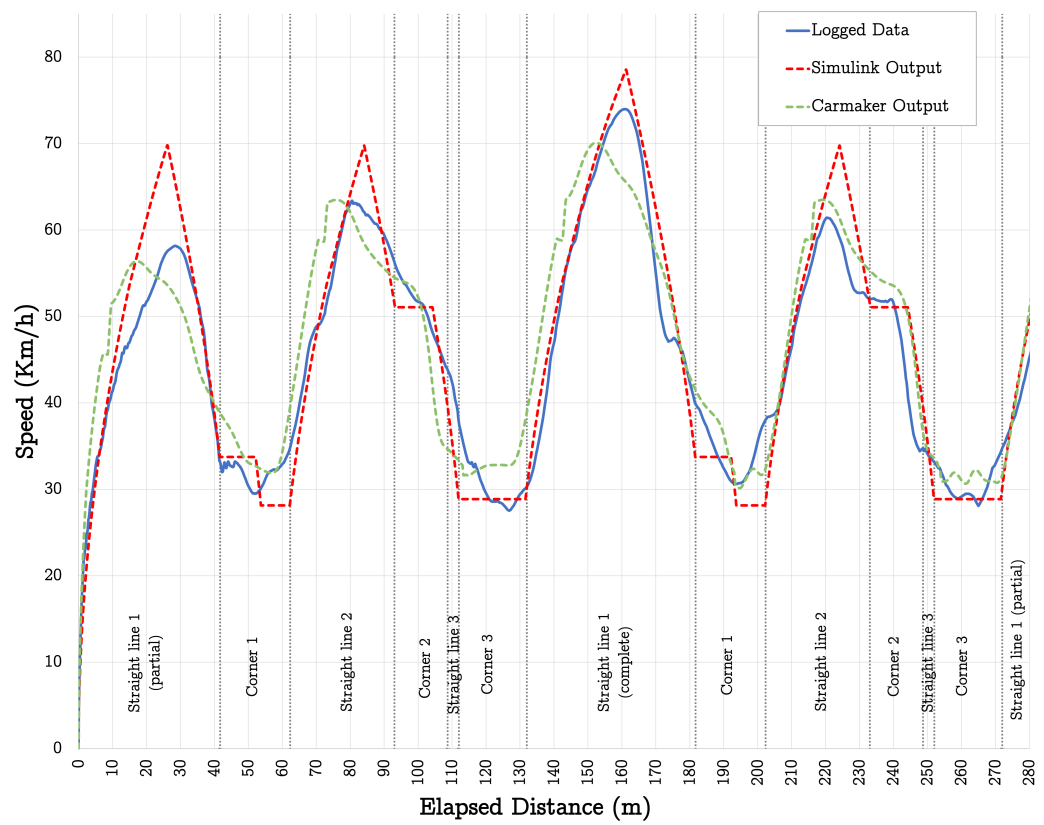

Figure 63: Carmaker, Simulink simulation and real speed results for pilot 1.

7.3.2 *Longitudinal and Lateral Accelerations*

7.3.2.1 *Acceleration X-X*

At the beginning of the run, the simulation results reached a maximum value considerable higher than the logged data. This is due to the fact that in the experimental procedure the vehicle launch induces a substantial amount of wheel spin reducing the maximum longitudinal net force of the tyres. The simulator algorithm controls the wheel spin therefore the oscillations visible at the start of the plot in Figure 64. During gear changes, for example, at an elapsed distance near 70 meters, the results for longitudinal acceleration fall sharply. This was also recorded during the test because the engine power is cut momentarily to engage a new gear. Despite being predicted in the simulation, this phenomenon was not recorded at the first gear change event (elapsed distance $\approx 10\text{m}$). This might be related to the storage inertia promoted by the spinning rear wheels, in other words, the gear change cut the engine power but at the same time slipping wheels started to recover grip and the acceleration did not fall sharply. The carmaker output acceleration also reached higher negative peaks resembling the predictions of the Simulink algorithm and the recorded data. Finally, it is important to note that the longitudinal acceleration is still present at the corning stage, i.e., the simulator is capable of operating with combined slip, which was a limitation factor of the Simulink model.

7.3.2.2 *Acceleration Y-Y*

The lateral acceleration profile exhibits a very close tendency when compared to the real data as depicted in Figure 65. The lateral tyre force generated was higher, as a result of the optimal grip simulation scenario. In consequence, the overall lateral acceleration was also higher promoting faster cornering speeds.

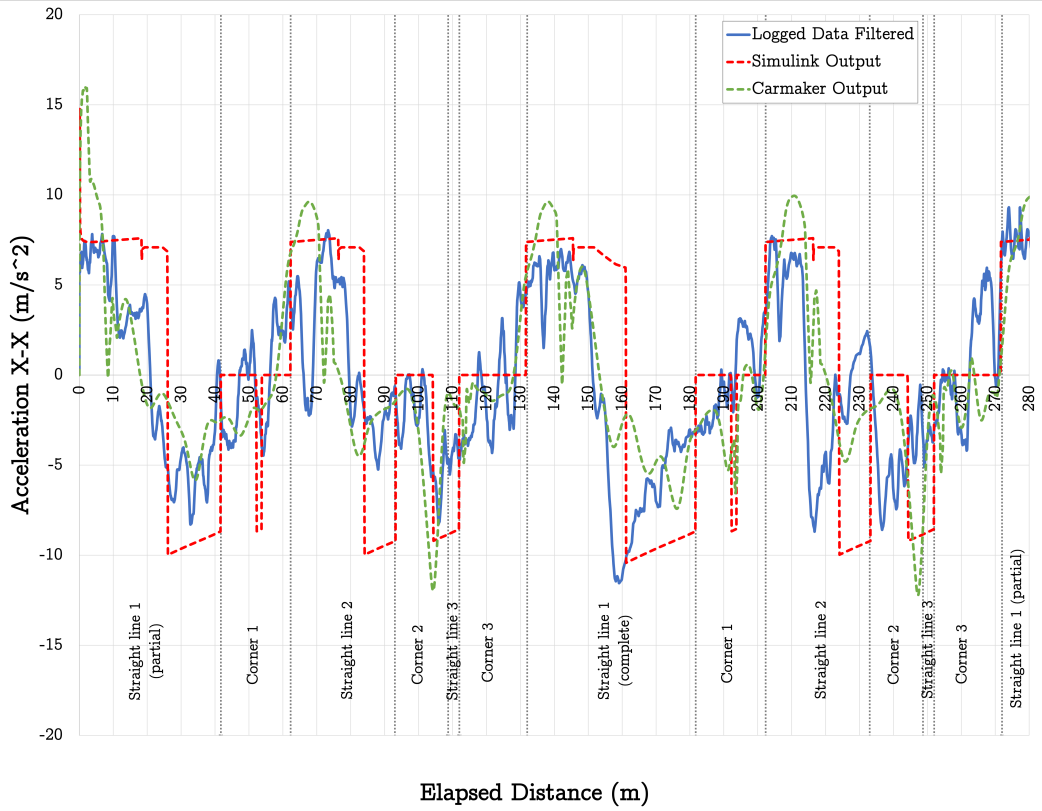

Figure 64: Carmaker, Simulink simulation and real longitudinal acceleration results for pilot 1.

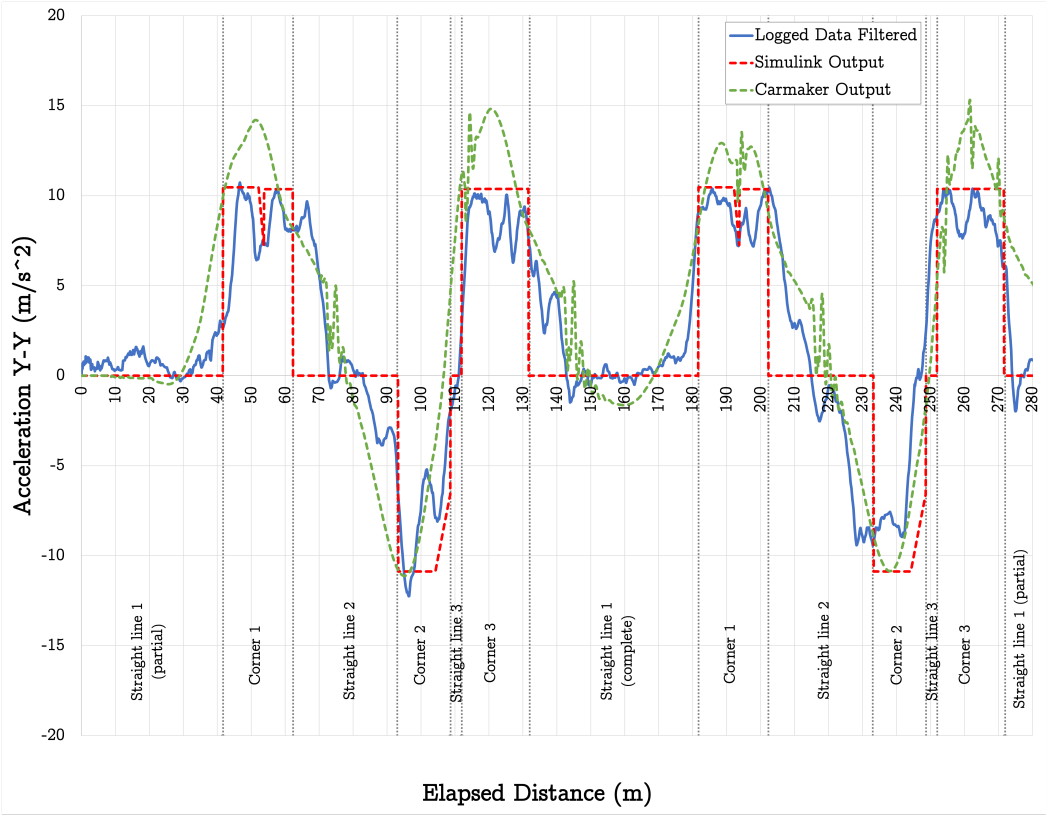

Figure 65: Carmaker, Simulink simulation and real lateral acceleration results for pilot 1.

7.3.3 *Powertrain*

7.3.3.1 *Gear position*

In the Figure 66, it is possible to see the gear strategy employed by the simulator and its similarities to the pilot approach. Likewise the Simulink results, the gear change occurs sooner than the real data at the start of the lap. The simulation predicts the use of third gear on corner 2, while in the real test the pilot chooses to use 2 gear. This discrepancy might happen because of the user-defined lower range of engine speed. However, the acceleration results were not much influenced by this dissimilarity once it arises during the braking stage.

7.3.3.2 *Engine speed*

Analogous to the analysis done in sub-section 7.2.3.2, the engine speed despite being closer is still different from the logged data. The algorithm used in the simulation does not account for the wheel spin induced by the excessive throttle in some

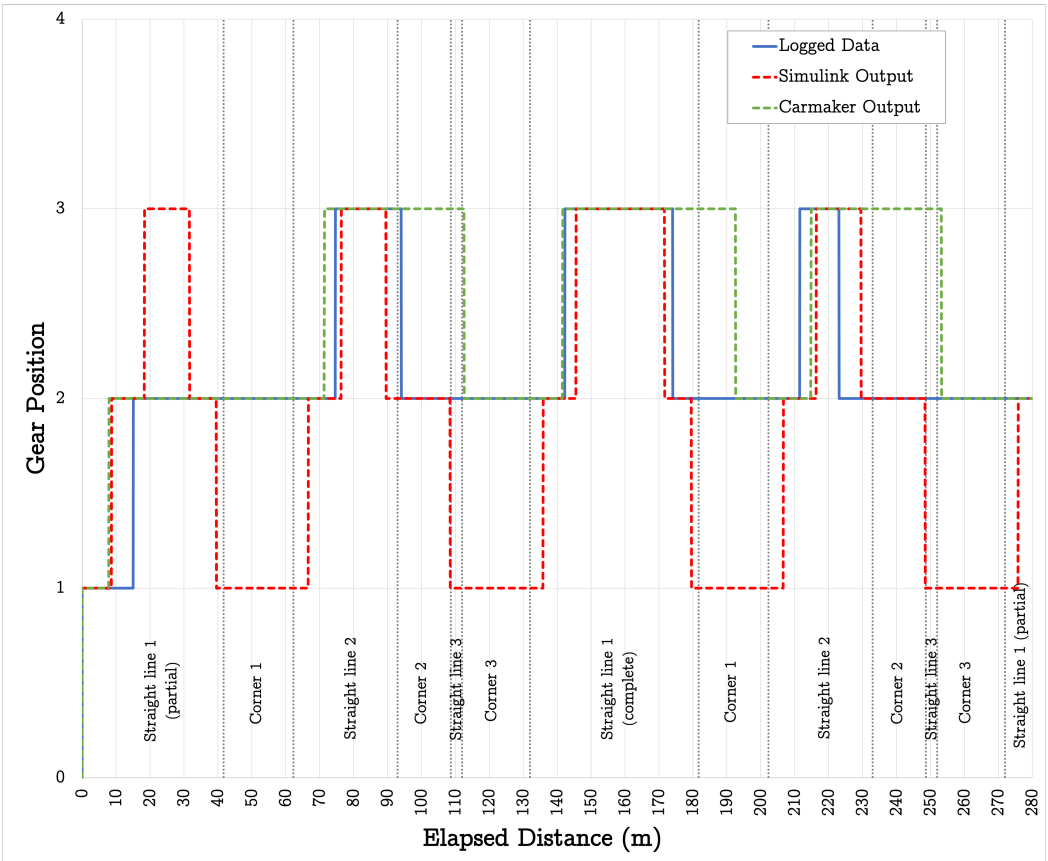

Figure 66: Simulink simulation and real gear position results for pilot 1.

situations. It should be noted that the minimum and maximum engine operation speed is defined as an input (upper and lower limit of the green line profile visible in Figure 67). That constrains the freedom of the algorithm to select gear position based only on maximum performance.

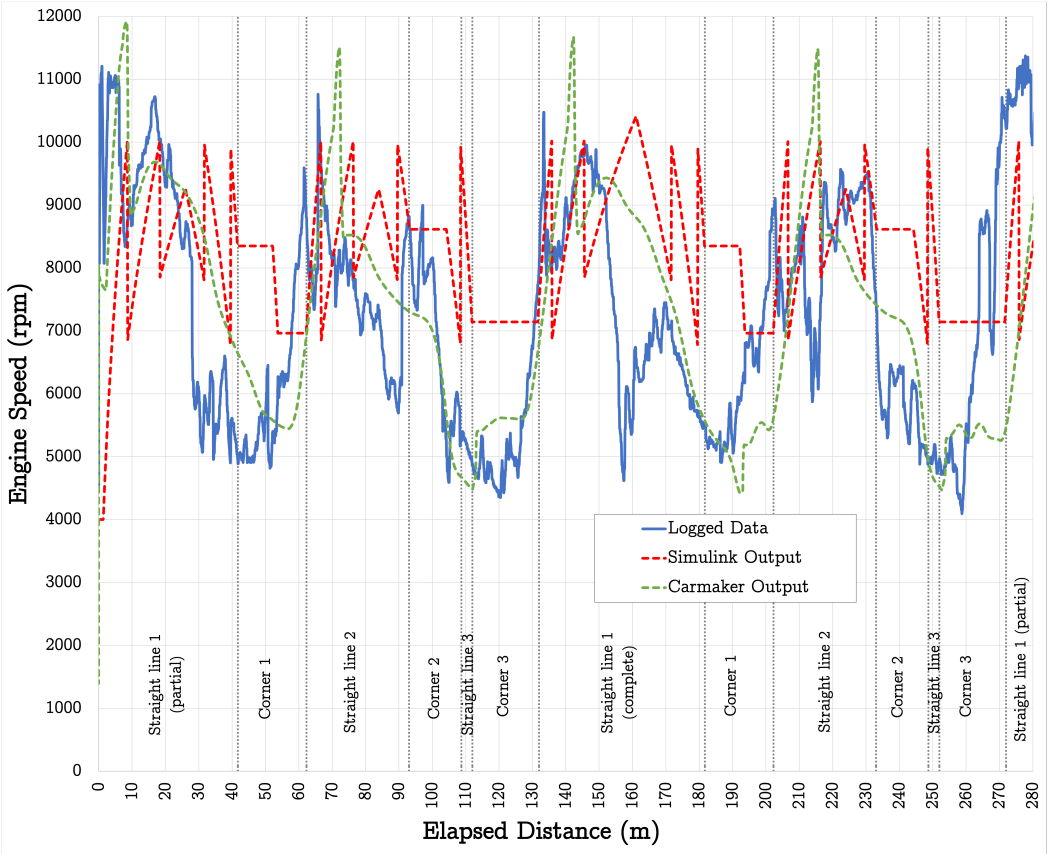

Figure 67: Carmaker, Simulink simulation and real engine speed results for pilot 1.

7.3.3.3 *Fuel consumption*

The Carmaker also utilizes break-specific fuel consumption to calculate the amount of fuel used. Instead of a 1D LUT, it uses a 2D LUT to define fuel usage as a function of engine load, speed and torque. Broadly speaking, the fuel consumption results show similar behaviour. In particular, the Carmaker predicts less fuel consumption when compared to the Simulink model, once the fuel cut off was extended to corner entry as shown in Figure 68. At the same time, when the vehicle is accelerating with the engine, the slope of fuel usage is higher than the Simulink. As a result, the Carmaker prediction for fuel usage was 48.42g (22.9l/100km). This represented a 12.2% less fuel than the Simulink calculations.

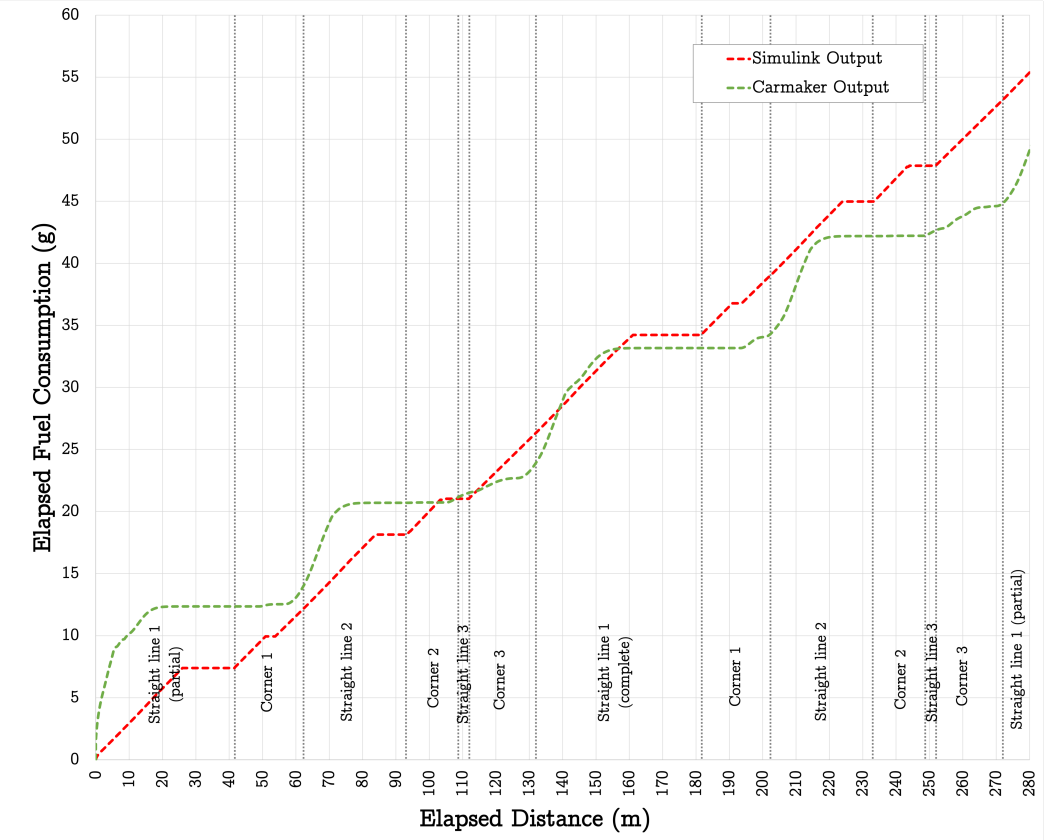

Figure 68: Carmaker, Simulink simulation fuel consumption results for pilot 1.

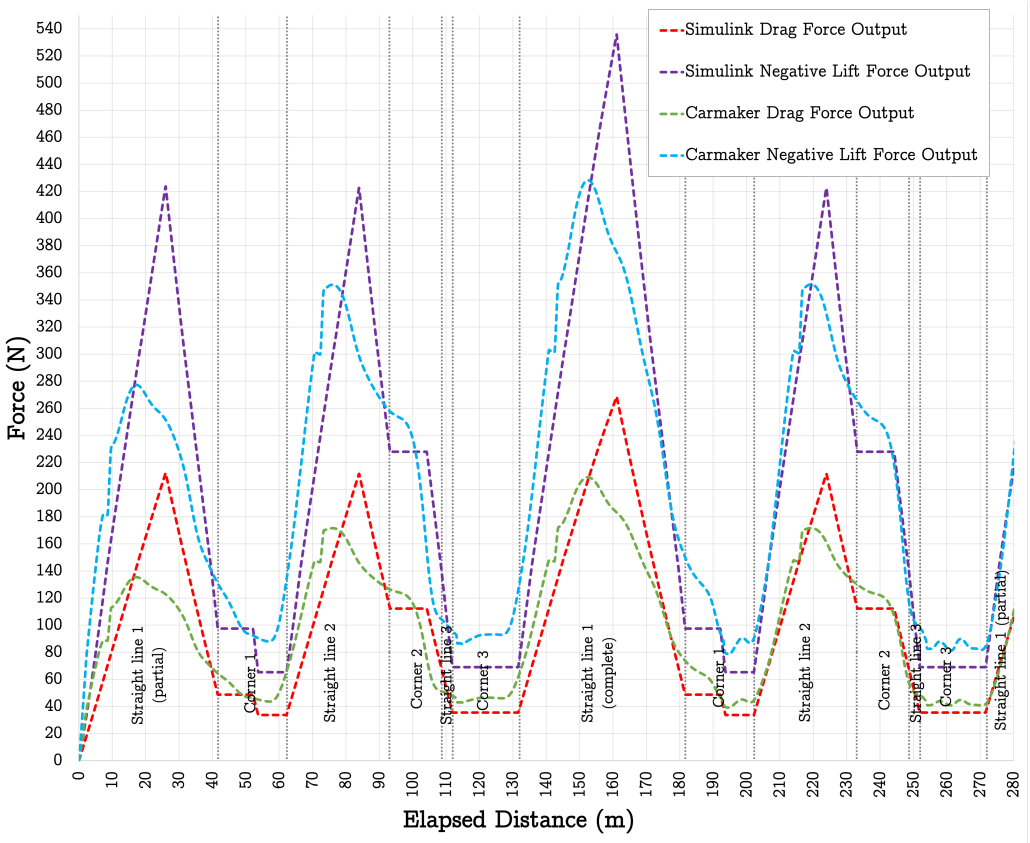

Figure 69: Carmaker, Simulink simulation aerodynamic results for pilot 1.

7.3.4 *Aerodynamics*

In comparison to the Simulink model, the Carmaker utilizes a similar approach to calculate the aerodynamic forces with the exception of having an inclination angle additional variable in the formulation. Despite this, the model defined did not predict such changes (same input for different angles) so the algorithm behind the two simulators was set to be in its own limitations the same. With that in mind, the disparity between results of negative lift and drag illustrated in Figure 69 was mainly caused by the speed differential, once the final result varies with the second power of flow velocity. The effects of such forces on the acceleration of the vehicle were not substantial, according to the results of Table 10. Once the tyre force generated did not increase significantly with the downforce, the engine power remained grip limited in some parts of the track so the estimated fuel consumption also represented a small percentage difference ($\approx 0.2\%$).

	Simulation Time (s)	Fuel Consumption (g)
Aero	27.93	48.42
No Aero	27.94	48.32
Difference %	0.04	0.21

Table 10: Carmaker simulation, aerodynamic vs no aerodynamic devices results for pilot 1.

7.3.5 *Summary:*

Due to the principle of operation and tyre model, the Simulink model shows a 16% difference in the lap time result. Despite that, it predicted with accuracy the disparity in results of the first and second pilots. The output profiles do not show a good transition between different manoeuvres (straight and corner). This happens because the model uses a steady-state approach, jumping from a longitudinal to a lateral accelerations without smoothly combining the two.

As expected, the Carmaker software shows superior outputs because it is not only capable of combining the lateral and longitudinal forces but also it calculates the load transfer and individual motion of suspension and tyres. This represented a lap time percentage difference of approximately 6%.

8

CONCLUSIONS AND RECOMMENDATIONS FOR FUTURE WORK

8.1 CONCLUSIONS

Due to the extremely complex behaviour of the vehicle, it is impossible to have a 100% accurate simulation, that is why there is a commonly used quote about vehicle dynamics models: 'All models are wrong but some are useful'. Nevertheless, one can find practical uses even in the most simple simulations. In the case of this thesis, two approaches have been implemented and validated using recorded data from a formula student vehicle. This provided critical information to analyse the results of the two numerical approaches.

Based on the analysis of the results, the first method (Simulink model) resulted in a significant percentage difference in lap time. One hypothesis for this is an oversimplified tyre model, which had some limitations concerning the effects of normal force, mainly in longitudinal force generation. This promoted higher longitudinal accelerations therefore less lap time in comparison to the real experimental procedure. Despite its limitations, this model has some practical uses in the research and development area. It provides the user with valuable outputs regarding powertrain and inertial effects, for example, fuel consumption, gear position, available engine torque, equivalent mass rotational inertia and others. For this reason, it is possible to conclude that the Simulink model provided the team with a simple and quick first approach tool to simulate some vehicle components for a given manoeuvre.

The second method was based on a commercially available solution to simulate vehicle behaviour that promoted more accurate results in the overall lap time. In particular, the use of a four-track vehicle model that predicted not only the individual tyre and suspension forces but also the load transfer, shown as expected a higher result consistency. The use of a tyre model with the magic formula reduced the biggest problem of the previously used Simulink algorithm, once the effects of tyre slip angle, slip ratio and load sensitivity were implemented. In the final analysis, the coherence of the results indicates that this detailed simulation environment could

be used by the team to further evaluate the effects of a particular component on a related vehicle subsystem and on the overall lap time performance.

8.2 RECOMMENDATIONS

This work provides a solid vehicle dynamic base for the formula student team but the models should continue to be optimized. The Simulink model is completely open-source therefore there are no boundaries regarding its improvement. It is recommended to start with the implementation of a different tyre model and vehicle model. Presumably, the best approach is to base the tyre model on the magic formula and the vehicle model on the bicycle model. Another interesting feature is the implementation of an electric motor model instead of the regular internal combustion engine. One can do that by simply defining the gearbox with a single gear ratio and utilizing the torque curve of the electric motor. With that in mind, the break-specific fuel consumption should be replaced by a power consumption algorithm preferentially connected to a regenerative braking block set.

Despite the current complexity of the Carmaker model, further work can be done. More precisely, it is recommended to improve the suspension model to have better predictions of the wheel movement during the cornering manoeuvre. This allows the user to have greater levels of understanding regarding suspension set-up optimization for a particular track achieving better lap times!

BIBLIOGRAPHY

Abe, Masato (2015). *Vehicle Handling Dynamics*. Butterworth-Heinemann.

Anderson, J. D. (2017). *Fundamentals of aerodynamics*. 2 Penn Plaza, New York, NY 10121: McGraw-Hill.

Automotive, IPG (2021a). *CarMaker*. Website. https://ipg-automotive.com/en/products-solutions/software/carmaker.

— (2021b). *CarMaker Reference Manual*. IPG Automotive Group.

Balkwill, James (2018). *Performance Vehicle Dynamics*. Butterworth-Heinemann.

Brayshaw, D L and M F Harrison (2005). "A quasi steady state approach to race car lap simulation in order to understand the effects of racing line and centre of gravity location". In: *Proceedings of the Institution of Mechanical Engineers, Part D: Journal of Automobile Engineering* 219.6, pp. 725–739. DOI: 10.1243/095440705X11211. URL: https://doi.org/10.1243/095440705X11211.

Candelpergher, Andrea, Marco Gadola, and David Vetturi (2000). "Developments of a Method for Lap Time Simulation". In: DOI: 10.4271/2000-01-3562.

Casanova, Daniel (2000). "On minimum time vehicle manoeuvring: the theoretical optimal lap". In:

COMSOL (2017). Website. https://www.comsol.com/blogs/which-turbulence-model-should-choose-cfd-application, last accessed on 15/02/2022.

Cornering of Vehicle (2015). Website. https://iith.ac.in/, last accessed on 20/02/2022.

Eng. ToolBox (2008). Website. https://www.engineeringtoolbox.com/rolling-friction-resistance-d_1303.html, last accessed on 16/07/2021.

Franck, Nicoud (2007). "Unsteady flows modeling and computation". In:

Frazza, Loïc, Frederic Alauzet, and Adrien Loseille (n.d.). "Mesh adaptation strategies using wall functions and low-Reynolds models". In: *2018 Fluid Dynamics Conference*. DOI: 10.2514/6.2018-4153. URL: https://arc.aiaa.org/doi/abs/10.2514/6.2018-4153.

Gianpiero Mastinu, Manfred Ploechl (2014). *Road and Off-Road Vehicle Systems Dynamics Handbook*. CRC Press.

Gillespie, Thomas D. (1992). *Fundamentals of Vehicle Dynamics*. Warrendale, PA: SAE International.

Henrique Amaral, Tiago. Pinheiro (2018). "Validation and development of a variable geometry intake system." Undergraduate Project.

I.J.M. Besselink, A.J.C. Schmeitz and H.B. Pacejka (2010). *An Improved Magic Formula/Swift Tyre Model That Can Handle Inflation Pressure Changes*.

IMechE (2021). *IMechE*. Website. https://www.imeche.org/events/formula-student/about-formula-student/history-of-formula-student.

Kang, Dongsoo et al. (2005). "Implementing the Milliken Moment Method using Controlled Dynamic Simulation". In: DOI: 10.4271/2005-01-0417.

Kelly, Daniel P. (2008). "Lap time simulation with transient vehicle and tyre dynamics". In:

Mason, Stephen (2020). *The Effects of Rotational Inertia on Automotive Acceleration*. Website. http://stephenmason.com/cars/rotationalinertia.html.

Miguel Ribeiro, Nuno Clara (2021). "Aerodynamic Study of a Undertray for a Formula SAE Vehicle." Undergraduate Project.

Milliken, W.F. and D.L. Milliken (1995). *Race Car Vehicle Dynamics*. Warrendale, PA: SAE International.

Molland, Anthony F and Stephen R Turnock (2007). *Marine Rudders and Control Surfaces*. Butterworth-Heinemann.

Nakajima, Yukio (2019). "Cornering Properties of Tires". In: *Advanced Tire Mechanics*. Singapore: Springer Singapore, pp. 707–806. DOI: 10.1007/978-981-13-5799-2_11. URL: https://doi.org/10.1007/978-981-13-5799-2_11.

NASA (2021). Website. https://www.grc.nasa.gov/www/k-12/airplane/boundlay.html, last accessed on 15/02/2022.

Novotny, Tomas (2016). "Lap Time Simulation". Master Thesis.

Oglieve, Callum, Mahdi Mohammadpour, and Homer Rahnejat (2017). "Optimisation of the vehicle transmission and the gear-shifting strategy for the minimum fuel consumption and the minimum nitrogen oxide emissions". In: *Proceedings of the Institution of Mechanical Engineers, Part D: Journal of Automobile Engineering*. DOI: 10.1177/0954407017702985.

Pacejka, H.B. (2005). *Tyre and Vehicle Dynamics*. Butterworth-Heinemann.

Pacejka, H.B. and I.J.M Besselink (1997). "Magic Formula Tyre Model with Transient Properties". In: *Vehicle System Dynamics* 27.sup001, pp. 234–249. DOI: 10.1080/00423119708969658. URL: https://doi.org/10.1080/00423119708969658.

Patton, Christi L. (2013). "Development of vehicle dynamics tools for motorsports". In:

SAE (1976). *Vehicle Dynamics Terminology*. https://doi.org/10.4271/J670_197607. Warrendale, PA: SAE International.

SangDo et al. (2015). "Dynamic vehicle model for handling performance using experimental data". In: *Advances in Mechanical Engineering* 7. DOI: 10.1177/1687814015618126.

Santos, Rodrigo (2014). *Racing Car Dynamics*. Website. http://racingcardynamics.com/racing-tires-lateral-force/.

Siegler, Blake, Andrew Deakin, and D. Crolla (2000). "Lap Time Simulation: Comparison of Steady State, Quasi- Static and Transient Racing Car Cornering Strategies". In: *SAE transactions* 109, pp. 2575–2581.

Smith, C. (2004). *Tune to Win*. Motorbooks International.

Wong, J.Y. (2001). *Theory of Ground Vehicles*. John Wiley & Sons, Inc.

APPENDIX

APPENDIX A

A.1 SIMULINK ENVIRONMENT

A.1.1 *Processor*

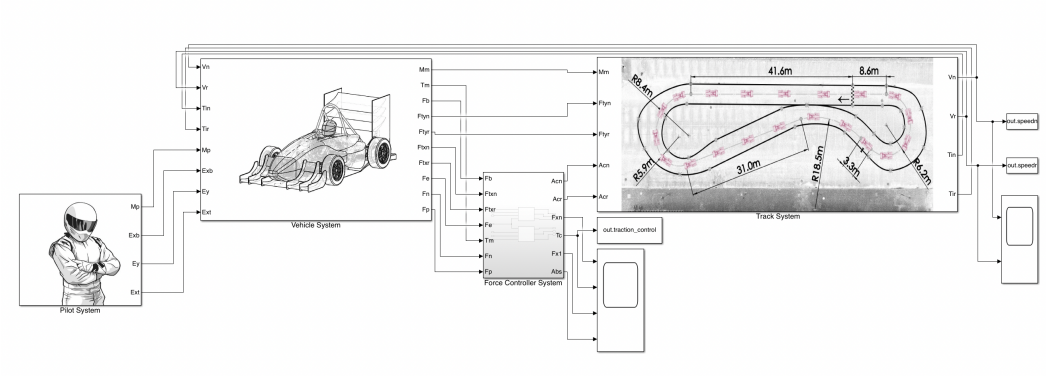

Figure 70: Processor overview.

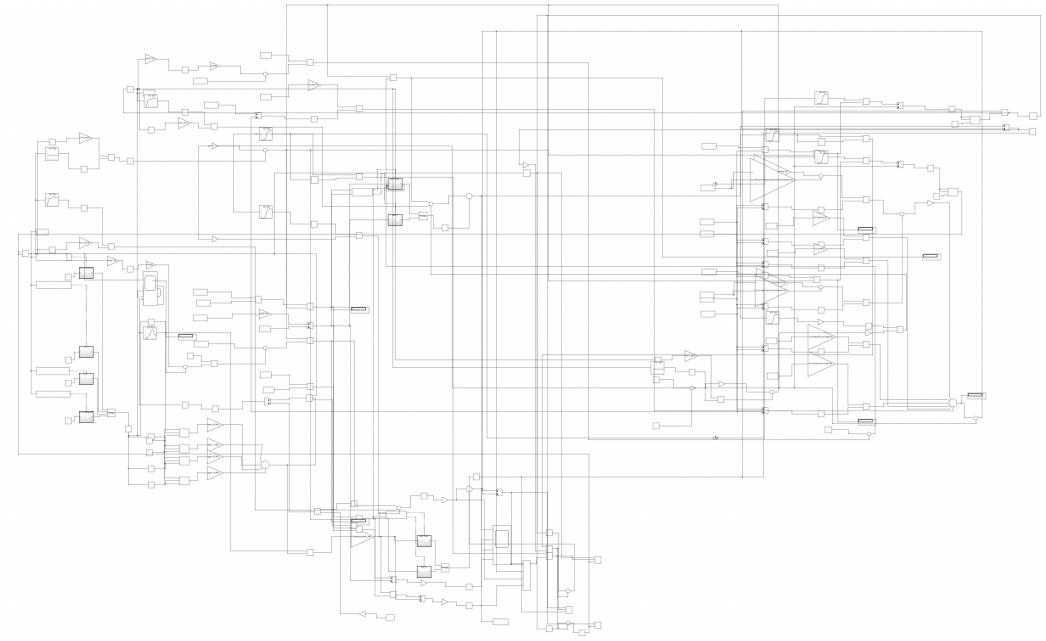

Figure 71: Processor expanded view.

A.1.2 *Post-Processor*

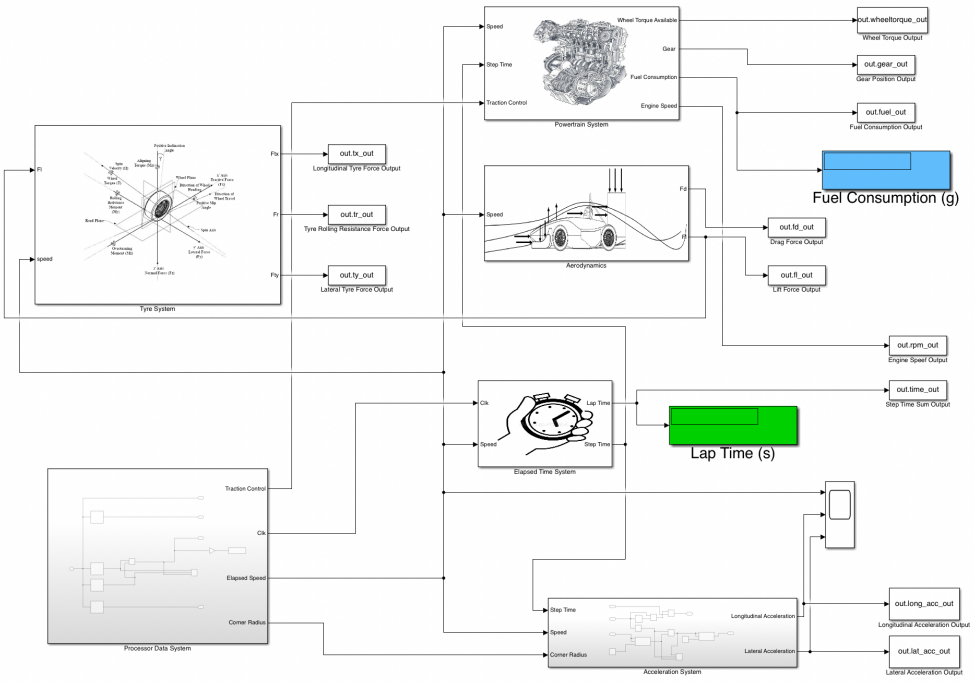

Figure 72: Post-Processor overview.

A.2 SIMULINK DATA SET

```
 Lap Time Simulator
By Henrique Amaral 2021

%::::::GENERAL PROPERTIES:::::%
d_air = 1.22; %air density for aero (kg/m^3)
g = 9.81; %gravitational acceleration (m/s^2)
%:::::::::::::::::::::::::::::%

%:::::::PILOT DATA::::::::::::%
mp = 75; %pilot mass (kg)
ext = 0.8; %pilot efficiency at throttle (0-1)
exb = 0.7; %pilot efficiency at brake (0-1)
ey = 0.6; %pilot efficiency at corner (0-1)
%:::::::::::::::::::::::::::::%
```

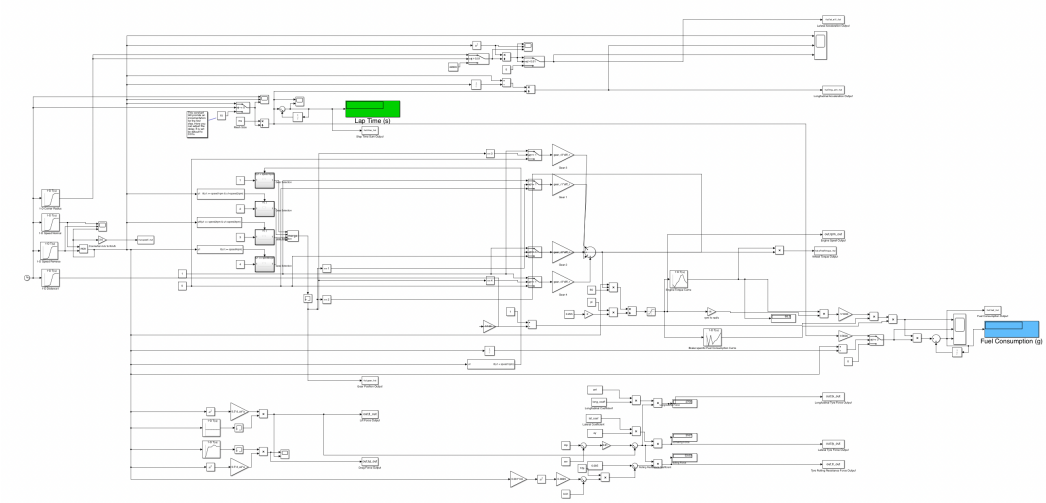

Figure 73: Post-Processor expanded view.

```
%:::::::::VEHICLE DATA::::::::::%
mv = 236.9; %vehicle mass(kg)
wradius = 0.255; %wheel radius(m)

%TYRES%
long_coeft = 1.126; %ideal longitudinal coefficient for throttle
long_coefb = 1.427; %ideal longitudinal coefficent for brakes
lat_coef = 1.725; %ideal lateral coefficient for cornering
grip_factor = 1; %factor for defining the road condition
roll_coef = 0.02; %rolling resistance coefficient
tp = 0.80; %tyre pressure (bar)

%AERODYNAMICS%
sp1 = 5.56; %speed1 (m/s)
sp2 = 11.11; %speed2 (m/s)
sp3 = 16.67; %speed3 (m/s)
sp4 = 22.22; %speed4 (m/s)
sp5 = 27.78; %speed5 (m/s)
sp6 = 33.33; %speed6 (m/s)

cd1 = 0.744; %drag coefficient for sp1
cd2 = 0.758; %drag coefficient for sp2
cd3 = 0.758; %drag coefficient for sp3
```

```
cd4 = 0.761; %drag coefficient for sp4
cd5 = 0.759; %drag coefficient for sp5
cd6 = 0.759; %drag coefficient for sp6

cl1= 0;%1.37; %lift coefficient for sp1
cl2 = 0;%1.57; %lift coefficient for sp2
cl3 = 0;%1.515; %lift coefficient for sp3
cl4 = 0;%1.518; %lift coefficient for sp4
cl5 = 0;%1.538; %lift coefficient for sp5
cl6 = 0;%1.557; %lift coefficient for sp6
a = 1.206; %cross sectional area (m^2)

%POWERTRAIN%
drive_effic = 0.9; %drivetrain efficiency
gear_r1 = 5.06; %first gear ratio
gear_r2 = 3.45; %second gear ratio
gear_r3 = 2.7; %third gear ratio
gear_r4 = 1.93; %fourth gear ratio
diff_r = 4.7; %diffirential ratio (final drive)
shiftrpm = 10000; %maximum rpm for shifting purposes
launchrpm = 4000; %rpm launch control

%\\target rpm to speed converter for auto-shifting\\%
speed1rpm = ((shiftrpm*2*pi*wradius)/(60*gear_r1*diff_r));
speed2rpm = ((shiftrpm*2*pi*wradius)/(60*gear_r2*diff_r));
speed3rpm = ((shiftrpm*2*pi*wradius)/(60*gear_r3*diff_r));
speed4rpm = ((shiftrpm*2*pi*wradius)/(60*gear_r4*diff_r));
%-----------------------------------------------%

%\\engine torque curve\\%
nm1 = 55; %engine torque point 1 (n.m)
nm2 = 52; %engine torque point 2 (n.m)
nm3 = 57; %engine torque point 3 (n.m)
nm4 = 59; %engine torque point 4 (n.m)
nm5 = 66; %engine torque point 5 (n.m)
nm6 = 67; %engine torque point 6 (n.m)
nm7 = 60; %engine torque point 7 (n.m)
nm8 = 57; %engine torque point 8 (n.m)
```

```
rpm1 = 4000; %engine speed point 1 (rpm)
rpm2 = 5000; %engine speed point 2 (rpm)
rpm3 = 6000; %engine speed point 3 (rpm)
rpm4 = 7000; %engine speed point 4 (rpm)
rpm5 = 8000; %engine speed point 5 (rpm)
rpm6 = 9000; %engine speed point 6 (rpm)
rpm7 = 10000; %engine speed point 7 (rpm)
rpm8 = 11000; %engine speed point 8 (rpm)


%\\fuel consumption\\%
bsfc1 = 305.40; %brake-specific fuel consumption point 1 (g/kw.h)
bsfc2 = 287.83; %brake-specific fuel consumption point 2 (g/kw.h)
bsfc3 = 306.08; %brake-specific fuel consumption point 3 (g/kw.h)
bsfc4 = 289.91; %brake-specific fuel consumption point 4 (g/kw.h)
bsfc5 = 295.57; %brake-specific fuel consumption point 5 (g/kw.h)
bsfc6 = 297.74; %brake-specific fuel consumption point 6 (g/kw.h)
bsfc7 = 303.21; %brake-specific fuel consumption point 7 (g/kw.h)
bsfc8 = 310.49; %brake-specific fuel consumption point 8 (g/kw.h)
%----------------------------------------%

%BRAKES%
rm = 0.165; %mean radius of the pad force on the disc (m)
ap = 0.00158; %pad area (m^2)
ph = 8000000; %hidraulic maximum pressure (Pa)
up = 0.6; %pad coefficient of friction
np = 2; %number of friction pads

%INERTIAS%
mdiff = 5.8720; %differential mass (kg)
mpinion = 0.1; %pinion mass (kg)
mrack = 1.83; %rack mass (kg)
mrim = 3.4; %wheel rim mass (kg)
mshaft = 7.84; %shaft mass (kg)
mtyre = 5.7; %tyre mass (kg)
mfw = 0.6; %fly wheel mass (kg)
rch = 0.05; %center hub radius (m)
```

```
rdiff = 0.05; %differential radius (m)
rpinion = 0.025; %pinion radius (m)
rirack = 0.06; %rack inner radius (m)
rishaft = 0.01; %shaft inner radius (m)
rorack = 0.123; %rack outter radius (m)
roshaft = 0.022; %shaft outter radius (m)
rfw = 0.120; %flywheel radius (m)
rrim = 0.165; %rim radius (m)
trim = 0.005; %rim thickness (m)
ttyre = 0.015; %tyre thickness (m)
htyre = 0.178; %tyre height (m)
wdr = 0.65; %rim weight distribution
wdt = 0.35; %tyre weight distribution
%:::::::::::::::::::::::::::::::::%
```

B

APPENDIX B

B.1 CARMAKER 3D SIMULATION

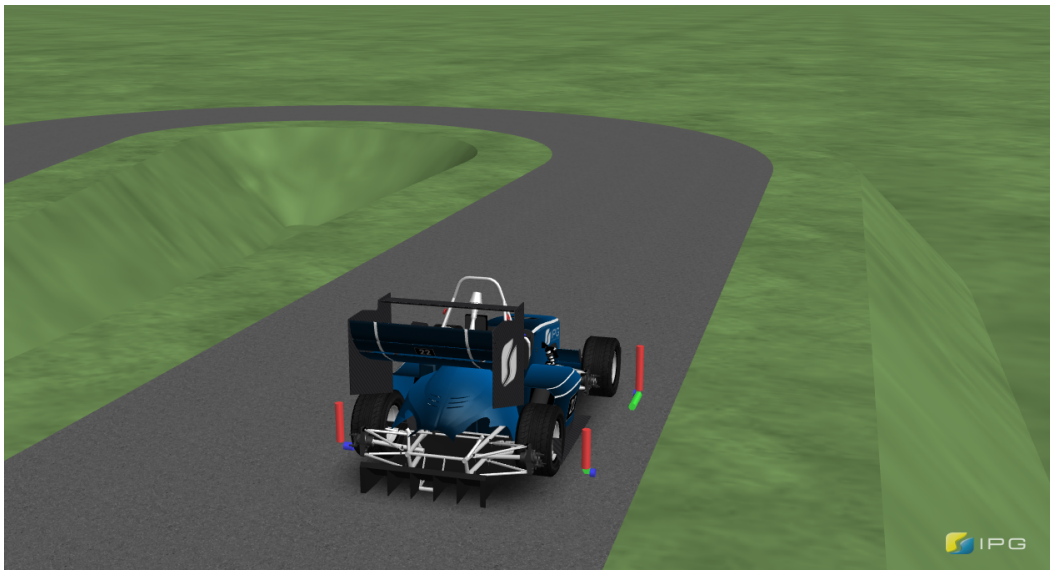

Figure 74: Simulation 3d environment.

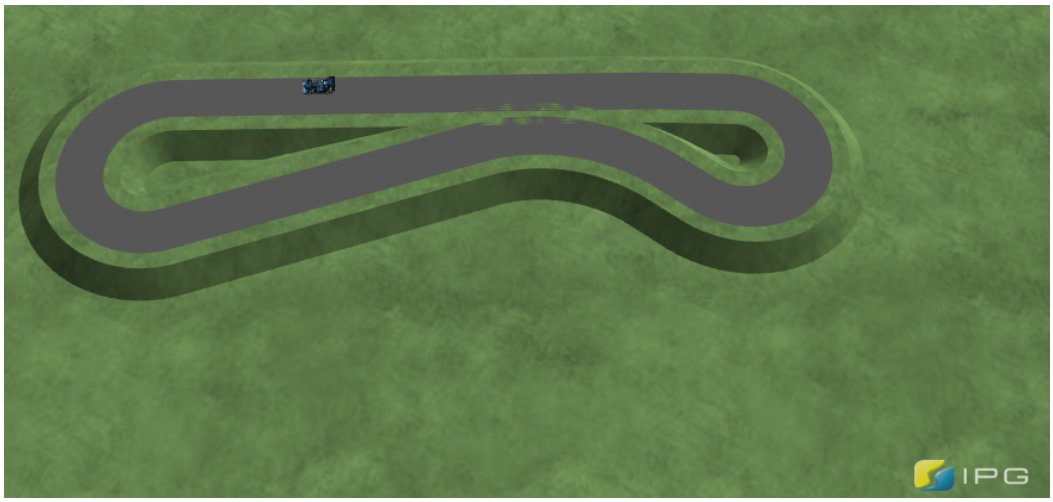

Figure 75: Simulation 3d track aerial view.

B.2 EXPERIMENTAL PROCEDURE

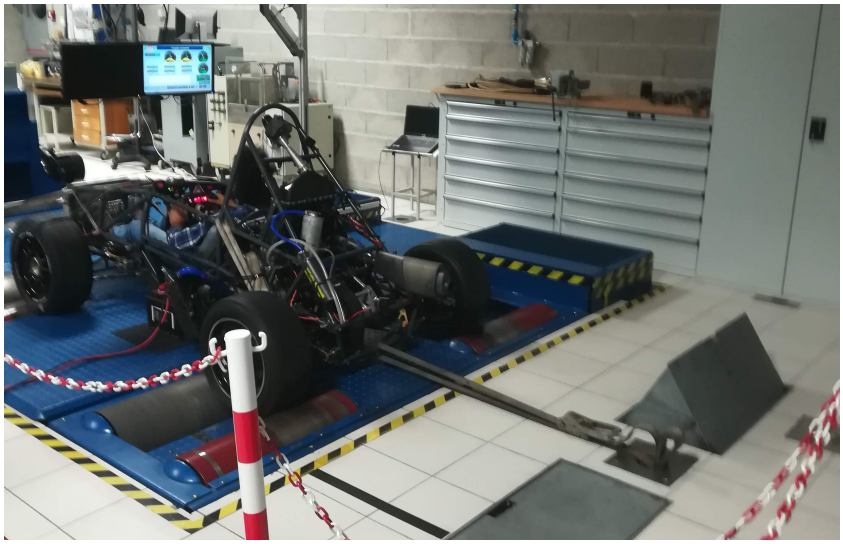

Figure 76: Power dyno trail for measuring engine torque at WOT condition.

Figure 77: Experimental test.

Figure 78: Experimental test aerial view.